Available online at www.sciencedirect.com
ScienceDirect
Icarus 192 (2007) 187–222
ICARUS
www.elsevier.com/locate/icarus

Antarctic dry valleys: Microclimate zonation, variable geomorphic processes, and implications for assessing climate change on Mars

David R. Marchant [a,*], James W. Head III [b]

[a] *Department of Earth Sciences, Boston University, Boston, MA 02215, USA*
[b] *Department of Geological Sciences, Brown University, Providence, RI 02912, USA*

Received 17 October 2006; revised 18 June 2007

Available online 16 August 2007

Abstract

The Antarctic Dry Valleys (ADV) are generally classified as a hyper-arid, cold-polar desert. The region has long been considered an important terrestrial analog for Mars because of its generally cold and dry climate and because it contains a suite of landforms at macro-, meso-, and microscales that closely resemble those occurring on the martian surface. The extreme hyperaridity of both Mars and the ADV has focused attention on the importance of salts and brines on soil development, phase transitions from liquid water to water ice, and ultimately, on process geomorphology and landscape evolution at a range of scales on both planets. The ADV can be subdivided into three microclimate zones: a coastal thaw zone, an inland mixed zone, and a stable upland zone; zones are defined on the basis of summertime measurements of atmospheric temperature, soil moisture, and relative humidity. Subtle variations in these climate parameters result in considerable differences in the distribution and morphology of: (1) macroscale features (e.g., slopes and gullies); (2) mesoscale features (e.g., polygons, including ice-wedge, sand-wedge, and sublimation-type polygons, as well as viscous-flow features, including solifluction lobes, gelifluction lobes, and debris-covered glaciers); and (3) microscale features (e.g., rock-weathering processes/features, including salt weathering, wind erosion, and surface pitting). Equilibrium landforms are those features that formed in balance with environmental conditions within fixed microclimate zones. Some equilibrium landforms, such as sublimation polygons, indicate the presence of extensive near-surface ice; identification of similar landforms on Mars may also provide a basis for detecting the location of shallow ice. Landforms that today appear in disequilibrium with local microclimate conditions in the ADV signify past and/or ongoing shifts in climate zonation; understanding these shifts is assisting in the documentation of the climate record for the ADV. A similar type of landform analysis can be applied to the surface of Mars where analogous microclimates and equilibrium landforms occur (1) in a variety of local environments, (2) in different latitudinal bands, and (3) in units of different ages. Documenting the nature and evolution of the ADV microclimate zones and their associated geomorphic processes is helping to provide a quantitative framework for assessing the evolution of climate on Mars.

Keywords: Earth; Geological processes; Ices; Mars, climate; Mars, surface

1. Introduction

Climate, the average weather conditions in a region over periods of years to decades, is defined by variations in factors such as temperature, the amount of rainfall, wind velocities, solar radiation, etc. These variations lead to different geological processes operating with different intensities in specific climate zones and thus in different geomorphic landforms characterizing these environments. On Earth, the recognition of groups of climate-related landforms has led to the definition of different morphogenetic regions (e.g., Wilson, 1969; Baker, 2001) which can be classified in terms of mean annual temperature and precipitation (Fig. 1). For example, climate zones with high mean annual temperatures (e.g., 30–40 °C; 303–313 K) can range from arid, with low mean annual precipitation (e.g., 10–20 mm), to selva (hot, wet, tropical rainforest), with extremely high mean annual precipitation (e.g., 1500–2000 mm).

* Corresponding author.
E-mail addresses: marchant@bu.edu (D.R. Marchant), james_head@brown.edu (J.W. Head III).

0019-1035/$ – see front matter
doi:10.1016/j.icarus.2007.06.018

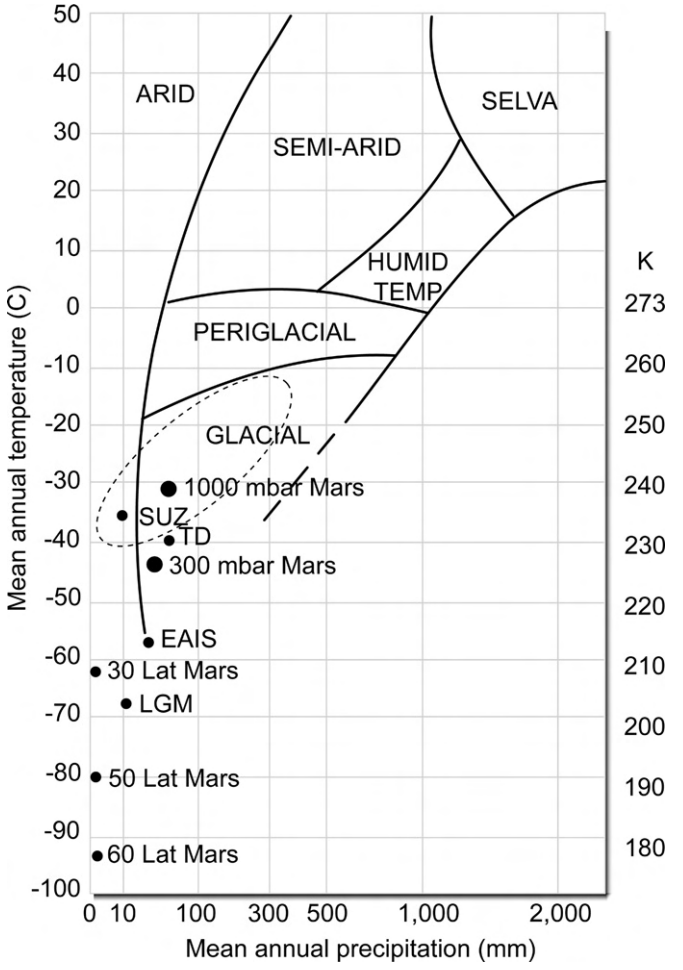

Fig. 1. Morphogenetic regions for climate related landforms on Earth [adapted from Baker (2001)]. Dashed oval shows region comprising the Antarctic Dry Valleys (ADV), including the stable upland zone SUZ (shown as a dot), the inland mixed zone IMZ, and the coastal thaw zone CTZ. Also plotted are modern Mars conditions at 30°, 50°, and 60° latitude, as well as an ancient Mars at 300 and 1000 mbar. TD, modern conditions at Taylor Dome, 35 km south-west of the ADV; EAIS, modern conditions at Vostok, interior East Antarctica (78° S); LGM, conditions during the last glacial maximum (∼18 ka) in interior East Antarctica.

A major key to the geological processes and geomorphic landforms characterizing different climate zones or environments is the abundance and state of water. In the high mean temperature arid–selva comparison, arid landscapes show less water-related fluvial activity, whereas the copious amounts of rainfall in the selva produce significant fluvial erosion. The state of the water is also important. Climate zones characterized by mean annual temperatures near or below the freezing point of water (Fig. 1) will clearly be much less influenced by fluvial activity. Instead, periglacial or glacial morphogenetic zones will prevail, and landscapes will be formed and modified by freeze-thaw cycles and the movement of ice.

These relationships (Fig. 1) offer a powerful tool for the definition of climate zones, an understanding of how they form and evolve, and even for predictions about the nature of landforms under different climate conditions on the Earth and Mars. For example, some modern terrestrial glacial environments, such as Taylor Dome and Vostok in Antarctica (TD and EAIS respectively in Fig. 1), have extremely low mean annual temperatures (−40 to −58 °C; 215–233 K) and extremely low mean annual precipitation (between 10 and 100 mm). In comparison, however, current conditions on Mars at mid to high latitudes (see 30, 50, 60, indicating Mars conditions at these latitudes in Fig. 1) are much colder (−60 to −95 °C; 178–213 K) and dryer (∼0 mm mean annual precipitation). Climates, however, change with time. Conditions inferred from the period of the last glacial maximum in Antarctica about 18 ka (LGM in Fig. 1) are much colder and dryer (−68 °C, 205 K; ∼10 mm mean annual precipitation) than those at Taylor Dome and Vostok today, and indeed are more comparable to mid-latitude conditions that exist currently on Mars (compare position of LGM and 30 in Fig. 1). In a similar manner, predicted climate conditions thought to have characterized earlier parts of Mars' history on the basis of climate models (e.g., Pollack et al., 1987) can also be plotted. In this scenario, modeled conditions for Mars at ∼300 mbar atmospheric pressure and ∼1000 mbar atmospheric pressure predict that ancient Mars could have been characterized by cold glacial climate conditions similar to those of modern Earth (Fig. 1).

The very low atmospheric temperatures and limited availability of liquid water in Earth's polar deserts make for compelling comparisons to a dry and cold Mars. Among polar deserts on Earth, the Antarctic Dry Valleys (ADV) have long been considered as the most Mars-like (e.g., Anderson et al., 1972; Gibson et al., 1983; Mahaney et al., 2001; Wentworth et al., 2005). Classified broadly as a cold and hyper-arid region, plotted as a dashed oval in Fig. 1, the valleys feature a diverse suite of surface landforms that provide a geomorphological framework for both assessing differences within the ADV, and interpreting features and microclimate zones on Mars.

In this contribution we examine the nature and evolution of the hyper-arid polar desert of the Antarctic Dry Valleys, defining three main microclimate zones, and assess the role of small variations in mean annual temperature and precipitation in producing and sustaining different characteristic landforms at a variety of scales. We then explore the application of these concepts to the assessment of climate change in the ADV and to the definition of microclimate zones on Mars and exploring evidence for recent climate change on that planet.

2. The Antarctic Dry Valleys

2.1. Physical setting

Located in the central Transantarctic Mountains, the ADV (also known as the McMurdo Dry Valleys) lie between the East Antarctic Ice Sheet (EAIS) and seasonally open water of the Ross Sea (Denton et al., 1993; Sugden et al., 1995a) (Fig. 2). Local relief is ∼ 2800 m. Most surfaces are generally free of ice and there are no vascular plants. Major east–west trending valleys, each ∼80 km long and up to 15 km wide, extend across the region.

A high-elevation bedrock threshold (∼2000 m) currently prevents significant influx of the EAIS into the ADV (western

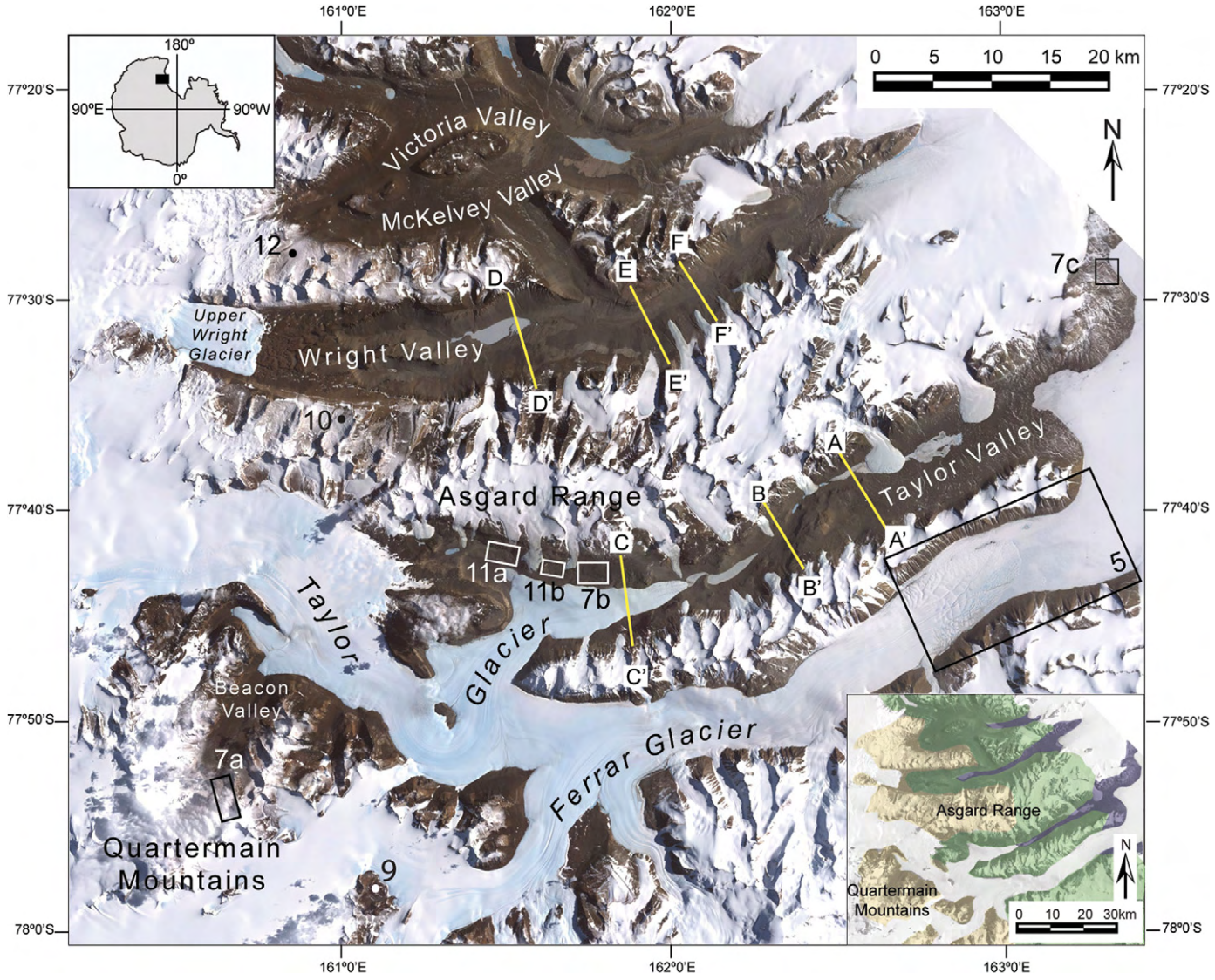

Fig. 2. Antarctic Dry Valleys: Location map showing major geographic features. Location of cross-valley profiles (Fig. 4) plotted as yellow lines; location of other figures in text shown as labeled boxes and dots. Upper left inset: Black square shows location of Dry Valleys within Antarctica. Lower right inset: Map showing general range for coastal thaw zone (CTZ; blue), inland mixed zone (IMZ; green), and stable upland zone (SUZ; yellow).

part of Fig. 2). Two small outlet glaciers, Taylor Glacier and Upper Wright Glacier, just pass over this threshold and terminate on land 75 to 50 km from the coast; only one outlet glacier reaches the coast (Ferrar Glacier) (Fig. 2). Alpine glaciers, nourished by local precipitation and wind-blown snow from the Polar Plateau, occur on elevated benches and on plateaus between the main valleys.

The local bedrock consists of a basement complex that includes pre-Cambrian to Paleozoic age granites and gneisses, most of which were produced and/or deformed during the Cambrian–Ordovician Ross Orogeny. These rocks crop out below ~800 m elevation near the coast and in the central portions of the ADV. Inland, exposed bedrock consists of generally flat-lying sedimentary rocks of the Beacon Supergroup (Devonian-to-Triassic age sandstones, siltstones, and conglomerates) and 200–300 m thick sills of Ferrar Dolerite (Jurassic age intrusives representing the break-up of Gondwana; Elliot and Fleming, 2004).

2.2. Dominant geomorphic processes

Katabatic winds, active-layer cryoturbation, and cold-based glaciation are the three fundamental processes that influence the morphology of the ADV.

2.2.1. Katabatic winds

Gravity-driven katabatic winds flow off the EAIS and gather speed as they pass through the ADV; winds commonly exceed 50 km/h (Schwerdtfeger, 1984; Marshall and Turner, 1997; Nylen et al., 2004). These winds entrain sand grains and scour bedrock landscapes (Lancaster, 2002; Malin, 1984, 1987; Selby, 1977). They also warm adiabatically as they descend the ice-sheet slope, resulting in slightly elevated air temperature excursions that are particularly apparent during winter months (Doran et al., 2002; Nylen et al., 2004; Fountain et al., 1999). The katabatic winds also transport significant snow from the Polar Plateau, some of which is deposited in the lee of topo-

graphic obstacles in the ADV. The fate of this snow—to melt or sublimate—is a critical factor in the development of most unconsolidated landforms.

2.2.2. Active-layer cryoturbation

A traditional active layer is defined as the surface horizon in permafrost regions that experiences seasonal temperature fluctuations above and below 0 °C (273 K) (Davis, 2001; Yershov, 1998). Its thickness depends primarily on atmospheric temperature, and secondarily on substrate heat conduction. We distinguish a "wet" active layer from a "dry" active layer on the basis of subsurface moisture content. A wet active layer contains visible ice and/or liquid water, whereas a dry active layer contains minimal soil moisture, generally <5% gravimetric water content (GWC). In coastal regions of the ADV, a wet-active layer up to ∼25 cm in thickness is common. In inland regions, dry active layers are the norm, and in some places they are only a few cm thick (Kowalewski et al., 2006).

2.2.3. Cold-based glaciers

All of the alpine glaciers in the ADV are presently cold-based. Unlike wet-based glaciers, which entrain debris by regelation and slide across bedrock surfaces, cold-based glaciers flow only by internal deformation; a rate for bedrock erosion beneath a typical cold-based alpine glacier in the ADV is calculated at $\sim 10^{-7}$ m/yr (Cuffey et al., 2000). Not only is this bedrock erosion rate several orders of magnitude less than that for typical wet-based alpine glaciers (Hallet et al., 1996; Spotila et al., 2004; Koppes and Hallet, 2006; Brook et al., 2006), it is also several orders of magnitude less than that for bedrock erosion arising from the impact of saltating sand grains in the ADV (Malin, 1984, 1987). Hence, rather than eroding underlying bedrock and/or unconsolidated debris, cold-based glaciers in the ADV tend to preserve underlying landscapes (e.g., Kleman and Hattestrand, 1999; Borgstrom, 1999; Fabel et al., 2002).

2.3. Microclimate variation

Observed and measured variations in weather patterns across the ADV show that the region is best divided into a series of microclimate zones (Marchant and Denton, 1996; Marchant and Head III, 2004). Slight changes in atmospheric temperature and soil-moisture, particularly along microclimate boundaries, are sufficient to produce major changes in equilibrium geomorphic processes and surface topography. As is the case for most cold-desert regions, the geomorphic impacts of minor variations in soil moisture and temperature are disproportionately large when compared to similar shifts in humid-temperate latitudes due to the crossing of geomorphic thresholds (Langbein and Schumm, 1958; Schumm, 1965; Schumm and Lichty, 1965).

On the basis of measured climate variation in the ADV (Table 1), we distinguish a coastal thaw zone (CTZ), an inland mixed zone (IMZ), and a stable upland zone (SUZ) (Fig. 2, inset). Alternative subdivisions are possible (e.g., Campbell and Claridge, 1969, 1987, 2006; Bockheim, 2002, 2003), but this three-fold microclimate classification captures the major trends in geomorphic processes and in landscape features across the region. At issue here is not the precise geographic boundary for each microclimate zone, but rather the identification of diagnostic equilibrium processes and geomorphic landforms within each zone. Details on the boundaries of each zone are presented in Marchant and Denton (1996) and are the focus of ongoing research.

2.3.1. Coastal thaw zone (CTZ)

Modern summertime air temperatures in the CTZ show a mean season-long temperature of ∼−5 °C (268 K), and a mean daily maximum of ∼−2 °C (271 K); relative humidity (RH) averages ∼64%; the rather high RH value is due to the prevalence of south-easterly winds, which carry moisture from the Ross Sea (Table 1). Due to large variations in surface albedo in the CTZ (which arise from the presence of numerous tills capped by different lithologies; Hall et al., 1993; Denton and Marchant, 2000), surface and subsurface ground temperatures vary considerably over relatively short horizontal distances of ∼10 m; in all places, however, subsurface soil temperatures in the CTZ rise well above 0 °C (273 K) (Table 1). Snowfall in the CTZ exceeds 80 mm of water equivalent per year (Schwerdtfeger, 1984); a large fraction of the snowfall melts and infiltrates near-surface soils. The GWC of most soils in the CTZ is thus >30% (Campbell et al., 1997a, 1997b).

2.3.2. Inland mixed zone (IMZ)

Alternating winds passing across the IMZ (westerly katabatic and easterly from the Ross Sea) produce variable RH in the IMZ, but the mean summertime RH is close to that of the coast, ∼67%. Summertime air temperatures show a mean of ∼−7 °C (266 K), with a mean daily maximum of ∼−4 °C (269 K) (Table 1). Snowfall is most probably less than that of the coastal thaw zone; the uncertainty lies in the unknown quantity of wind-blown snow from the Polar Plateau in this region. Apart from regions alongside ephemeral streams and isolated snow patches, near-surface soils contain <30% GWC (Campbell et al., 1997a, 1997b).

2.3.3. Stable upland zone (SUZ)

The low value of summertime RH for the SUZ, ∼41%, reflects the passage of dry, katabatic winds originating over the EAIS. Summertime air temperatures show a mean of ∼−10 °C (263 K), with a mean daily maximum of ∼−8 °C (265 K) (Table 1; Fig. 3 soil-temperature profile, SUZ). Precipitation is limited, but snow blown off the Polar Plateau may accumulate on small glaciers and feed perennial snow banks. Glaciers and snow banks lose mass by sublimation and the upper horizons of most soils contain <5% GWC (Campbell et al., 1997a).

2.4. The importance of salts and brines

These major microclimate zones, and the variations in geomorphic processes produced by differences in the presence and activity of water, are locally modified by soil salinity (e.g., Claridge and Campbell, 1968, 1977, 2005; Bockheim, 1997, 2002; Mahaney et al., 2001; Campbell and Claridge, 2006).

Table 1
General climate data for three microclimate zones in the Antarctic Dry Valleys

		Summer (annual)[a]		
		Stable upland zone[b]	Inland mixed zone[c]	Coastal thaw zone[d,e]
Atmospheric temperature	Mean (°C)	−10 (−22)	−7 (−18)	−5 (−20)
	Mean daily maximum	−8 (−18)	−4 (−14)	−2 (−15)
	Mean daily minimum	−12 (−25)	−10 (−21)	−7 (−24)
Soil temperature	Mean @ 0 cm depth	−5 (−22)	–	2 (−18)
	Mean @ 10 cm depth	−6 (−21)	–	1 (−17)
RH	Mean relative humidity (%)	41 (43)	67 (55)	64 (63)

Note. All Data from McMurdo LTER weather stations. Available at http://huey.colorado.edu/LTER/meteordata.html.
[a] Summer months: December, January, February; annual conditions shown in parentheses.
[b] Beacon Valley; 1176 m a.s.l., 74 km from coast.
[c] Howard Glacier; 472 m a.s.l., 16 km from coast.
[d] Explorers Cove; 26 m a.s.l., 4 km from coast.
[e] Soil data for coastal zone from near Lake Bonney; 60 m a.s.l., 25 km from coast.

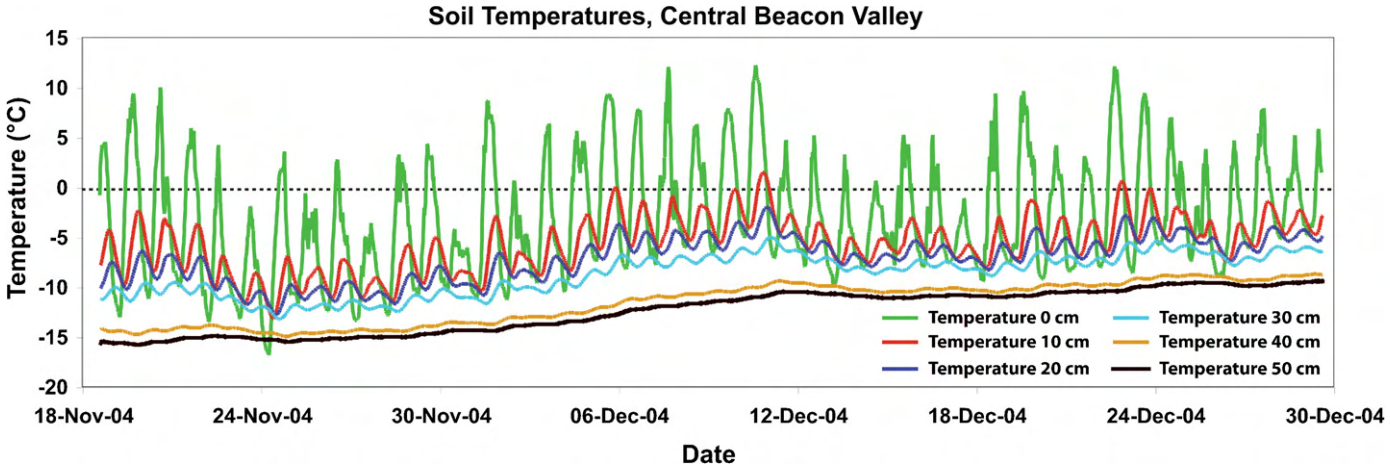

Fig. 3. Soil-temperature data for December, January, February 2004, Beacon Valley, stable upland zone (for details on data acquisition; see Kowalewski et al., 2006).

Several factors tend to enhance the importance of salts in the ADV (Bao and Marchant, 2006). Salts that are deposited by precipitation of snow generally become concentrated and remain near the site of deposition because of the hyper-arid environment, in which evaporation/sublimation exceeds precipitation. Salts released during weathering of rocks and soils accumulate continuously in the soils because of the paucity of liquid water. Local surface environments of salt occurrence include soil and rock coatings and efflorescences, interiors of weathering pits on rock surfaces (see below), cracks and joint surfaces in surface rocks, and accumulations underneath surface rocks deposited by saline solutions draining from rock surfaces and their evaporation/sublimation. Below the surface, salts are observed as widely distributed efflorescences, and as discrete horizons sometimes up to 15 cm in thickness (e.g., Campbell and Claridge, 2006; Bockheim, 1997).

Local areal and vertical concentrations of salts can induce variations in soil moisture. Surface liquid water has been observed at temperatures of $<-4\,^{\circ}C$ (269 K) in small damp, salty hollows (e.g., Campbell and Claridge, 2006), and in upper Wright Valley at Don Juan Pond, surface water remains below the solidus even at temperatures below −40 to −50 °C (223 to 233 K) (e.g., Marion, 1997; Takamatsu et al., 1998; Healy et al., 2006). Water cycled laterally through hyporheic zones (regions beneath and lateral to stream beds, where mixing of shallow groundwater and surface water occur) associated with ADV streams can mobilize salts, forming saline solutions, brines, and seeps, and can locally redeposit salts in soil horizons and on the surface (e.g., McKnight et al., 1999; Lyons et al., 2005; Harris et al., 2007). Vertical migration of water through soils can also result in mobilization and concentration of salts (e.g., Gibson et al., 1983; Dickinson and Rosen, 2003; Wentworth et al., 2005). These variations in vertical concentrations result in salt aggregations and layers that can be characterized by significant locally elevated water contents; such variations can produce local complexities in the geochemistry and thermal states of soils, and can influence geomorphic processes and resultant surface landforms.

Salt types include a very wide variety of crystalline phases of sodium, potassium and magnesium chlorides, nitrates and sulfates. Salts increase in importance and abundance with increasing soil age (e.g., Claridge and Campbell, 1977; Mahaney et al., 2001; Wentworth et al., 2005; Bao and Marchant, 2006; Campbell and Claridge, 2006). These same trends have important implications for the very ancient terrains and soils of the ultrastable, hyper-arid environment of Mars.

2.5. Geomorphic approach and methods

We now outline the geomorphic processes that give rise to the various equilibrium landforms in the three ADV microclimate zones (Marchant and Head III, 2004, 2005). Pertinent goals are to (1) document the spatial variability of periglacial landforms in the ADV; (2) identify palimpsest landscapes that reflect shifting microclimate conditions; (3) evaluate future landscape change that might arise from lateral displacement of climate zones due to atmospheric warming and; and (4) assess the application of similar geomorphic approaches towards understanding the magnitude and direction of recent and future climate change on Mars.

3. Landform analysis

Our analysis of landforms in the ADV is organized by microclimate zone and the size of mapped geomorphic features. Subdivisions include (1) macroscale landforms (>250 m in areal extent and/or those features incised in bedrock); (2) mesoscale landforms (unconsolidated deposits from 1 to ∼250 m in areal extent); and (3) microscale landforms (features ≪1 m in size). One benefit of this scale-dependent organization is that size-specific analyses can be performed for Mars, taking advantage of Viking and Odyssey-scale image data sets (macroscale), MOC and HiRise image data and MOLA altimetry data (mesoscale), and Viking Lander-Pathfinder-MER-scale image data (microscale).

3.1. Macroscale landforms: slope asymmetry, drainage-basin asymmetry, and gullies

3.1.1. Coastal thaw zone (CTZ)

Slopes in the CTZ display a classic asymmetry (Fig. 4). North-facing slopes that receive relatively high levels of incident solar radiation (e.g., Dana et al., 1998) are shallower (averaging ∼20°) than south-facing slopes (∼25°). Consistent with this marked valley-side asymmetry is a well-expressed drainage-basin asymmetry [drainage basin asymmetry is defined here as the ratio of the valley-half width (measured south of the valley "thalweg," i.e., south of the main valley axis) to the total valley width]. A symmetrical valley would show an asymmetry factor (AF) of ∼50, whereas an asymmetrical valley would show an AF above or below 50. An AF of ∼65 for the CTZ indicates preferred degradation along north-facing walls (Table 2). The size and spacing of gullies on valley walls in the CTZ also displays local variation with aspect. In lower Ferrar Valley, for example, gullies on the north-facing slopes appear deeper and spaced further apart than those on south-facing slopes (Fig. 5).

Melting occurs preferentially on north-facing slopes, with meltwater commonly percolating centimeters to tens of centimeters into soils. In places, this meltwater elevates soil-pore pressures sufficiently to induce downslope movement via solifluction, e.g., the slow flow of saturated materials. Elsewhere, evaporation of meltwater produces visible salts that coat rock surfaces and intervening soil. Variations in the size of these salt crystals, arising from expansion and contraction upon hydration–dehydration, permits rock breakdown, as salts pry away loosely bound crystals (Huinink et al., 2004). In the CTZ the most common salt species are chlorides and sulfates, reflecting proximity to the Ross Sea (Claridge and Campbell, 1977; Bao et al., 2000). Overall, the melting of snow and glaciers on north-facing slopes in the CTZ is a rather minor process of ice loss, only accounting for ∼10% of the total ablation; the majority of the loss takes place by sublimation (Chinn, 1980, 1981; Frezotti, 1997; Fountain et al., 1999). Nonetheless, the meltwater produced is sufficient in places to cut channels 3–5 m deep in loose debris. A saturated hyporheic zone, 1–2 m wide (Gooseff et al., 2003a), commonly fringes these channels during summer months and helps sustain a unique biota of several varieties of cold-adapted nematodes (Gooseff et al., 2003b; Nkem et al., 2006). Snow that falls on south-facing slopes in the CTZ tends to lose mass via sublimation and in a relative sense produces minimal geomorphic impact.

3.1.2. Inland mixed zone (IMZ)

The IMZ shows less valley-side asymmetry and less drainage basin asymmetry than the CTZ (Table 2; Fig. 2). In addition, gullies in the IMZ are relatively shallow, appear closely spaced, and show sharp, knife-like interfluves. Although the average air temperature in the IMZ is less than that of the CTZ (Table 1), minor snowmelt fringes most snowbanks: snow melts alongside rocks that are heated by solar radiation to temperatures >0 °C (273 K). In addition, snow may be blown from local snowbanks onto the surface of solar-heated rocks; in this way the distribution of meltwater is increased well beyond the immediate margins of snowbanks, although it is localized in the downwind direction. The total meltwater contributed by these processes is minor (and does not commonly support solifluction), but appears sufficient to maintain a shallow, discontinuous ice-cemented layer within the upper few centimeters of debris, and may also contribute to shallow subsurface meltwater flow in saline soils (e.g., Lyons et al., 2005; Harris et al., 2007). Perennial snowbanks and seasonal windblown snow trapped in lows (alcoves, channels, polygon troughs) may form significant sources for meltwater that can lead to gully formation in the IMZ (Head et al., 2007; Dickson et al., 2007a; Morgan et al., 2007; Levy et al., 2007).

3.1.3. Stable upland zone (SUZ)

Given that the current climate conditions in the SUZ (Table 1) prohibit significant meltwater, there is little evidence for ongoing, macroscale geomorphic change. Gullies, where present in this zone, are interpreted to be relict and inactive because overlying colluvium is commonly interbedded with near-surface ashfall dated to as much as 11 Ma (Marchant et al., 1993a, 1993b, 1996; Marchant and Denton, 1996). Unlike slopes in the CTZ and IMZ, which are incised in relatively uniform igneous and metamorphic rocks of the basement complex, the slopes of the SUZ are incised in sedimentary rocks and intervening sills of dolerite. Lithology thus plays a significant role in the macroscale geomorphology of the region: cliffs are formed in resistant sills of Ferrar Dolerite and Beacon Heights

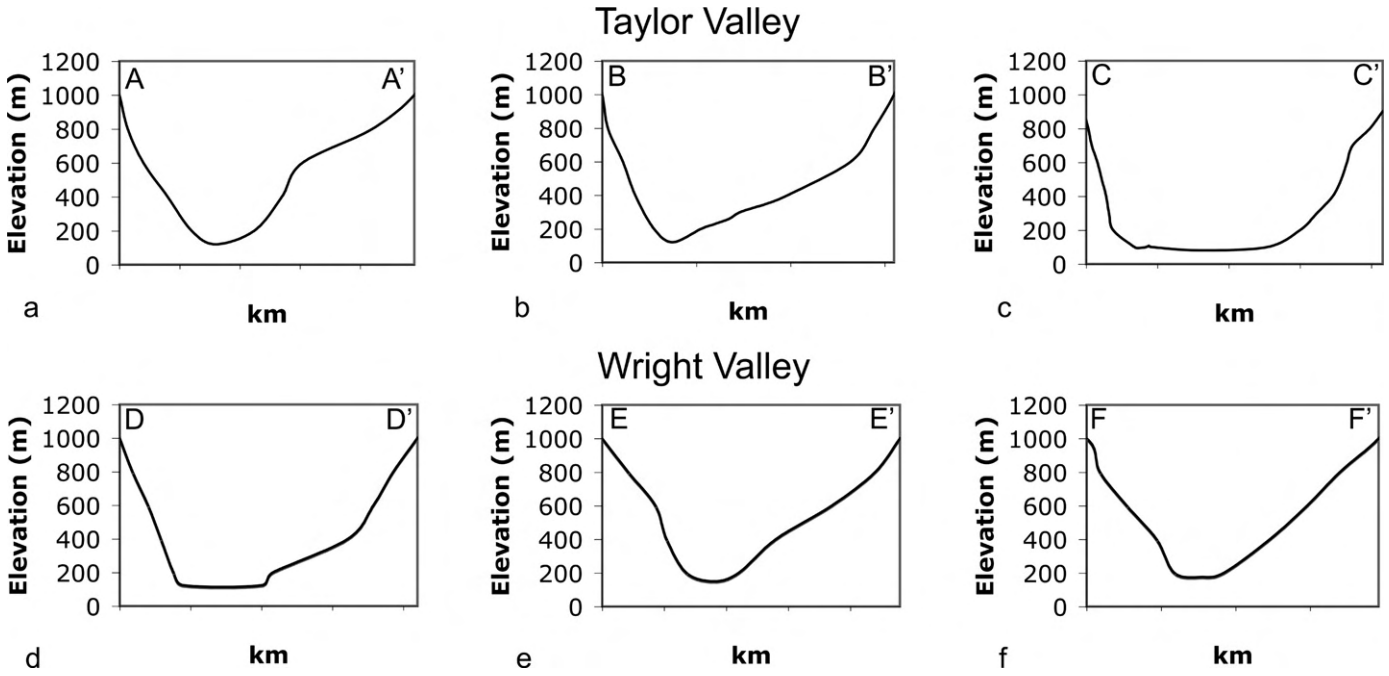

Fig. 4. Cross-valley profiles for the CTZ and IMZ; locations shown in Fig. 2. North-facing (equator-facing) slopes possess gentle slope angles.

Table 2
Distinctive geomorphic features, equilibrium landforms, and erosion rates for each microclimate zone

Process/feature	Stable upland zone	Inland mixed zone	Coastal thaw zone
Thermal contraction	Sublimation-type polygons	Sand-wedge and composite polygons	Ice-wedge polygons
Viscous flow	Debris-covered glaciers	Gelifluction lobes	Solifluction lobes
Average near-surface soil moisture[a]	<3%	⩽10%	⩾10%
Bedrock erosion rate[b]	~0.06–0.27 m/Ma	Mixed	~1 m/Ma
Drainage-basin asymmetry	N/A	52	65
Additional features/process	Pitted surface cobbles, salt-cemented duricrusts, puzzle rocks, and relict gullies	Desert pavements with wind-polished cobbles; immature, closely spaced gullies	Thermokarst, tafoni, low-gradient slopes with mature, low-density gullies

[a] Gravimetric water content, defined as weight of soil moisture/weight of dried soil. Data from Campbell et al. (1997a, 1997b).
[b] Data from Summerfield et al. (1999) and Brook et al. (1995).

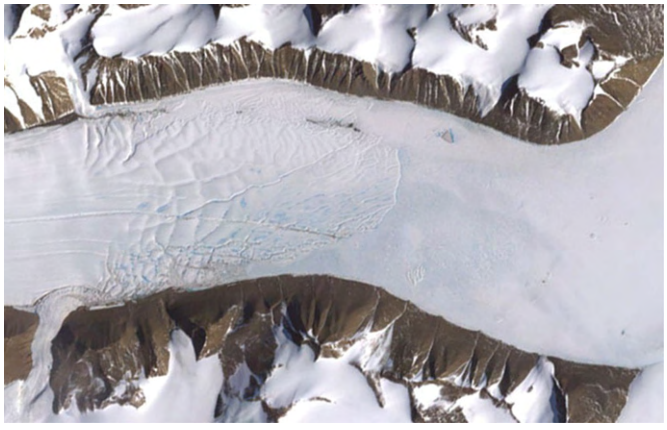

Fig. 5. Landsat satellite image of lower Ferrar Valley illustrating gully asymmetry on north-facing (bottom of image) and south-facing (top of image) slopes. See Fig. 2 for location and scale.

Orthoquartzite, whereas smooth, rectilinear slopes (~25°–30°) form on weakly cemented sandstones (Altar Mountain Sandstone, New Mountain Sandstone) (Sugden et al., 1995a; Selby, 1971a, 1974; Augustinus and Selby, 1990; Prentice et al., 1998).

Glaciers in the SUZ lose mass almost entirely by sublimation. The margins of some glaciers and perennial snow banks may experience melting where intense re-radiation off nearby surfaces elevates local temperatures (e.g., Dana et al., 1998; Fountain et al., 1999), and/or where a thin cover of wind-blown sands lowers the surface albedo and induces melting of underlying ice and snow (this phenomenon occurs in all microclimate zones, but it is the only mechanism for relatively significant melting in the SUZ). In all cases, however, the geomorphic impact of this meltwater in the SUZ is negligible. Although meltwater may moisten the upper 5–15 cm of soil, it does not induce solifluction, and evaporation removes most of this water within hours (Kowalewski et al., 2006).

3.1.4. Synthesis

The observed variation in valley-side asymmetry, drainage-basin asymmetry, and gully development in the ADV is plausibly related to spatial variations in the melting of snow and ice (and where appropriate, the distribution of resistant bedrock lithologies). The mature gully system of the CTZ most likely reflects (1) the preponderance of rock breakdown associated with snowmelt, freeze-thaw, and salt weathering, and (2) the downslope transport of these weathering products by water, solifluction, and wind. Given the direct correlations among the magnitude of observed surface melting and the size and spacing of gullies in the IMZ and CTZ, we suggest that gully maturation may be analogous to the development of rills to master rills observed in cohesive sands in humid temperate regions (Bocco, 1991). If so, mature gullies form at the expense of immature gullies by progressive capture, a process that requires significant meltwater and some component of lateral flow. As gullies grow, they are capable of trapping increasing amounts of wind-blown snow, which on melting enables cross grading (i.e., lateral flow on walls of newly formed gullies); the latter promotes the wide spacing of gullies. If the above sequence is correct, then the relatively high density and narrow morphology of gullies in the IMZ could reflect stagnation within the maturation sequence due to insufficient meltwater.

Among additional parameters that could be responsible for the observed variation in gully morphology is the *duration* of gully incision. We contend that time is not *the* most critical factor in differentiating gully morphology because many slopes in the IMZ (as well as in the SUZ) have been dated on the basis of $^{40}Ar/^{39}Ar$ analyses of overlying ashfall to $\geqslant 7$ Ma (Marchant and Denton, 1996). Given the time available for slope evolution in the IMZ, we postulate that gullies would have achieved mature forms if sufficient meltwater had been available (i.e., comparable to that now found in the modern CTZ). The extremely low levels of meltwater produced in the SUZ lead to a preponderance of inherited slopes that likely formed under wetter, and most likely warmer, climate conditions before the onset of cold-polar desert conditions (e.g., Sugden et al., 1995a, 1995b; Lewis et al., 2007).

3.2. Mesoscale landforms: contraction-crack polygons and viscous-flow features

3.2.1. Ice-wedge, sand-wedge, and sublimation-type polygons

Contraction-crack polygons form by thermal cracking of ice-rich permafrost and subsequent infilling of cracks with a variety of materials. In plan view, the vertical cracks intersect to form a variety of polygon shapes (Fig. 6). Cracking is favored in regions that experience abrupt seasonal cooling (Berg and Black, 1966; Black, 1973) and where near-surface materials are cohesive. Once initiated, various geomorphic processes operating in each microclimate zone yield different classes of contraction-crack polygons (Fig. 6).

3.2.1.1. Coastal thaw zone Ice-wedge polygons are widespread in the CTZ (Fig. 6). The seasonal influx of liquid water from wet active layers into open thermal-contraction cracks, along with subsequent growth of ice on freezing, leads to the development of downward-tapering ice wedges outlining raised-rim polygons (Berg and Black, 1966). Polygons in the CTZ average ~10–20 m in diameter. The maximum width of most ice wedges is ~2 m, considerably less than that for comparable ice-wedge polygons of Arctic regions (e.g., Mackay, 1977). The smaller size of ice wedges in the CTZ, relative to those of the Arctic, likely reflects the limited availability of liquid water in the CTZ, rather than the duration of ice-wedge growth.

3.2.1.2. Inland mixed zone Sand-wedge polygons and composite polygons are the dominant forms of contraction-crack polygons in the IMZ (Fig. 6). Sand-wedge polygons develop in a manner analogous to ice-wedge polygons except that contraction cracks fill with sand, rather than with ice (Péwé, 1959; Murton et al., 2000). Composite polygons show wedges that exhibit alternating lenses of ice and sand (Ghysels and Heyse, 2006).

The retention of open contraction cracks at the ground surface, and the availability of sands to fill these cracks are two key factors that determine the growth of sand-wedge polygons (Berg and Black, 1966; e.g., Marchant et al., 2002). Because cracks tend to be wider and remain open longer in soils with cohesive ice and/or salt-cemented horizons, sand-wedge polygons are most active near the margins (and downwind) of perennial snow banks that experience minor snowmelt. To a first order, growth rates of sand wedges appear correlated with the abundance of available sediment and with the presence of shallow ice and salt-cemented soil horizons (e.g., Marchant et al., 2002).

3.2.1.3. Stable upland zone A special type of sand-wedge polygon, a sublimation-type polygon, forms where sediment overlies buried, massive ice in the SUZ (Marchant et al., 2002; Marchant and Head III, 2003) (Fig. 6). The formation and evolution of sublimation-type polygons is tied to the thermal cracking and sublimation of underlying ice (Fig. 6). As cracks form in buried ice, the finest fraction of overlying debris (<2 cm) percolates down into the cracks. Material that is too large ($\gtrsim$2 cm) collects at the buried-ice surface. This process of passive sifting and removal of fine-grained material creates a zone of relatively coarse-grained debris at polygon margins (i.e., above contraction cracks). Due to the relatively high porosity and permeability of this debris, sublimation of the underlying ice is locally enhanced (Marchant et al., 2002). Ultimately, elevated rates of ice sublimation at polygon margins leads to the development of deep troughs, >2–3 m deep, that outline conical, sediment-covered mounds of buried ice (Fig. 6).

A negative feedback prevents runaway ice loss. As sublimation troughs deepen, they become preferred sites for collection of windblown snow. The downward flux of vapor and/or minor melt from the base of these snowbanks creates a thin layer of superposed ice that effectively seals the remaining ice from sublimation (Marchant et al., 2002; Kowalewski et al., 2006; Levy et al., 2006). Ultimately, cohesive plugs of ice-and-salt-cemented sands that form at the top of contraction cracks prevent further infiltration of overlying sediment and reduce the

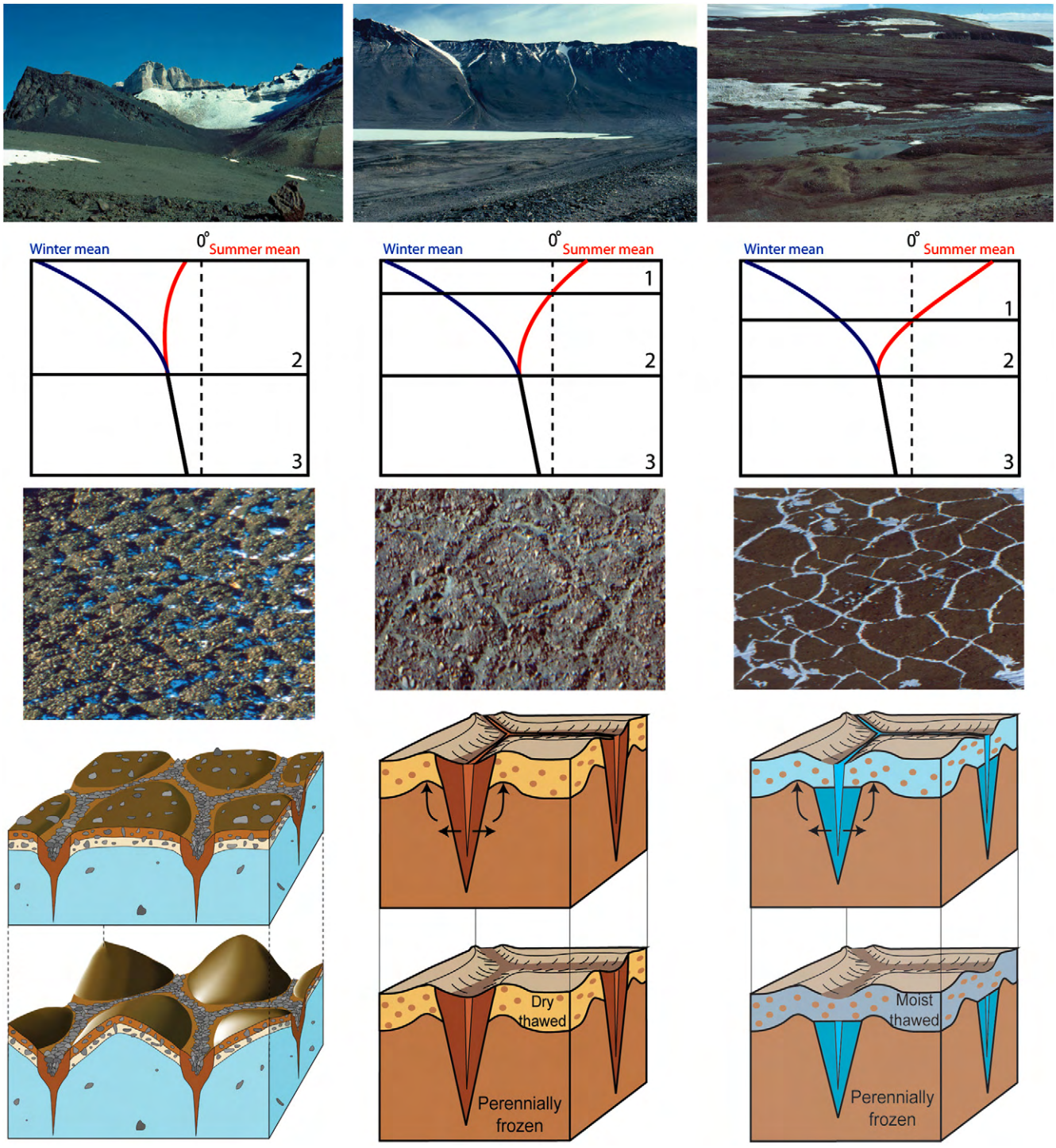

Fig. 6. Landscapes, near-surface thermal profiles, and polygons as a function of microclimate zones in the ADV. Top (row 1): photographs showing typical landscapes in each microclimate zone; left to right: stable upland zone (SUZ), inland mixed zone (IMZ), and coastal thaw zone (CTZ). Second (row 2): schematic showing vertical thermal profiles for each zone. Dashed line represents 0 °C (273 K) baseline; blue and red lines show winter-mean and summer-mean soil temperatures as a function of depth. Numbered soil "horizons" are defined on the basis of temperature profiles. Horizon 1 is a surface layer that experiences summer temperatures above 0 °C (273 K). In the case of the CTZ (right), soils are seasonally moist and thus seasonal oscillation about 0 °C (273 K) produces a classic active layer (see text for discussion). For the IMZ (center), soils are too dry to produce classic active-layer disturbance, even though summer soil temperatures rise above 0 °C (273 K). Horizon 1 is not present in the SUZ (left) because mean-summer soil temperatures fail to rise above 0 °C (273 K); this zone thus lacks a traditional active layer. Horizon 2 reflects the depth to which near-surface materials experience seasonal temperature change. Temperature oscillation results in material expansion/contraction and is responsible for the initiation of polygonal terrain; see text. Horizon 3 reflects a zone of uniform temperature increase with depth; the base of the permafrost would occur where temperatures exceed 0 °C. Third (row 3): left, oblique-aerial view of sublimation-type polygons in SUZ; field of view (FOV) is ∼100 m; center, oblique-aerial view of sand-wedge polygons in IMZ; FOV is ∼50 m; right, oblique-aerial view of ice-wedge polygons in CTZ; FOV is ∼75 m. Bottom (row 4): Block diagrams illustrating the development of sublimation-type polygons (left), sand-wedge polygons (center), and ice-wedge polygons (right). Blue color indicates ice; see text for explanation.

potential for compressive stress and ice deformation at depth (e.g., Marchant et al., 2002).

3.2.1.4. Synthesis Contraction-crack polygons of different types are strong morphological indicators of conditions prevailing in a particular microclimate zone. As shown in Fig. 6 morphologic variation arises from the abundance of liquid water in near-surface soils. Ice-wedge polygons of the CTZ require wet active layers. Sand-wedge polygons of the IMZ signal soil moisture sufficient to induce widespread thermal cracking but insufficient to fill cracks with ice. Sublimation polygons of the SUZ indicate the location of near-surface buried ice in regions without wet active layers (Fig. 6).

All three types of contraction-crack polygons provide information on the distribution and concentration of subsurface ice. For ice-wedge polygons, the highest concentration of ice occurs in polygon troughs. For sand-wedge polygons, the ice commonly occurs distributed evenly as pore ice in near-surface sediment (generally $<30\%$ ice by volume). For sublimation polygons, excess ice (ice exceeding available pore space and with values $\gg 30\%$ ice by volume) generally occurs $\leqslant 1$ m from the ground surface (Marchant et al., 2002). In sharp contrast with ice-wedge polygons, the lowest concentrations of ice in sublimation polygons are found in the troughs.

3.2.2. Solifluction lobes, gelifluction lobes, and debris-covered glaciers

The terms solifluction and gelifluction are sometimes used interchangeably (e.g., Matsuoka, 2001), just as are the terms rock glacier and debris-covered glacier (e.g., Whalley and Palmer, 1998; Giardino et al., 1987). The confusion exists because these features form by a continuum of processes that are all related to the slow movement of hillslope materials. Previously, we defined solifluction as the slow flow of saturated materials, with or without the presence of nearby ice. Our usage of the term gelifluction differs in that in addition to saturated flow, gelifluction lobes advance by internal deformation (and perhaps slippage along) buried-ice lenses and/or pore ice. Although rock-glaciers and debris-covered glaciers both flow by creep deformation of internal ice, we distinguish rock-glaciers as having ice of secondary origin (i.e., not glacial), including ice that forms by the freezing of pore water. Debris-covered glaciers are those viscous-flow features that have a demonstrable core of buried glacier ice.

3.2.2.1. Coastal thaw zone Solifluction is the dominant form of viscous flow in the CTZ (Fig. 7c). Solifluction lobes are commonly 20–30 cm thick and occur en echelon on slopes as low as 5° (Nichols, 1968; Selby, 1971b). In places, soil pore-pressures, and thus rates of solifluction, are elevated where meltwater is unable to penetrate impermeable subsurface horizons, such as a local ice table. As the summer season progresses, shallow ice commonly melts and gives rise to typical, though relatively small, thermorkarst features (shallow depressions, planar slides). The wetting of near-surface debris also commonly produces saline brines (Campbell and Claridge, 1987; Bockheim, 1997; Campbell et al., 1998; Lyons et al., 2005). These brines remain in a liquid state, facilitating solifluction even as temperatures drop below the freezing point for pure water.

3.2.2.2. Inland mixed zone Many slopes in the IMZ show well-developed gelifluction lobes (Fig. 7b). These lobes flow by downslope movement of saturated debris and internal deformation of pore ice and/or ice lenses at depth. Gelifluction lobes may emanate from steep slopes, though this is not required, and commonly display a series of stacked surface lobes and/or nested ridges that terminate along coarse-grained, lobate fronts. Gelifluction lobes may exceed the angle of repose and show a relief of 3–5 m.

3.2.2.3. Stable upland zone Debris-covered glaciers are the most common form of viscous-flow features in the SUZ. Most debris-covered glaciers occur downwind from dolerite-capped cliffs and originate through accumulation of rockfall debris on alpine glaciers (Fig. 7a). Debris that falls onto glacier accumulation zones may move englacially before rising toward the surface as overlying ice sublimes. The stratigraphic contact between ice and overlying debris is smooth and dry, and mimics the modern ground surface (Marchant et al., 2002). The rate of ice sublimation is dependent on the thickness, porosity, and permeability of overlying debris (sublimation till) (Marchant et al., 2002; Schaefer et al., 2000; Kowalewski et al., 2006; Levy et al., 2006).

Most debris-covered glaciers in the SUZ show concentric surface ridges characteristic of subsurface ice flow (Fig. 7a; Levy et al., 2006). Horizontal ice-surface velocities are generally $\lesssim 40$ mm per year (Rignot et al., 2002), which is considerably less than that for comparably sized gelifluction lobes in the IMZ (~ 3 cm per year; Hassinger and Mayewski, 1983). One explanation for this difference in flow rate involves ice temperature and its control on ice rheology: all other things being equal, warm ice flows faster than cold ice (Patterson, 2001). Ice in most debris-covered glaciers in the SUZ is $\leqslant -25\,^{\circ}\mathrm{C}$ (248 K) (Kowalewski et al., 2006, and unpublished data), whereas that in gelifluction lobes in the IMZ may approach $\sim -18\,^{\circ}\mathrm{C}$. Beheaded debris-covered glaciers (those where topographic hollows exist in former snow-and-ice accumulation areas) occur in many places in the SUZ. These hollows may reflect a change in climate leading to a marked reduction in ice accumulation, or alternatively, may reflect a reduction in rockfall debris, leading to greater expanses of exposed glacier ice, rapid sublimation, and ice-surface lowering (e.g., Marchant and Head III, 2004). Sugden et al. (1995b) argue that some stagnant glacier ice in the SUZ has survived for least 8.1 Ma beneath a dry, debris layer ~ 50 cm thick (see also Kowalewski et al., 2006).

3.2.2.4. Synthesis The style of viscous-flow feature developed in each microclimate zone depends on the availability and state of water. If water saturates near-surface soils, as it does in the CTZ (aided in places by the freezing point depression associated with brines), then flow is best accommodated by solifluction. If water freezes at depth to form excess pore ice, then gelifluction lobes may dominate, as they do in the IMZ. In

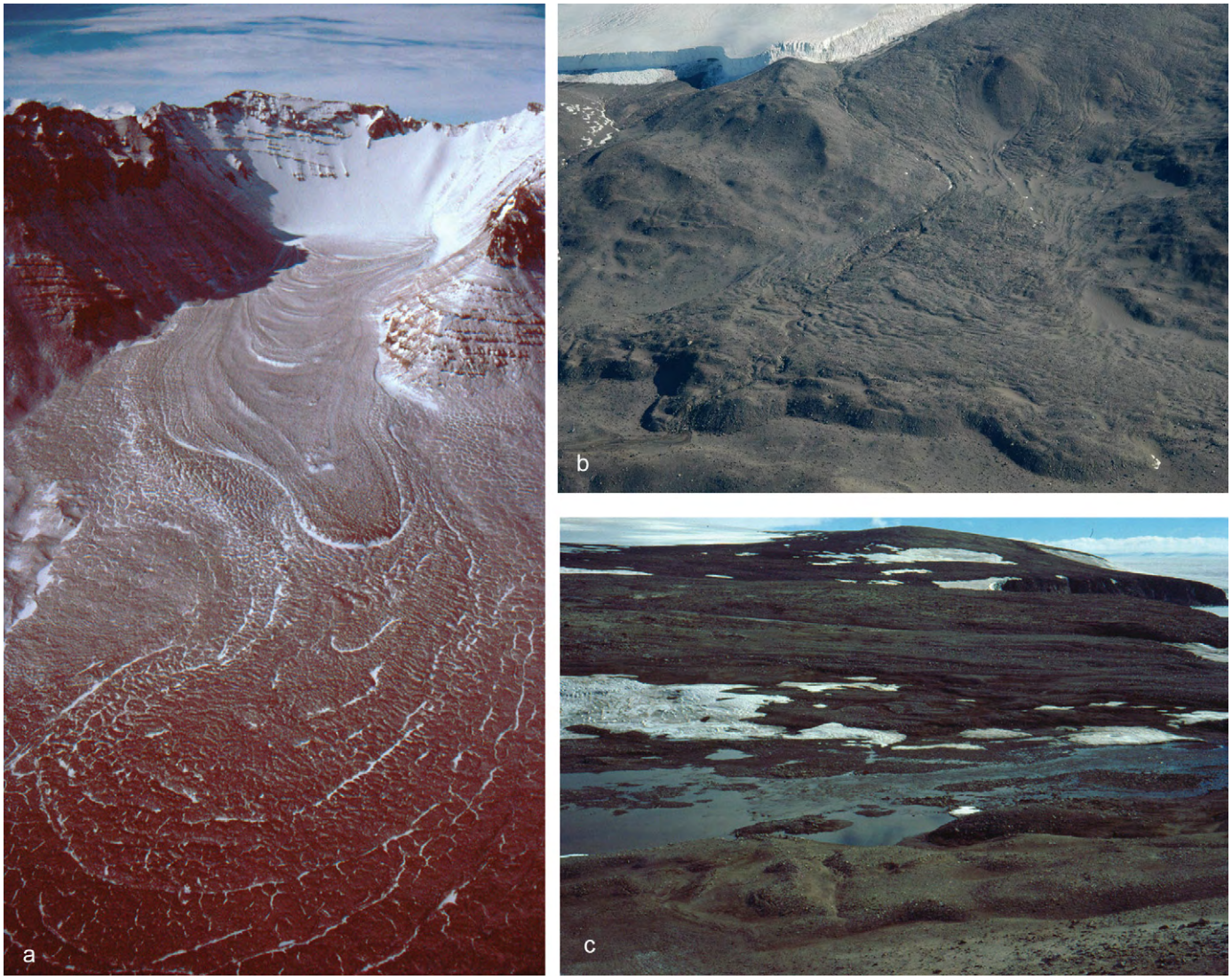

Fig. 7. Styles of viscous flow. (a) Debris-covered glacier ice in the SUZ (Mullins glacier). The small alpine glacier at the valley head transitions into a debris-covered glacier that extends for ∼3.5 + km. The debris originates from rockfall onto the alpine glacier. Most debris travels englacially before rising to the surface as overlying ice sublimes. The till thickens from about 10 cm in the upper portion of the valley, to ∼50 cm near the base of the photograph; field of view at base of the photograph is ∼0.75 km. (b) Gelifluction lobe in IMZ, central Taylor Valley. The steep front is up to 5 m high. In places, ice occurs ∼1 m below the ground surface in the upper half of this lobe; field of view at the base of the photograph is ∼1 km. (c) Solifluction lobes/terraces occur just beyond the small meltwater pond and snow banks in the central portion of this photograph. The lobes show 20 to 25 cm relief and are stacked en echelon. Linear features in foreground are small ice-wedge polygons; field of view at base of the photograph is ∼4 m. See Fig. 2 for specific locations.

the SUZ, where there is insufficient meltwater to promote solifluction and/or produce excess subsurface ice, debris-covered glaciers dominate. As a check on alternate source mechanisms for subsurface ice in the SUZ, Kowalewski et al. (2006) showed that the downward flux of vapor into soils is currently incapable of producing requisite pore-ice volumes that would sustain viscous flow.

3.3. Microscale topography and rock weathering: tafoni, weathering pits, desert pavements, and duricrusts

3.3.1. Coastal thaw zone

Most rocks at the surface in the CTZ and other zones show salt encrustations (Nichols, 1968; Campbell and Claridge, 1987; Gibson et al., 1983; Hall, 1991) (Fig. 8). These salts are produced by evaporation of near-surface brines and saline meltwater. The growth and expansion of salts pry loose mineral grains, particularly on coarse-grained rocks, and lead to the development of widespread grus (loose collections of mineral grains). Some salt-coated rocks are weathered flat to the soil surface (Beyer et al., 1999); traces of these former upstanding boulders appear as tails of grus, elongated in the downwind direction. Salt weathering in the CTZ also leads to the development of tafoni through cavernous weathering of coarse-grained rocks (Conca and Astor, 1987). Typical salt species in the CTZ include gypsum ($CaSO_4{\cdot}2H_2O$), halite (NaCl), mirabilite ($Na_2SO_4{\cdot}10H_2O$), and nitratine ($NaNO_3$). As measured over 10 m baselines, the long-term effect of salt weathering in the CTZ is to smooth bedrock slopes. Observations of slopes at

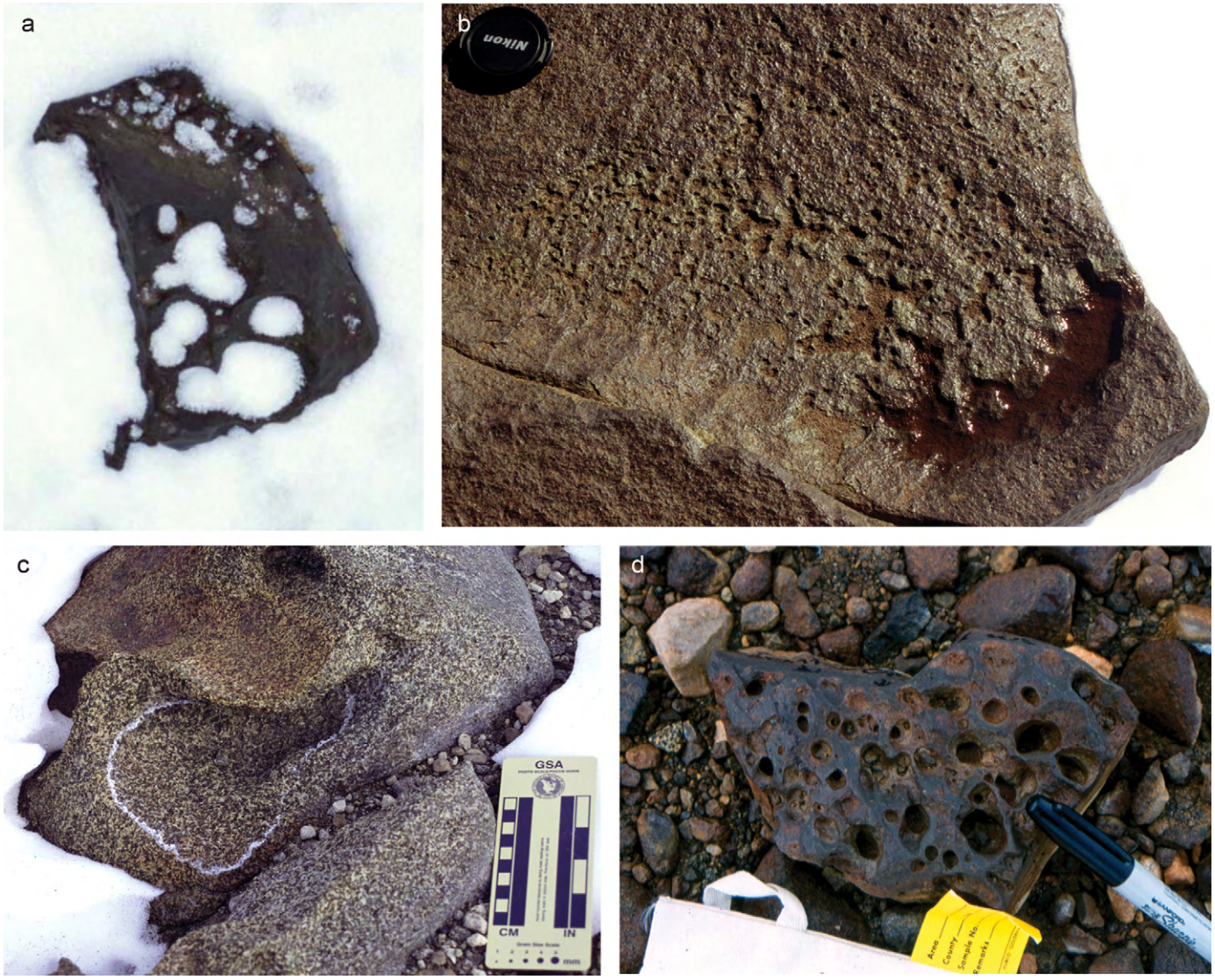

Fig. 8. Modification of rock-surface textures in the ADV by salt weathering. (a) Snow collects in lows and pits in low-albedo dolerite in the SUZ; the largest snow-filled pit is ∼1.5 cm in diameter, (b) Preferential heating of the surface of low-albedo dolerite rocks in the SUZ causes snow in the pits to melt; subsequent evaporation of snowmelt creates brines that ultimately form salt-encrusted pits. [The surface slope of the rock in panel (b) dips to the lower right corner, where melt water accumulates.] The maximum meltwater level in one pit is shown in (c) as a white (salt-encrusted) line (e.g., "bathtub ring"); this relatively coarse-grained dolerite shows a greater susceptibility to salt weathering than do the relatively fine-grained dolerite rocks (with crystals <1 to 2 mm in size) shown in (a), (b), and (d). Ultimately, snowmelt, evaporation, and crystal growth (including hydration/dehydration cycles) processes produce deep pits (d) that for fine-grained dolerite rocks tend to increase in width and depth linearly with age (see Fig. 9). Note the rill-like forms in (b); these are produced as brines repeatedly overfill small pits and trickle downslope. See text for details.

sub-meter scales, however, show considerable relief (Conca and Astor, 1987).

3.3.2. Inland mixed zone

The climate conditions of the IMZ foster the development of widespread desert pavements, with wind-faceted cobbles (ventifacts) and intervening lags of coarse-grained sand and gravel. In regions with fine-grained extrusive rocks (best suited for developing wind-polished facets; Selby, 1977), the spacing of ventifacts varies approximately with soil age. Surfaces with interlocking ventifacts and little intervening sand are generally older than are sandy surfaces with widely spaced ventifacts.

3.3.3. Stable upland zone

Because rocks in the SUZ are not subjected to episodes of burial and exposure, as commonly occurs in areas with traditional, wet active layers (e.g., Hallet and Waddington, 1991), rock surface textures are almost exclusively a function of wind erosion and salt weathering. Given the very dry conditions of the SUZ, salt weathering proceeds at an extremely slow pace. Rates of surface erosion in the SUZ that are based on analyses of in situ produced cosmogenic nuclides in boulders are as low as ∼6 cm/Ma, the lowest measured on Earth (Summerfield et al., 1998, 1999; Brook et al., 1995; Margerison et al., 2005; Staiger et al., 2006) (Table 2).

Micro-relief on rock surfaces is initiated by minor snowmelt that forms on solar-heated rocks (Figs. 8a and 8b). This melt-

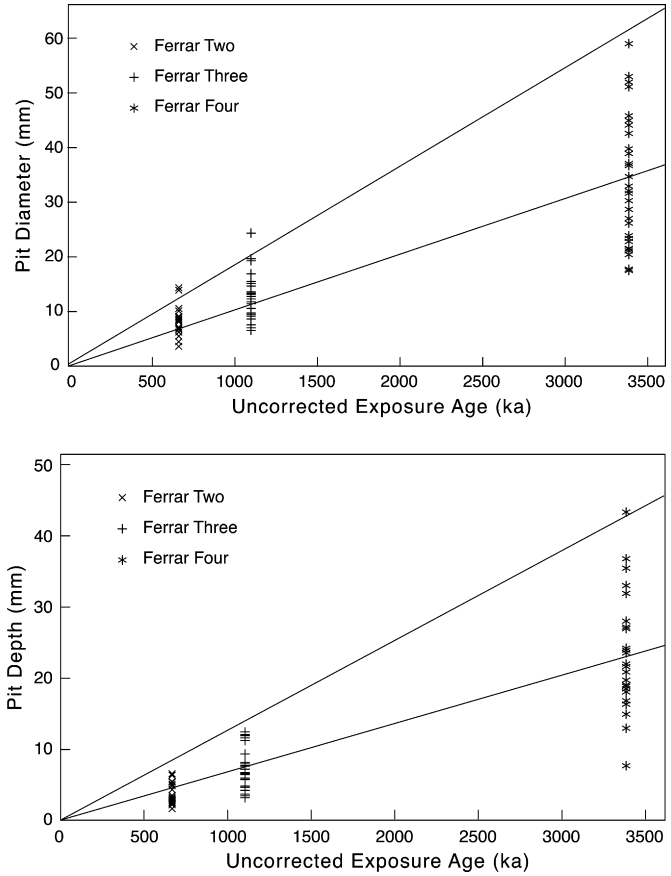

Fig. 9. The maximum diameter and depth of weathering pits on surface cobbles from dated moraines in the SUZ [see Fig. 2 for location and Staiger et al. (2006) for details on cosmogenic dating]. In each panel, the lower trendline was determined from measuring the mean value for pit size on selected rocks; the upper trendline highlights maximum values. Using mean values, Staiger et al. (2006) concluded that the mean width and depth of the largest surface pits on boulders from dated moraines increases by ∼10 and ∼6.7 mm/Ma, respectively [adapted from Staiger et al. (2006)].

water tends to occupy shallow surface depressions, which originally may have formed by wind scour on exposed rock surfaces (Selby, 1977). Repeated cycles of melting and concentration of ions through water evaporation in depressions are sufficient to produce visible salt encrustations (Fig. 8c). Microfracturing and undercutting of rock minerals by the growth and hydration of these salts creates pits that, through positive feedback, attract more snow, producing more salts and ever deeper and wider pits (Allen and Conca, 1991; Parsons et al., 2005; Staiger et al., 2006) (Fig. 8d). This process can produce a network of pits and micro-rills on the surface of rocks in the SUZ (Figs. 8b and 8d). Micro-rills form where rock surfaces are inclined such that saline meltwater spills out from pits and flows down the rock surface (Fig. 8b). As shown in Fig. 9, the average depth and width of weathering pits at one locality in the SUZ shows a linear increase with exposure age (Staiger et al., 2006). The salts in the SUZ are most commonly enriched in nitrates, reflecting derivation from snow blown off the ice-sheet margin (Claridge and Campbell, 1977; Bao and Marchant, 2006).

Puzzle rocks, those rocks that are fringed with thermally cleaved and spalled fragments, are also common in the SUZ (Fig. 10). For rocks composed of low albedo Ferrar Dolerite (∼0.07; Campbell et al., 1997b), the transition from solid boulders to partially disintegrated puzzle rocks in the SUZ likely requires 3 to 5 Ma (Marchant et al., 1993a; Staiger et al., 2006).

Infiltration of snowmelt into the upper few centimeters of silty soils in the SUZ helps create a fragile, salt-cemented duricrust. This fragile crust, held together by crystals that bind detrital grains, is susceptible to breakdown upon wetting. Wetted crusts may yield saline solutions that locally enhance downslope movement of near-surface soil–water mixtures (millimeter-to-centimeter-scale thickness). On the other hand, in the absence of surface water, as is commonly the case in the SUZ, the salts are enduring and tend to retard downslope movement and aeolian deflation. Additionally, owing to their chemical properties and physical ability to reduce near-surface porosity and permeability, salts in duricrusts may slow the flux of water vapor into and out of underlying soil (Marchant et al., 2002; Kowalewski et al., 2006).

3.3.4. Synthesis

The relatively wet climate conditions of the CTZ foster the development of widespread near-surface brines. Successive hydration and dehydration cycles lead to the formation of multiple salt species and relatively rapid rates of salt weathering. In the CTZ, these rates of rock disintegration appear to outpace the development of well-formed ventifacts and small, rock-weathering pits on most rock surfaces. The rate of degradation via salt weathering decreases inland, with measured rates for bedrock erosion in the SUZ being an order of magnitude lower than that measured near the coast (Summerfield et al., 1999). The effects of salt weathering are, however, visible in the SUZ as thin duricrusts and pitted-rock surfaces; well-formed pits appear only on rocks in the SUZ that have been exposed at the ground surface for >1-to-2 Ma (Parsons et al., 2005; Staiger et al., 2006). Duricrusts tend to be most extensive where wind blown snow commonly melts on the surface of solar heated rocks. This meltwater may infiltrate the upper few centimeters of soil, evaporate, and over time leave behind appreciable salts (e.g., Claridge and Campbell, 1977; Bockheim, 1997; Bao and Marchant, 2006). In binding adjacent sand grains, the salt mixture creates a thin duricrust from 1 to 2 cm thick. A simple but important point to emphasize is that surface and near-surface brines in the ADV may remain in a liquid state at temperatures <0 °C. In extreme situations, such as the case for Don Juan Pond, upper Wright Valley, surface water remains below the solidus even as temperatures drop below −40 to −50 °C (e.g., Marion, 1997; Takamatsu et al., 1998; Healy et al., 2006). In addition to effecting geomorphic change, such a situation could impact microbial activity (Siegel et al., 1979; Torii et al., 1989).

4. Equilibrium landforms

The key landforms that are diagnostic of individual microclimate zones in the ADV are summarized in Table 2. Because

Fig. 10. In situ breakdown of rocks from thermal cycling to produce "puzzle rocks." (a)–(d) show rocks in progressive stages of breakdown. Ultimately, single, coherent boulders (a) are transformed into multiple pieces (d). The pieces, like puzzles, can be reassembled; material is conserved and the pieces fit together without gaps. Smallest increments on scale bars are 1 cm.

these landforms are produced by specific geomorphic processes endemic to, and in balance with, local microclimate conditions (e.g., Fig. 1), we term these features equilibrium landforms.

Our assemblage of CTZ equilibrium landforms includes tafoni, solifluction lobes, thermokarst, ice-wedge polygons, and low-gradient slopes with mature, low-density gullies. Equilibrium landforms of the IMZ include gelifluction lobes, sand-wedge and composite polygons, desert pavements with wind-polished cobbles, and immature, closely spaced gullies. Finally, equilibrium landforms that best characterize the SUZ include sublimation polygons, debris-covered glaciers, pitted surface cobbles, salt-cemented duricrusts, and puzzle rocks.

5. Geomorphic evidence for climate change

Changes in the spatial distribution of equilibrium landforms over time, or the presence of relict equilibrium landforms, provide a morphological basis for interpreting past and on-going climate change. For example, a slight climatic warming might be registered as a landward shift of the CTZ at the expense of the IMZ (e.g., Marchant and Denton, 1996). Such a shift would likely increase the area of active-layer cryoturbation; wind-blown snow in gullies of the IMZ might undergo greater melting, promote solifluction and salt weathering, and possibly lead to the development of wide, low-density gullies with rounded interfluves such as those that today occur in the CTZ. In addition, composite and sand-wedge polygons of the IMZ would likely give way to ice-wedge polygons, and soils would show an overall increase in moisture content.

For larger climate shifts, evidence for traditional active layer cryoturbation might extend well inland into the SUZ. This could manifest as (1) the development of solifluction lobes and shallow active-layer detachment slides (Swanger and Marchant, 2007); (2) an inland migration of gelifluction lobes at the expense of debris-covered glaciers; (3) the growth and evolution of active gullies; (4) the introduction of extensive ice-wedge polygons; and (5) significant melting of buried ice leading to widespread thermokarst.

Detailed geomorphic inspection of the IMZ does in fact reveal geomorphic evidence for climatic warming. Although the majority of landforms appear in equilibrium with the local environment, some gelifluction lobes in the IMZ show evidence for considerable stream dissection, with channels bisecting lobes and producing locally extensive fans of stratified debris (Fig. 11). Given the magnitude of stream dissection, it is unlikely that these gelifluction lobes could have sustained this level of incision for >1 Ma, the likely age of sediment in some of these lobes (Hartman, 1998). Rather, we argue that these lobes are no longer in equilibrium with current microclimate conditions, and the data may be a harbinger of local climate warming in the ADV. The stream dissection that crosses these lobes occurs over a range of elevations and slope gradients, and so does not appear related to potential insolation changes that might arise as lobes descend to lower elevations along valley walls. We argue that the gelifluction lobes and superposed channels reflect a palimpsest landscape, showing the migration of dominant geomorphic processes of the CTZ to the IMZ. This conclusion is consistent with observations for rising lake levels in the ADV since 1900 (Chinn, 1993; Priscu, 1998, and references therein; see also Lyons et al., 1997).

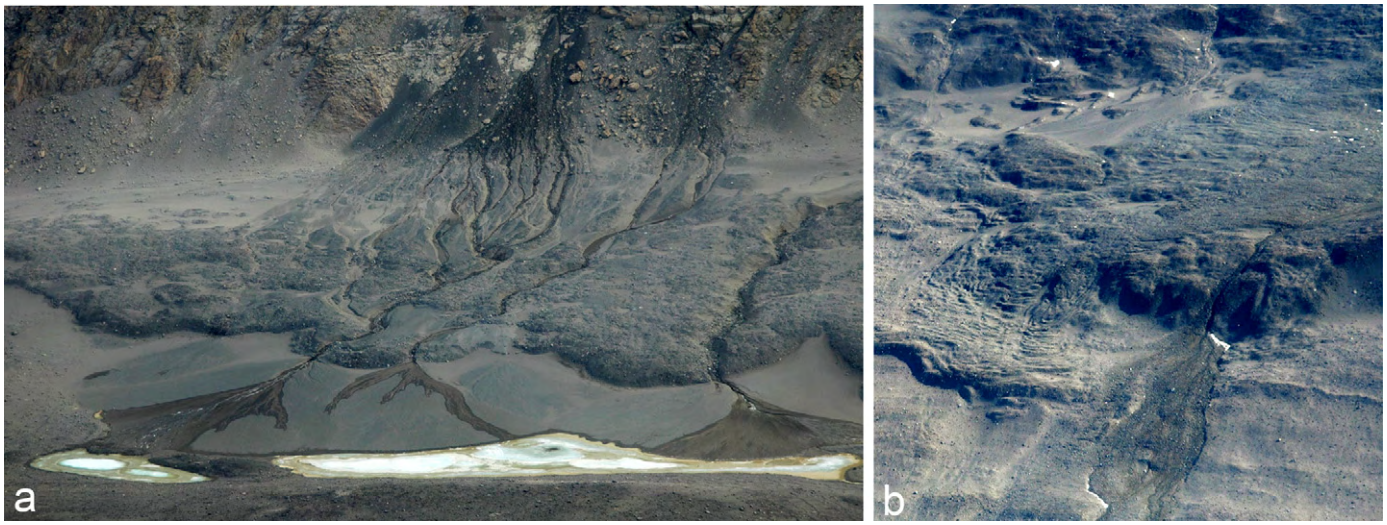

Fig. 11. Modern stream dissection of gelifluction lobes in the IMZ (see Fig. 2 for locations). Wind-blown sands (tan) cover a portion of the upper part of each lobe. (a) Meltwater channels derived from snowmelt higher up on the valley wall (snow banks not shown) cut up to 5 m into prominent lobes. Buried ice is exposed in places along channel walls. The channels feed large fans that spread out just beyond lobe fronts. Excess water fills saline ponds beyond the fans. The darker colors on the fans show places where meltwater is flowing in channels and where surrounding sands are moistened and/or saturated (e.g., hyporheic zones). The noted dissection may be a harbinger of climate warming in the Dry Valleys (see text). The photograph was taken on December 12, 2004; field of view at base is ∼0.65 km. (b) A stream cuts through a gelifluction lobe in central Taylor Valley. The stream, which has incised a deep notch along the front of one lobe, spreads out to form a braided channel network. Incision by this braided network has eroded a portion of a prominent lobe to the west (left) and removed a portion of a lateral moraine from Taylor Glacier to the east (right). Photograph taken on January 10, 1998; field of view at base is ∼0.45 km.

Is the warming apparent everywhere? The presence of ancient, in situ ashfall on slopes of the SUZ and in cracks in polygons there (Fig. 12) indicates that the relatively warm and wet microclimate conditions of the CTZ, which foster active layer cryoturbation and widespread solifluction, have not advanced into the SUZ for at least ∼13 Ma (Marchant et al., 1996; Marchant and Denton, 1996). The geomorphic stability of the SUZ likely arises from the lasting presence of a robust polar East Antarctic Ice Sheet (without extensive surface melting zones; Marchant and Denton, 1996). East–west thermal gradients across the ADV may have steepened during relatively warm periods (i.e., the middle Pliocene), but climate conditions in the SUZ have most probably remained little modified over the last ∼13 Ma (Staiger et al., 2006, and references therein; Lewis et al., 2007; Beyer et al., 1999).

The relative geomorphic and climate stability for the entire ADV is in stark contrast with measured, large-scale changes in climate and landscapes that have occurred in Arctic regions throughout the Pliocene and Quaternary Periods (for example, Baffin Island; Miller et al., 2005; Kleman et al., 2001). Consequently most macroscale (and perhaps mesoscale) landforms in the Arctic reflect the culmination of alternating geomorphic processes operating under a variety of climates (Bradley, 1999). This last point emphasizes the unique aspect of the ADV, its long-term climate stability, and makes them an ideal terrestrial analog for Mars. Moreover, the specific equilibrium landforms identified for the ADV formed under climate conditions comparable to those described for Mars over geologic time (Fig. 1) (Baker, 2001; Kreslavsky et al., 2007).

6. Application of Antarctic Dry Valley microclimate concepts to Mars, its present climate, and to past climate change

6.1. Introduction

Our geomorphic assessment of the Dry Valleys region emphasizes (1) the recognition of three microclimate zones, (2) the documentation of equilibrium landforms at various scales within each zone, and (3) the record of climate change as provided by the spatial variation of equilibrium landforms and microclimate zones over time. Given that the overall climate of the Dry Valleys is among the most Mars-like available for study on Earth (e.g., Anderson et al., 1972; Gibson et al., 1983; Mahaney et al., 2001; Baker, 2001; Wentworth et al., 2005; Fig. 1), we now focus our attention on documenting the potential for similar types of geomorphic investigations of cold-desert equilibrium landforms and "microclimate zones" on Mars. Just as in the Dry Valleys, we emphasize the potential for interpreting recent climate change on Mars in terms of the lateral displacement of microclimate zones and equilibrium landforms. Our discussion parallels that for the Dry Valleys in that we first outline current climate conditions on Mars and then document landforms at macro-, meso-, and micro-scales that appear in equilibrium with latitude-dependent climate zones (Head et al., 2003). We emphasize that although the spatial scale for broad climate zones on Mars (latitude dependent) is vastly greater than that for the Dry Valleys microclimate zones, many of the cold-desert landforms and the variability of specific landform types are remarkably similar for both planets. The zones in the Dry Valleys are condensed due to the steep thermal gradients that exist in the ∼100 km from sea level to

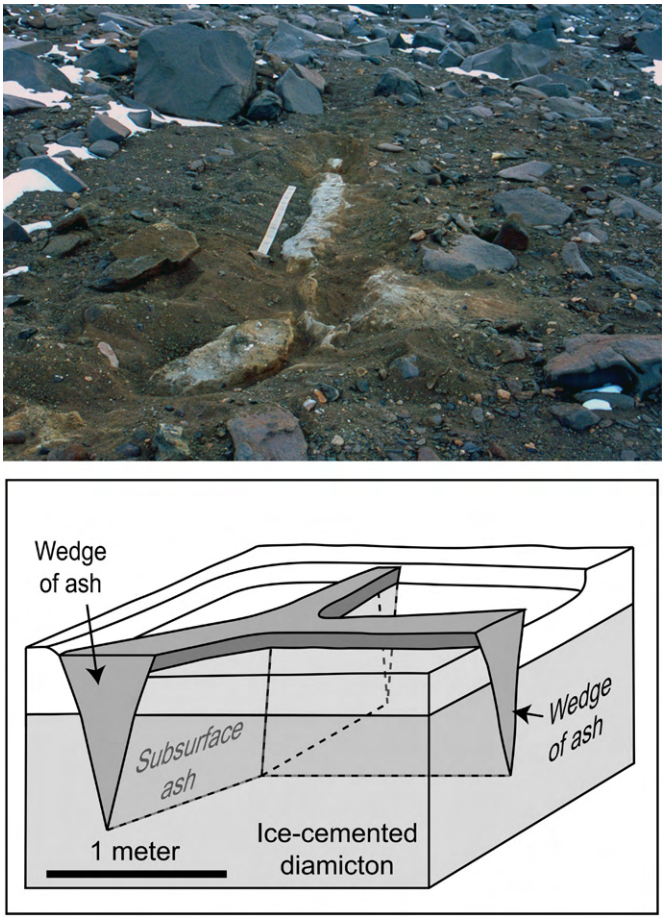

Fig. 12. In situ ashfall in association with relict sand-wedge polygons. The photograph shows a shallow soil pit locating the intersection of three, formerly buried wedges of concentrated volcanic ash (white) (sample ALS 00-30, dated to 13.94 ± 0.75 Ma; Lewis et al., 2007) (see Fig. 2 for location). Based on the morphology of the deposit, the ash most likely collected in a Y-shaped intersection of three former polygon troughs (e.g., Marchant et al., 1996). A near-surface sand-and-gravel layer (material that probably slumped down from former polygon margins) has been removed to expose the underlying ash. The white tape measure parallel to distal wedge of ash is 1 m. The ash is composed of 95% glass shards and is essentially unweathered (<4% clay-sized grains). The deposit indicates minimal post-depositional reworking, such as might occur with near-surface cryoturbation and development of saturated active layers, for at least the last 13.94 Ma (see text for details). Bottom panel, interpretive sketch, shows that the wedge-shaped ash deposit extends ~50+ cm into the subsurface [adapted from Lewis et al. (2007)].

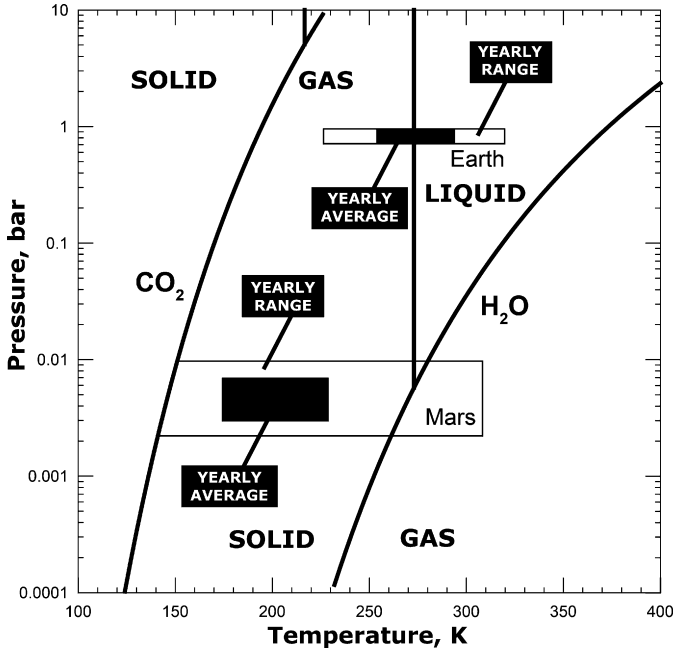

Fig. 13. Phase diagram in temperature–pressure coordinates for water and carbon dioxide for Earth and Mars. Larger boxes represent current overall ranges and inset boxes represent current yearly average surface temperature and near-surface atmospheric pressure for both Earth and Mars. The dimensions of the boxes represent the general latitudinal, elevational and temporal variations. On Earth, temperatures and pressures are in the range where liquid water and ice tend to dominate geomorphic processes (see Fig. 1), and CO_2 comprises only about 0.035% of the atmosphere, is in the gaseous state, and is not a direct geomorphic factor. The atmosphere of Mars is composed predominantly of CO_2; during winter at high latitudes, CO_2 condenses onto the surface to form the seasonal cap, a phenomena that is reflected in the seasonal variation of atmospheric pressure at the Viking Lander sites (Fig. 16, top). For H_2O on Mars, current year-average temperatures are much lower and well within the solid (ice) domain for all year-average temperatures (see Fig. 1). Temporal changes of temperatures cause sublimation of water ice and condensation of water vapor to produce snow and frost, such as is observed seasonally at the Viking Lander 2 site (see Fig. 24) (Jones et al., 1979; Wall, 1981). Note that at the range of temperatures and pressures on Mars, conditions for metastable liquid water can occur locally for short periods of time (e.g., Hecht, 2002) but liquid water is not a major factor in regional geomorphic processes (see also Fig. 1). The presence of salts and brines can modify these relations. Water may be locally important in some special microenvironments (e.g., pits in surface rocks, gullies), and in the recent history of Mars (e.g., Kreslavsky et al., 2007). Changes in spin axis and orbital parameters can cause changes in the distribution of ice stability zones (e.g., Figs. 15 and 17). For example, longer-term changes can result in (1) periods of much higher obliquity leading to sublimation of the polar caps and transport of water to the topics to form glacial deposits there (e.g., Forget et al., 2006), (2) periods of very low obliquity during which time the atmosphere collapses and condenses onto the surface (e.g., Kreslavsky and Head, 2005), or (3) periods of time in early Mars history when Mars may have been "warm and wet" and more Earth-like (e.g., Craddock and Howard, 2002) (Fig. 1; points labeled 300 mbar Mars, 1000 mbar Mars).

the polar plateau (Fig. 2). We conclude the discussion with an example showing how the recognition of key geomorphologic fingerprints of microclimate zones in the ADV and their migration during periods of climate change can be used to document similar trends of laterally migrating and overprinted landforms on Mars.

6.2. *Current climate conditions on Mars*

6.2.1. *Physical setting*

Mars today is a global hyper-arid, cold desert similar in many ways to the ADV [Figs. 1, 13–15; and see summary in Zurek (1992), Carr (1996) and Leovy (2001)]. The predominantly CO_2 atmosphere is thin, resulting in an atmospheric pressure that is less than 1/100th that of Earth (Fig. 13). Although the atmosphere is often close to saturation with water vapor, only very tiny amounts are actually present (an average of 10 precipitable microns) due to the low temperatures, and thus the global climate is hyper-arid (Fig. 1; e.g., Baker, 2001). Heat exchange between the surface and the thin atmosphere is much weaker than on the Earth; because of this, the eleva-

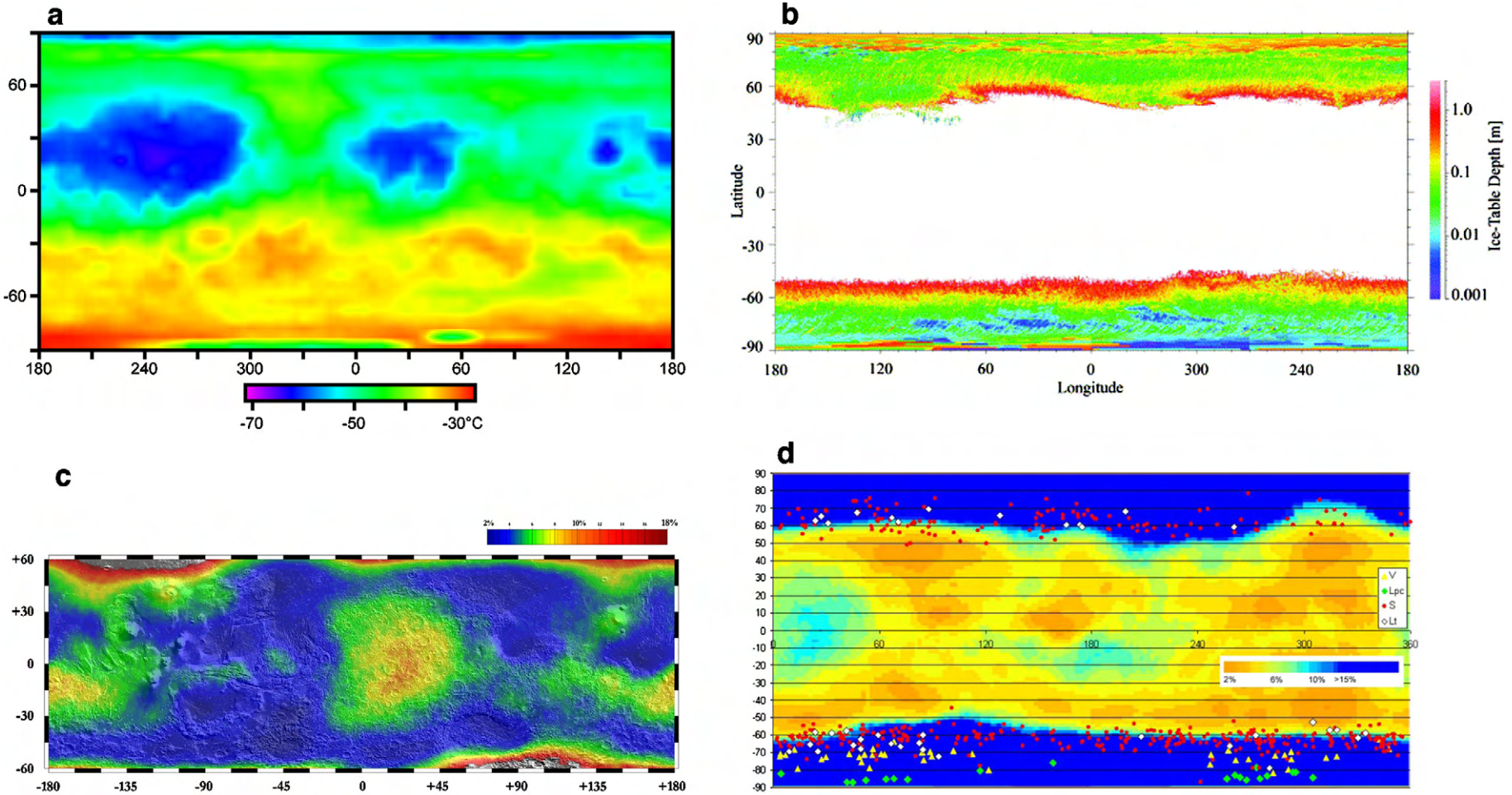

Fig. 14. Temperature, water stability, the presence and depth of ice on the martian surface and in the shallow subsurface, and the distribution of some ice-related landforms. (a) Year-maximum, day-average surface temperatures on Mars. Data on surface temperatures from the European Martian Climate Database (http://www-mars.lmd.jussieu.fr/). This data set has been generated using a general circulation model (GCM) (Forget et al., 1999) but represents the observed martian climate system well. From Kreslavsky et al. (2007). (b) Predicted depth to the ice table under present climate conditions (from Mellon, 2003). (c) Observed distribution of surface and near-subsurface ice (the ice table) from Mars Odyssey GRS/NS data (from Boynton et al., 2002; Feldman et al., 2002; Mitrofanov et al., 2002). (d) Distribution of polygons on Mars superposed on map of the ground ice proportion in mass as measured by the Mars Odyssey Neutron Spectrometer (Feldman et al., 2002). V = large heterogeneous polygons: LPC = straight crack networks close to the south polar cap; LT = large homogeneous polygons formed by cracks associated with topography; S = homogeneous polygons of a size <40 m. From Mangold et al. (2004).

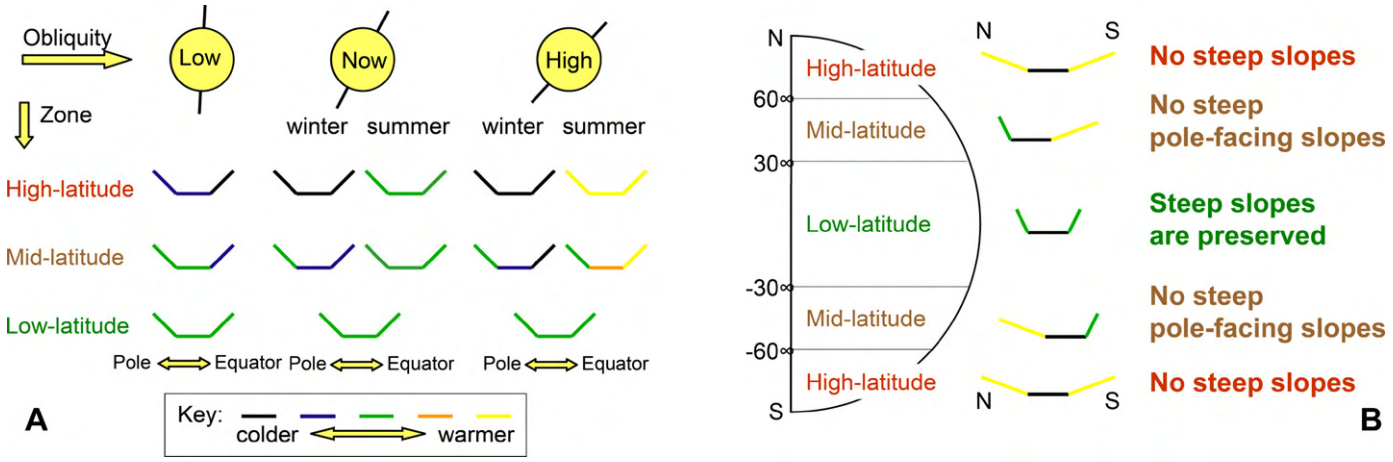

Fig. 15. Relationships of topography, slopes and insolation. (a) A qualitative representation of the dependence of insolation on obliquity, latitude and north–south facing slopes. (b) A qualitative representation of the global trend of steep north and south-facing slope occurrences. From Kreslavsky et al. (2007). Note that changes in obliquity can cause changes in insolation in crater interiors, a change in and redistribution of microenvironments, and consequent geomorphic effects (such as enhancement of slope degradation).

tion zonality of surface temperature is much less pronounced on Mars than in Antarctica.

Surface temperatures vary diurnally and with seasons. At the equator, daily mean surface temperature is ∼ −58 °C (∼215 K) (Fig. 14), but temperatures can range from −113 to −93 °C (160–180 K) at night to as high as −13 to 7 °C (260–280 K) during the day. Day-average air temperatures at the Viking Lander sites (Fig. 16) clearly show this latitude dependence (compare VL 1, 22.5° N and VL 2, 48.0° N), and daily maximum and minimum air temperatures at the VL 2 site differ by up to ∼60 K during northern summer. Due to the eccentricity of the orbit of Mars, and the obliquity of its rotational axis (e.g., Laskar et al., 2004), insolation and the exact temperature at any point on the surface of Mars are dependent on the latitude, the season, the albedo and thermal inertia of the surface, and the local variations in topography (Hecht, 2002). Dust in the atmosphere can vary significantly with time; its presence increases the absorption of solar radiation in the atmosphere, decreasing radiative and conductive heat exchange with the surface, making the vertical atmospheric temperature profile more isothermal, and affecting the temperature regime of the surface (for example, Fig. 16 shows the effects of global dust storms on air temperature at the VL 2 site; see arrows). Wind speeds measured at the surface landing sites are typically a few m/s, with daily maxima up to 8–10 m/s, and gusts up to 40 m/s (Zurek et al., 1992).

Just as topography, elevation, and roughness play important roles in defining the Antarctic Dry Valleys climate and their microclimate zones, so too do these parameters influence martian climate. On Mars, global trends in topography (e.g., Smith et al., 2001) and roughness (e.g., Kreslavsky and Head, 1999, 2000, 2002a) are observed. High elevations and rough topography dominate the southern heavily cratered uplands. Low elevations and smoother topography characterize the northern lowlands. Huge volcanoes, craters of all sizes, and extensive troughs and valleys (e.g., Carr, 1981, 2006) all create local microclimate environments through variations in elevation, albedo, slope, aspect, etc.

In a manner similar to the Antarctic Dry Valleys, rocks, soils, and bedrock exposures characterize the surface of Mars due to the lack of surface vegetation. Surface thermal inertia on Mars is thus dominated by variations in thermal conductivity, with blocky terrains and bedrock exposures having high thermal inertia, and granular soils and dust having low thermal inertia due to conduction of heat being largely restricted to the contact points between grains. Surface thermal inertia on Mars varies regionally and globally (e.g., Christensen et al., 2001; Jakosky and Mellon, 2001).

6.2.2. *Definition of microclimate zones on Mars*

An important factor in the definition of microclimate zones in the Antarctic Dry Valleys is the presence, abundance and state of water on the surface and in the soil. Comparison of the phase diagram of water for Earth and Mars surface conditions (Fig. 13) (Hecht, 2002) shows that pure liquid water is metastable under martian conditions. Thus, deposition of water as snow and frost (rather than pluvial activity associated with liquid water) and sublimation (rather than melting, runoff and fluvial activity) are currently the dominant processes on Mars. Liquid water is stable only where temperatures exceed 273 K (0 °C) and water partial pressure exceeds 6.1 mbar, an unlikely situation in the current climate period. The water vapor content in the atmosphere is so low that if the atmosphere is well mixed, the partial pressure of water is 2–3 orders of magnitude below that needed to stabilize liquid water. Over most of Mars, liquid water brought to the surface under current conditions would rapidly boil and freeze; surface ice would sublimate upon heating. In some low areas on Mars, atmospheric pressure exceeds 6.1 mbar; here liquid water would remain until rapidly consumed by evaporation and freezing (Kreslavsky and Head, 2002b). Localized conditions could also create microenvironments for liquid water. For example, if an ice-rich soil is heated at a high rate, and soil permeability was low enough so that soil pore water vapor pressure could build to 6.1 mbar, then liquid water could form if temperatures exceeded freezing. If salts and brines were involved, liquid water might be formed at even

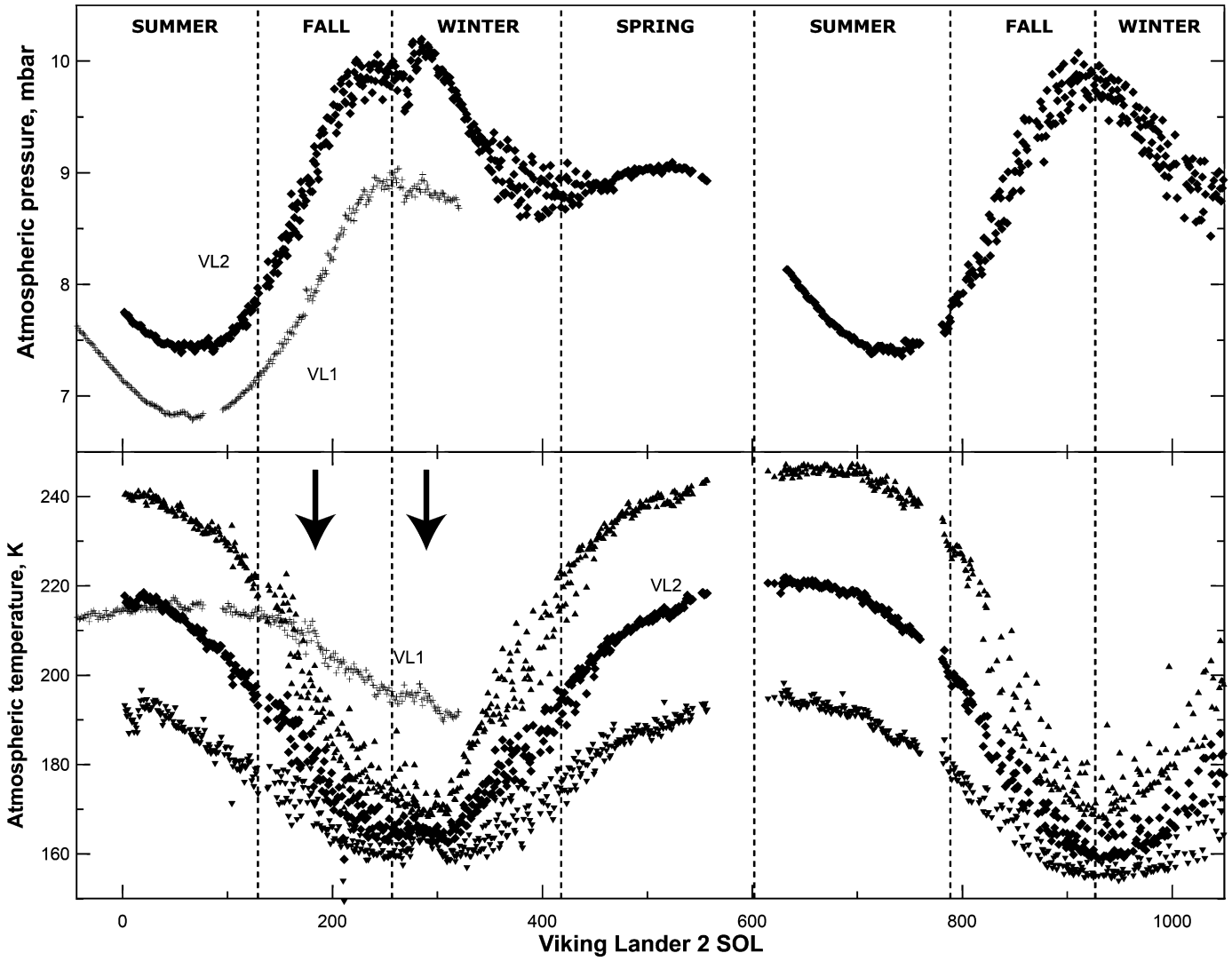

Fig. 16. Temperature and pressure conditions and variations at the Viking Lander 1 (22.48° N, 47.82° W) and Viking Lander 2 sites (47.97° N, 229.59° W). Top: Day-average atmospheric pressure at the Viking Lander 1 and 2 sites, both in the northern hemisphere; VL2 solid black diamonds; VL1, gray crosses. Atmospheric pressure at the more northerly VL2 site is always higher, and both sites display increased pressure during northern winter when CO_2 migrates from the warmer southern hemisphere. Perturbations in the pressure and temperature are caused by global dust storms, the two most prominent of which are indicated by the vertical arrows. Bottom: Atmospheric temperatures (T) at the VL1 and VL2 sites. For VL1, only the day-average temperature is shown; for VL2, the maximum (top line), mean (middle line; day-average), and minimum (bottom line) daily temperatures are shown. Note that the maximum T never approaches the melting point of water. The gap in the data around VL2 SOL 600 is caused by superior conjunction (Tillman, 1988; Zurek et al., 1992).

lower temperatures. Like the Antarctic Dry Valleys, any melting conditions would be very transient because of the limited period where required temperatures are met and the rapid decrease of daytime temperatures with depth (e.g., Fig. 3) (Carr, 2006).

On Mars, the thin, cold atmosphere is capable of holding little water (about 1/6500–13,000th of Earth's atmosphere), but seasonal/latitudinal temperature variations can cause interchange among several reservoirs (polar ice, the atmosphere, and the surface and soil layer). Seasonal insolation variations can cause cyclic mobilization of water (sublimation and desorption), redistribution latitudinally in the atmosphere, and deposition on the surface, and diffusive exchange with the soil layer or regolith (e.g., Farmer, 1976; Zent et al., 1986; Zurek, 1992; Zurek et al., 1992; Haberle et al., 2001; Richardson and Mischna, 2005).

The current distribution of mean surface temperatures on Mars can be used to predict the distribution of water ice on the surface and in the near-subsurface (Fig. 14). The distribution of maximum surface temperatures averaged over a day is a good indication of the presence and behavior of ice. For example, on Earth, those areas with many days of day-averaged surface temperatures above the freezing point of water will likely be characterized by rainfall (pluvial) and fluvial processes if sufficient water vapor is present in the atmosphere (Fig. 1, humid-temperate, selva climates). Those with few or no days of day-averaged surface temperatures above the freezing point of water will remain in periglacial, glacial or hyperarid glacial environments even over the full range of annual precipitation

on Earth (Fig. 1, bottom of diagram below freezing). For year-averaged temperatures, the current environment on Mars falls deep within this latter range (Fig. 1, mean annual temperature at 30°, 50° and 60° latitudes). Similarly, the maximum day-average surface temperatures during a year for the current environment on Mars are everywhere below freezing (Fig. 14a). Thus, on the basis of these standards, we can predict that at the present, Mars lies in periglacial, glacial or hyperarid glacial morphogenetic environments.

Several workers have combined incident solar radiation, thermal inertia, and albedo to calculate mean annual temperature as a function of position on the surface of Mars and then to map this into regolith ice stability zones (e.g., Farmer and Doms, 1979; Mellon and Jakosky, 1995). These calculations suggest that ground ice is currently unstable in the near subsurface at latitudes less than about 50°, but is currently stable at higher latitudes. More recent analyses permit the predictive mapping of the depth to the current ice table (Fig. 14b) (Mellon, 2003), and show that at latitudes greater than ∼60°, most depths to the ice table are between 1 and 10 cm. These predictions have largely been confirmed by the Mars Odyssey Gamma Ray Spectrometer experiment package (Fig. 14c), which mapped the global distribution of surface and near-surface water ice (Boynton et al., 2002; Feldman et al., 2002; Mitrofanov et al., 2002).

As is the case in the Antarctic Dry Valleys, mean annual temperatures on Mars and their variation with microclimate zones (Fig. 1) are important but tell only part of the story. Key to the formation and evolution of landforms at all scales is the range in annual temperature, the maximum temperatures, the period of time these maximum temperatures are achieved, their relationship to the melting point of water, and the presence and influence of salts and brines. For example, while the year-average (Fig. 1) and day-average (Fig. 14a) surface temperatures are well below the freezing point of water over the whole planet, surface temperature can exceed the freezing point in some places during a portion of the day. Currently, the surface temperature exceeds the freezing point of water for very short periods of the day in the equatorial zone throughout the year, and in the mid-latitudes during the summer, especially on equator-facing slopes (Kreslavsky et al., 2007) (Fig. 15). Temperatures at the Viking Lander 1 and 2 sites varied considerably daily and with seasons (Fig. 16).

Seasonal thermal cycling can be a significant factor in geomorphology, for example, in the formation of contraction-crack polygons (Figs. 6 and 18) (e.g., Lachenbruch, 1962; Mellon, 1997; Marchant et al., 2002; Sletten et al., 2003; Mangold et al., 2004; Mangold, 2005; Levy et al., 2006). In the current Mars environment, however, the summer day-average surface temperature never exceeds the melting point of water anywhere on the surface (Fig. 14a), and thus near-surface seasonal freezing and thawing are not predicted to occur (e.g., Paige, 2002; Costard et al., 2002; Kreslavsky and Head, 2004; Kreslavsky et al., 2007) (Fig. 1). Recent detailed calculations of spin axis/orbital parameter behavior in the recent geological past (e.g., Laskar et al., 2004), however, can be used to predict climate forcing sufficient to produce microenvironments with a seasonal active layer (Fig. 17). This, together with new altimetry data, can provide insight into where and when melting temperatures and an active layer could have occurred on Mars (Fig. 15) (e.g., Paige, 2002; Costard et al., 2002; Kreslavsky and Head, 2004; Kreslavsky et al., 2007) and what the related geomorphic processes might be.

6.2.3. *The importance of salts and brines*

One of the surprises of the initial analyses of surface chemical–elemental soil composition (Viking Lander) was that soils were not simply ground up basalt with minor oxidation of iron minerals, as generally expected before the mission (Banin et al., 1992). Very high S, high Fe, moderate Mg, and unexpected levels of Cl at the VL1 and VL2 sites indicated that the soils were not an admixture of weathering products of known rock types, but rather that other processes, such as the introduction of salts in the form of Mg and Ca sulfates and chlorides, by leaching or addition of volcanic gases, might account for the measurements (e.g., Toulmin et al., 1977; Clark and Baird, 1979; Settle, 1979; Clark and Van Hart, 1981; Clark et al., 1982; Gooding, 1992). For example, Toulmin et al. (1977) attributed the two-orders-of-magnitude higher S content of martian soils (compared to typical terrestrial rocks) to the fines being enriched in salt leachate. The localized concentration of salts and secondary minerals in the Mars environment has been emphasized further by observations at the Pathfinder and Mars Exploration Rover (MER) sites (e.g., Larsen et al., 2000; Rieder et al., 2004; Squyres et al., 2004a, 2004b, 2004c, 2006; Haskin et al., 2005; Tosca et al., 2005; Vaniman and Chipera, 2006; Wang et al., 2007).

The role of salts in the alteration of the martian surface has been confirmed by analysis of the martian SNC meteorites. Assessments of the interaction between martian crustal fluids and parent igneous rocks suggest that the most plausible models for secondary mineral formation (e.g., Fe–Mg–Ca carbonates, anhydrite, gypsum, clays, etc.) involve evaporation of low-temperature brines (e.g., Bridges et al., 2001). Furthermore, soils from parts of the ADV contain the same salt phases as those in SNC meteorites known to be formed on Mars (Gooding et al., 1991; Wentworth et al., 2005).

Brines have also been implicated on Mars (e.g., Kuzmin and Zabalueva, 1998). The high levels of Cl and S detected by Viking in the martian soil motivated Brass (1980) to perform a theoretical analysis of the stability of brines on Mars; equilibrium ternary phase diagrams indicated that the minimum temperature at which brines could be stable at the surface was 210 K (−63 °C), with a water concentration of ∼70 wt% and a high concentration of CaCl. The stability of chemically plausible (chloride–sulfate) brines in the near surface was further assessed by Zent and Fanale (1986, 1990) who showed that metastable brines could have long lifetimes and that chloride–sulfate brines could be consistent with Viking Lander elemental data. Knauth and Burt (2002) developed the eutectic brine hypothesis for Mars in which an original NaCl-rich hydrosphere became evapoconcentrated, pore fluids evolved into complex $CaCl_2$-enriched brines through chemical reaction with the re-

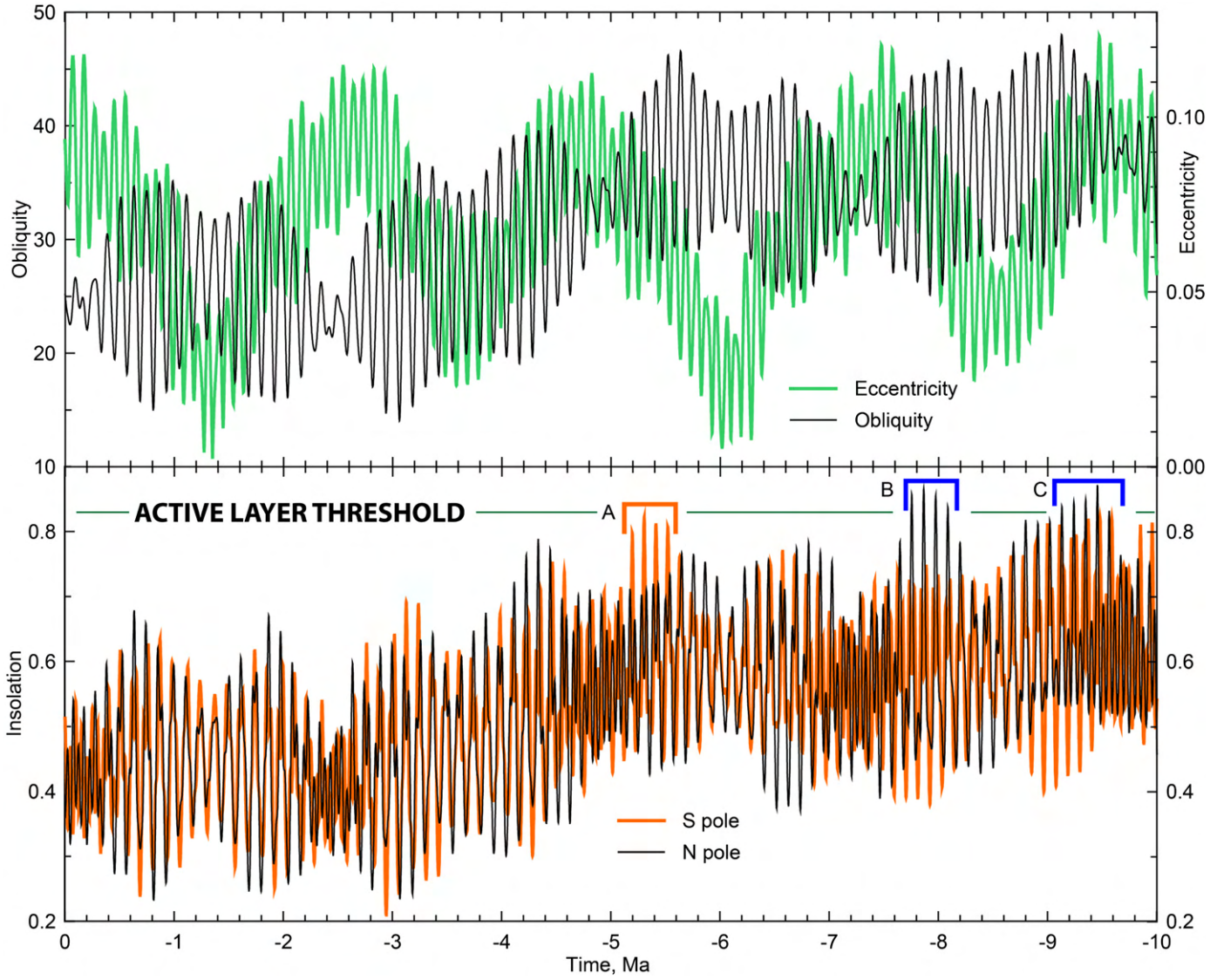

Fig. 17. The recent history of obliquity and eccentricity of Mars and its relationship to insolation and surface conditions [modified from Kreslavsky et al. (2007)]. Top: The history of obliquity and eccentricity for the last 10 Ma. The data are from Laskar et al. (2004). Bottom: The year-maximum day-average insolation at the poles of Mars, calculated from the spin axis/orbital evolution for the last 10 Ma. The thin horizontal line marks the estimated active layer threshold. Places where the insolation exceeds this threshold are predicted to result in an active layer during this time (~5.2, ~7.9 and ~9.2 Ma).

golith, and continuing freeze-down of Mars left eutectic brines as pore fluids. Knauth and Burt (2002) and Burt and Knauth (2003) describe brines with freezing points well below 225 K (−48 °C) in the Antarctic Dry Valleys of Earth (Don Juan Pond) and hypothesized that concentrated brines may currently be stable at temperatures between 180 and 210 K (−63° to −93°C) on Mars, and perhaps even be responsible for recent gully formation. In order to simulate the subsurface conditions where liquid water and rock interact on Mars today, Bullock et al. (2004) performed laboratory experiments in which a SNC-derived mineral mixture reacted with pure water under a simulated Mars atmosphere. The experiments produced dilute brines with dominant dissolved cations being Ca^{2+}, Mg^{2+}, Al^{3+}, and Na^{+}, and major dissolved anions being C, F^{-}, SO_4^{2-} and Cl^{-}. Elemental abundance patterns in their synthetic sulfate–chloride brines were quite similar to those measured in the martian fines at the Mars Pathfinder and VL 1 and 2 landing sites.

In summary, these observations and experiments suggest that salts are present and locally abundant in martian soils, and that salts and brines formed over time as a result of the interaction of surface or subsurface liquid water with basalts in the presence of the martian atmosphere. As is the case in the Antarctic Dry Valleys, salts and brines on Mars may thus modulate the effects of microclimate conditions (e.g., Clark, 1978, 1979) and influence geomorphic processes (e.g., Malin, 1974). Under current conditions, for example, if the eutectic freezing temperatures of $CaCl_2$-enriched brines were in the range of 180 to 210 K (−63 to −93 °C) (Knauth and Burt, 2002; Burt and Knauth, 2003), they would be frozen at extremely high latitudes, would have evaporated at low latitudes, but be stable in mid-latitude bands.

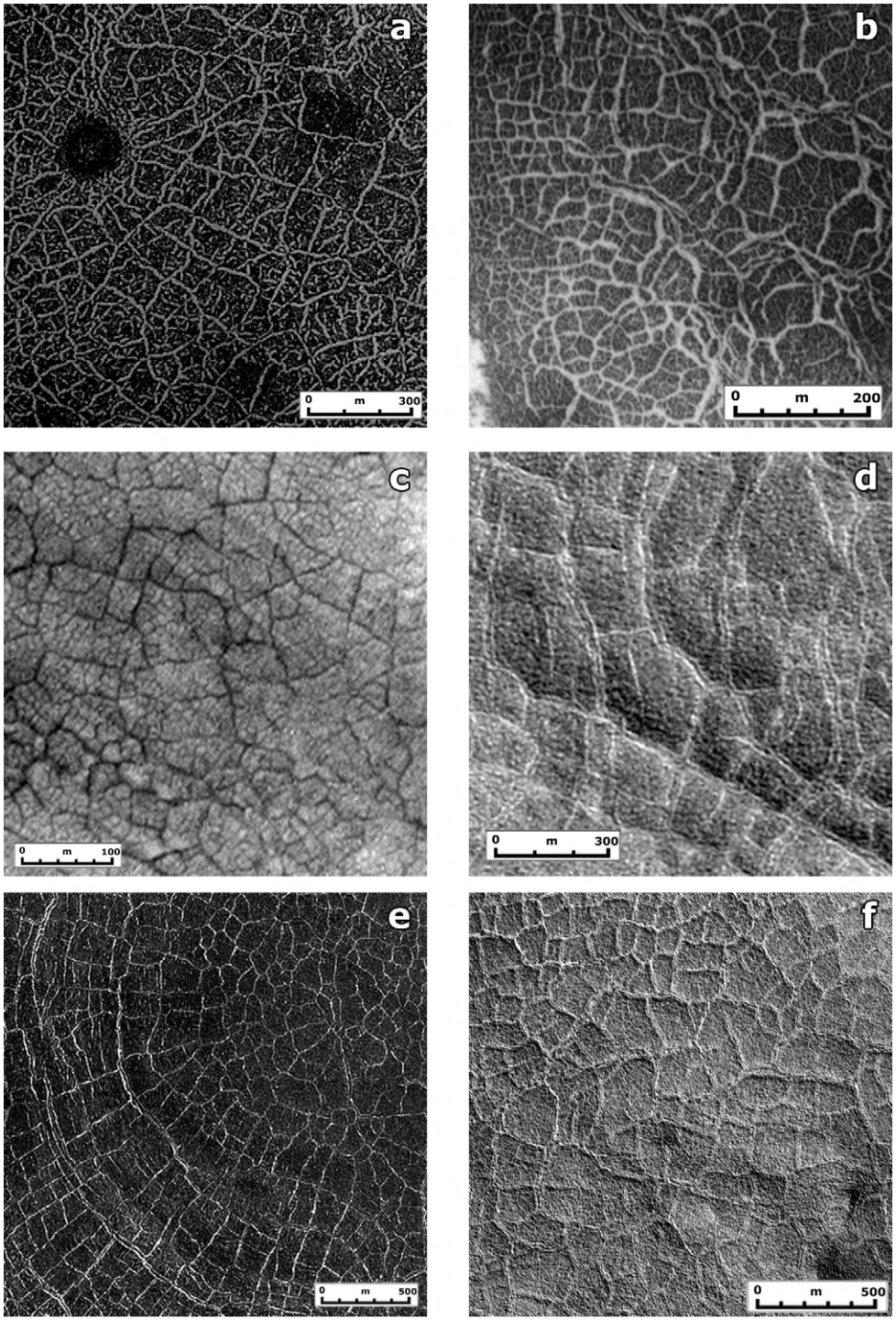

Fig. 18. Contraction crack polygons: (a) Candidate ice wedge or frost/snow filled polygons; 75.16° N, 331.52° W, MOC E09/00029. (b) Candidate ice wedge or frost/snow filled polygons; 71.74° N, 11.3° W, MOC E09/00249. (c) Aeolian activity (wind streaking NW–SE) has stripped some finer debris, leaving some open and some filled polygon cracks; 75.16° N, 331.52° W, MOC E12/02319. (d) Two scales of polygons with the smaller ones resembling "basketball terrain" or sublimation polygons (e.g., Marchant et al., 2002), and the larger ones having sloping margins and filled cracks; 75.16° N, 331.52° W, MOC E21/01593. (e) Differences in polygon size and structure on crater walls (lower left) and floor (upper right). Polygon structure is much more isotropic in the crater center; 65.55° N, 327.89° W, MOC M19/00047. (f) Polygon structure in the northern lowland plains. Note the two scales of polygons and the basketball terrain texture in the smaller polygons (http://mars.jpl.nasa.gov/mgs/msss/camera/images/7_19_99_fifthMars/07_npolys/, press release MOC2-150). (g) Polygon structure in the northern lowlands; typical "basketball terrain"; 60.66° N, 2.93° W, MOC M14/00154. (h) Polygon structure in the southern highlands; typical "basketball terrain"; 54.16° S, 119.52° W, MOC M03/04266. North is at top in all images.

6.2.4. Implications for dominant geomorphic processes

There are several implications of the current nature of the hyperarid, cold desert environment of Mars for geomorphological features at various scales on that planet (Figs. 18–21). First, there is a distinctive latitude-dependent variation in mean annual surface temperature (Fig. 14a) that is similar to the

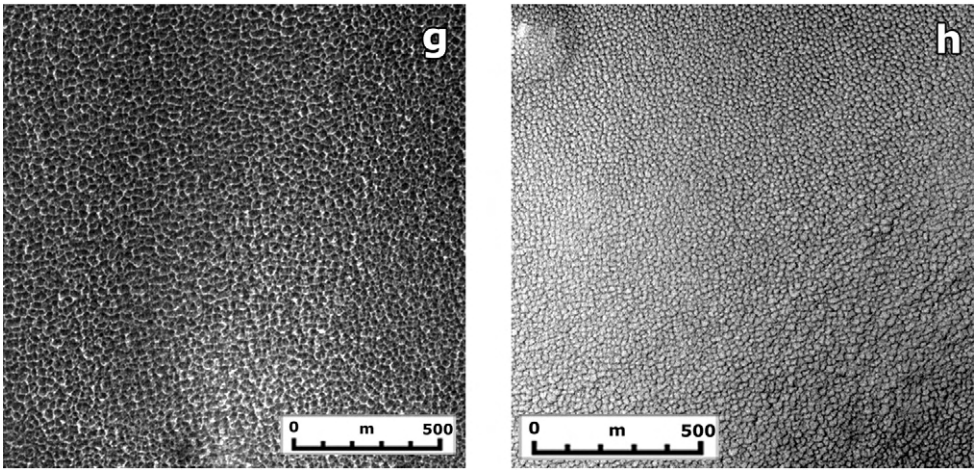

Fig. 18. (*continued*)

differences in mean annual temperatures seen in the different ADV microclimate zones (Fig. 1, compare the dashed oval with Mars mean annual temperature at 30°, 50° and 60° latitudes). Second, the presence of ground ice and the depth to the ice table is also dependent on latitude (Figs. 14b and 14c). These first two factors should map out into potentially significant differences in geomorphology. Third, due to the current pressure–temperature conditions on Mars and the phase relations of water (Figs. 1 and 13), liquid water is not predicted to be present on the surface or in the near subsurface in the current climate regime. A major implication of this is that under these conditions, there can be no active layer (see definitions and discussion in Section 2.2), and thus no typical cryoturbation of soils. However, new data on spin axis/orbital parameters and topography permit predictions of the nature of climates in the recent past, and where and when these conditions should have occurred (e.g., Kreslavsky and Head, 2004; Kreslavsky et al., 2007) (Fig. 17). Fourth, the seasonal deposition of CO_2 and H_2O snow and surface ice is strongly latitude dependent. Any geomorphic process linked to this seasonal deposition will also be strongly latitude-dependent. Fifth, although the current mean surface temperatures everywhere on Mars are typically well below 0 °C (273 K), variations in spin axis/orbital parameters can cause poleward-facing slopes at mid-latitudes (Fig. 15) to reach surface and shallow subsurface temperatures in excess of 0 °C (273 K) for days to perhaps weeks per year in the recent geological past (e.g., Costard et al., 2002; Paige, 2002; Kreslavsky and Head, 2004; Kreslavsky et al., 2007). This could potentially cause locally enhanced flow of ice, melting of snow, glacial ice and ground ice, and formation of a localized active layer and runoff gullies in topographically favored regions. Finally, the potential role of salts and brines in modifying melting temperatures and geomorphic responses needs to be taken into consideration (see Section 6.2.3). These factors together make the calculated erosion rates on Mars extremely low (Golombek et al., 1997, 1999), in the range of 0.2 m/Ma (Arvidson et al., 1979), very similar to those of the SUZ in the Antarctic Dry Valleys (~0.06–0.3 m/Ma; Summerfield et al., 1999; Brook et al., 1995).

6.3. Mars microclimate zones and their influence on equilibrium landforms and geomorphologic processes at various scales

Recent exploration of Mars has provided important new data on surface morphology, geology, topography, mineralogy, thermal inertia, and soil water ice content. Data from the Gamma Ray and Neutron Spectrometer Experiments show the presence of near surface water ice (Fig. 14c) (Boynton et al., 2002; Feldman et al., 2002; Mitrofanov et al., 2002) closely consistent with that predicted from theory for the shallow ice table at latitudes above ~50° (e.g., Mellon and Jakosky, 1995; Mellon, 2003) (Fig. 14b). Here we examine equilibrium landforms and geomorphologic processes at various scales and their relationship to microclimate zones.

6.3.1. Macroscale landforms

At the macro-scale, gullies similar to those seen in the ADV coastal thaw and inland-mixed zones are observed on Mars (Fig. 21) (e.g., Malin and Edgett, 2000, 2001), where they show a range in latitude distribution from 30° to 70°, are largely restricted to a band around 45°, and tend to have some preference for pole-facing slopes. Initially interpreted to have formed by groundwater release (e.g., Malin and Edgett, 2000; see also Heldmann and Mellon, 2004), the latitude distribution, orientation, and local geological environment of these features suggest to others that they formed by seasonal melting of snowpack or ground ice to form intermittent streams or debris flows (e.g., Costard et al., 2002; Christensen, 2003; Dickson et al., 2007b; Head and Marchant, 2006; Bridges and Lackner, 2006; Head et al., 2007). The lack of periods of extended surface melting temperatures in the current climate regime (Figs. 13, 14a, and 17) suggests that these features may date from the recent geological past (e.g., Costard et al., 2002; Head et al., 2003; Reiss and Jaumann, 2003; Kreslavsky et al., 2007), although some recent activity has been reported (e.g., Malin et al., 2006).

Also at the macro-scale, latitude-dependent asymmetries in the distribution of steep slopes have been observed (Kreslavsky and Head, 2003), similar to the situation in the ADV microclimate zones (Table 2; Fig. 4). The frequency of steep (>20°)

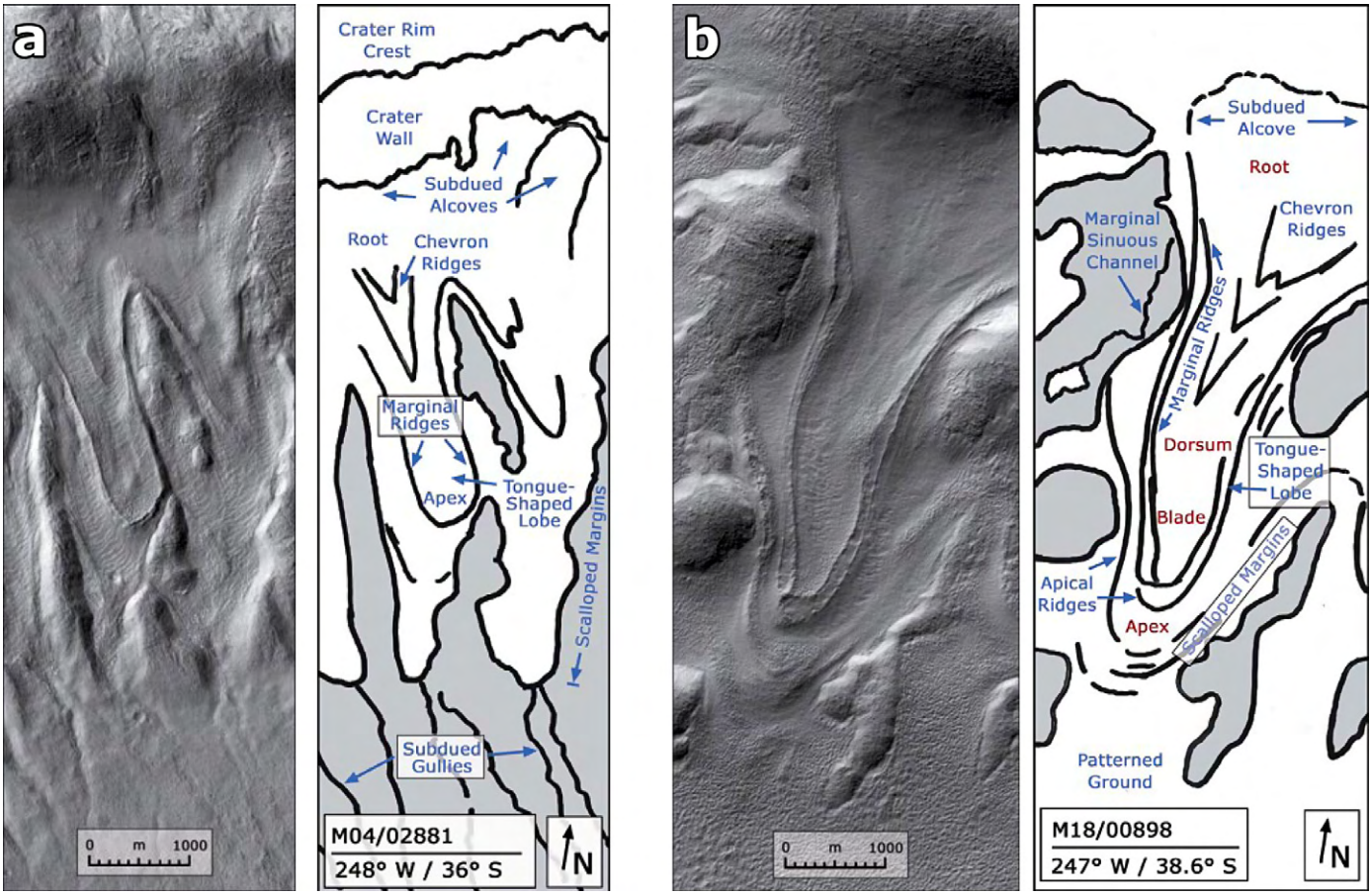

Fig. 19. Viscous flow features at mid-latitudes: (a) Image and sketch map of viscous flow features on the interior of an impact crater wall. Note the tongue-shaped lobes, the marginal ridges and the alcoves. Subdued gullies emerge from the distal portions of the depressions occupied by the tongue-shaped lobes. MOC image M04/02881, 248° W, 36° S. North is at the top of the image and illumination is from the northwest. (b) Image and sketch map of viscous flow features on the interior of an impact crater wall. Note the details of the tongue-shaped lobe, including multiple marginal ridges, multiple apical ridges, and the distal patterned ground. MOC image M18/00898, 247° W, 38.6° S. North is at the top of the image and illumination is from the northwest. From Marchant and Head III (2003).

slopes drops more than three orders of magnitude from equatorial to high-latitude regions on Mars (Fig. 22). This is interpreted to be due to the enhanced role of climate-related ice and dust mantling, and ice-assisted creep processes at higher latitude (Kreslavsky and Head, 2003). Further, the boundary between preserved (equatorial) and modified (higher latitude) steep slopes occurs at higher latitudes for pole-facing slopes and at lower latitudes for equator-facing slopes (Fig. 22), illustrating the importance of slope-related insolation and local microclimate environments (Fig. 15).

6.3.2. *Mesoscale landforms*

At the meso-scale, a variety of contraction-crack polygons (Fig. 18) have been observed in different environments above about 55° N and S latitudes, but are generally absent below these latitudes; polygon subtypes show evidence for latitude dependence and correlation with the presence of ground ice (Fig. 14d) (Seibert and Kargel, 2001). For example, types of patterned ground (e.g., polygons, slope stripes) were classified into ten different sub-types by Mangold et al. (2004) and Mangold (2005); their distribution was concentrated above ∼55° N and S latitudes and highly correlated with regional ground ice distribution interpreted from Odyssey Neutron Spectrometer data (Fig. 14d). At least five subtypes were interpreted to be controlled by climate zonation because they are located at the same latitudes between 55° and 75° in both hemispheres (Mangold, 2005). On the basis of comparisons to Earth, polygons were interpreted to be due to seasonal temperature variations, such as thermal contraction and seasonal thaw. Some polygons on Mars are larger than those on Earth by a factor of up to ∼5 (Fig. 18); the larger size could be due to deeper propagation of cracks due to colder temperature conditions and also larger temperature variations in past periods on Mars. Polygons similar to ice-wedge polygons on Earth formed (by a combination of thermal contraction and seasonal thaw) are homogeneous, 50–200 m in width, and found in crater interiors (Mangold, 2005). Small polygons and hummocks (15–40 m in width, i.e., similar in size to those observed in the ADV and in other periglacial environments on Earth) are the most abundant polygon type (Figs. 18g and 18h). For these polygons, cracks are usually not observed directly, but thermal contraction and widening by sublimation and desiccation of the surface layer appear to be important in their formation. These polygons are most similar to the sublimation polygons observed in the Antarctic Dry Valleys (e.g., Marchant et al., 2002) (Fig. 6). Mangold (2005) found that all types of patterned ground on

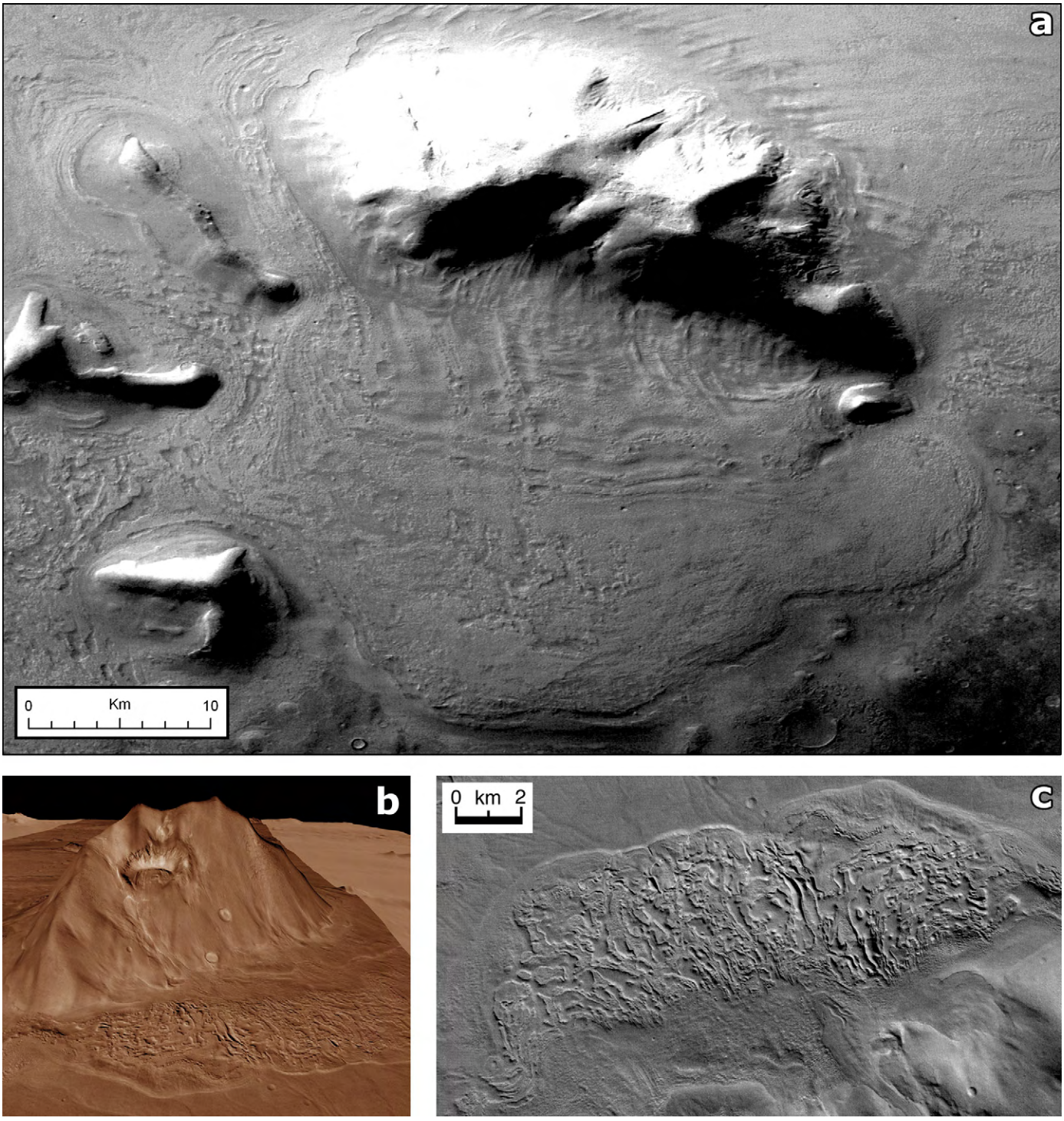

Fig. 20. Lobate debris aprons at mid-latitudes. (a) Lobate debris apron around a massif at the dichotomy boundary at northern mid-latitudes (north is at the bottom). MEX HRSC Orbit 1523; 49.25° W, 46.25° S. (b) Lobate debris apron around a massif on the eastern rim of the Hellas basin at southern mid-latitudes. Perspective view shows lobate debris apron at the base of the massif (vertical exaggeration ∼30×), and vertical view (c) shows extensive pitting suggesting that considerable sublimation of excess ice occurred and that the feature may have been a debris-covered glacier (e.g., Head et al., 2005). MEX HRSC Orbit 300; 262.8° W, 43.2° S.

Mars are geologically recent (<10 Myr) but that they did not form simultaneously; he found that some features may correspond to freeze-thaw cycles that occur during periods of higher obliquity (>35°), and that certain subtypes may have been enhanced by specific microenvironments. Kostama et al. (2006) found that in the northern high latitudes of Mars, polygonal patterned ground was developed on a thin mantling deposit with a very young surface crater retention age, and that the mantle was characterized by patterned ground textures that varied as a function of latitude.

The variety of contraction crack polygons thus offers clues to microclimates and climate change on Mars. For example,

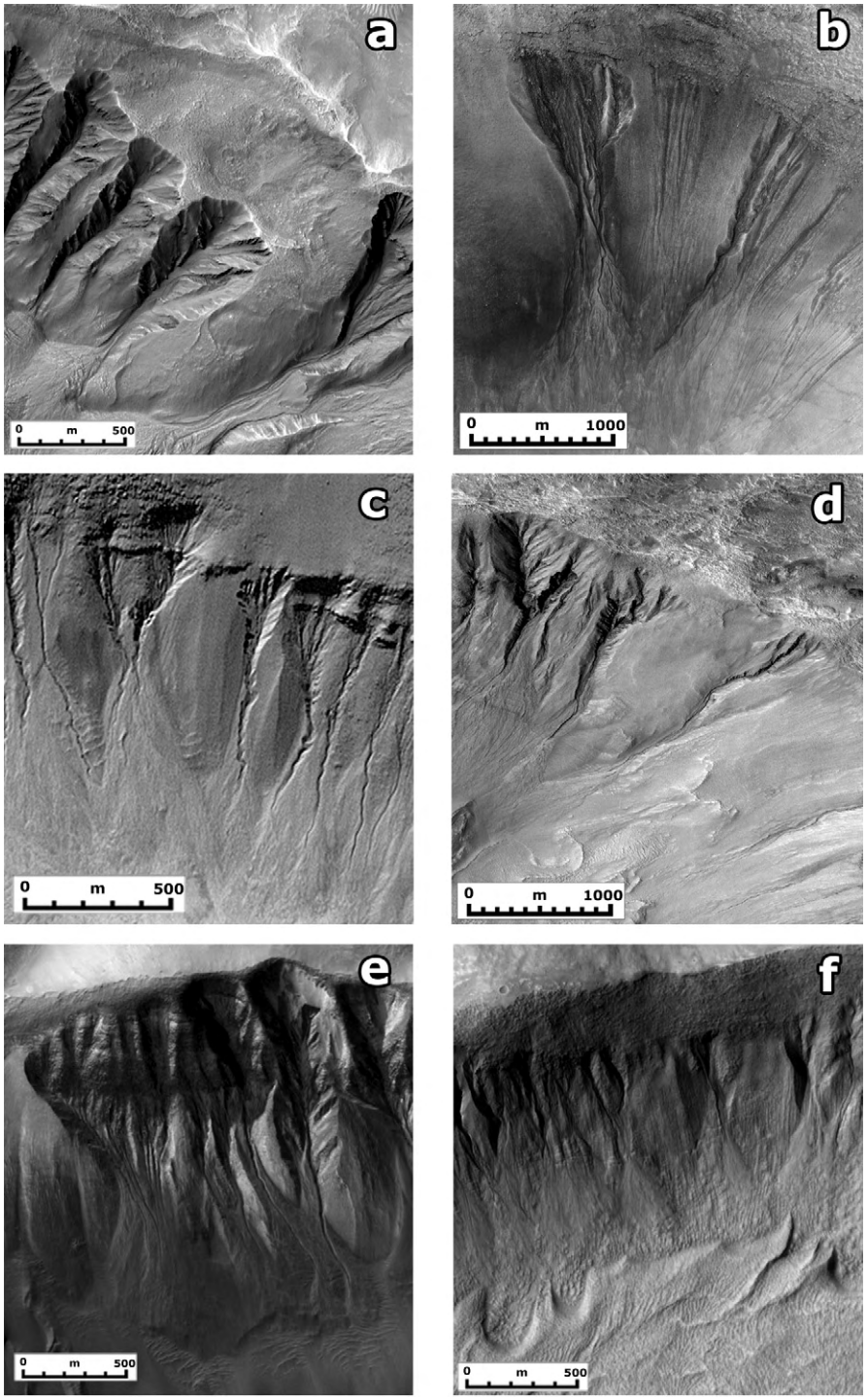

Fig. 21. As originally defined (Malin and Edgett, 2000), gullies occur on generally steep slopes, commonly on interior crater walls, and are made up of three components, an upper alcove, an intermediate channel, and a lower apron. Gullies occur on Mars in a highly restricted latitudinal distribution, suggesting important control by a specific microenvironment. A variety of these types of alcoves, channels and aprons are shown in (a)–(e). (a) 41° S, 205° W; portion of MOC image E13/01791. (b) 47° S, 162° W; portion of MOC image R10/02078. (c) 39° S, 201° W; portion of MOC image M17/00423. (d) 43° S, 162° W; portion of MOC image E10/04497. (e) 42° S, 158° W; portion of MOC image E03/02550. Some gullies also show evidence for the former presence of lobate viscous flow features (f)–(h). (f) Convex outward depressions at the base of the slope suggesting the former presence of debris-covered glaciers (compare to Fig. 19); gully fans fill the depression. 36° S, 133° W; portion of MOC image R05/02305. (g) Multiple lobes at the base of a crater wall; gully fans fill the depressions. 43° S, 162° W; portion of MOC image E09/02399. (h) Multiple lobes at the base of a crater wall with a much larger scalloped depression; here too, gully fans fill the depressions. 39° S, 166° W; portion of MOC image E11/04033.

many contraction-crack polygons at high latitudes (Figs. 18d, 18f, 18g and 18h) in areas having a shallow ice table (Figs. 14b and 14c) display the rounded texture, termed "basketball terrain" (Malin and Edgett, 2001; Kreslavsky and Head, 2000; Head et al., 2003; Mangold et al., 2004; Kostama et al., 2006), similar to the sublimation polygons of the SUZ in the Antarc-

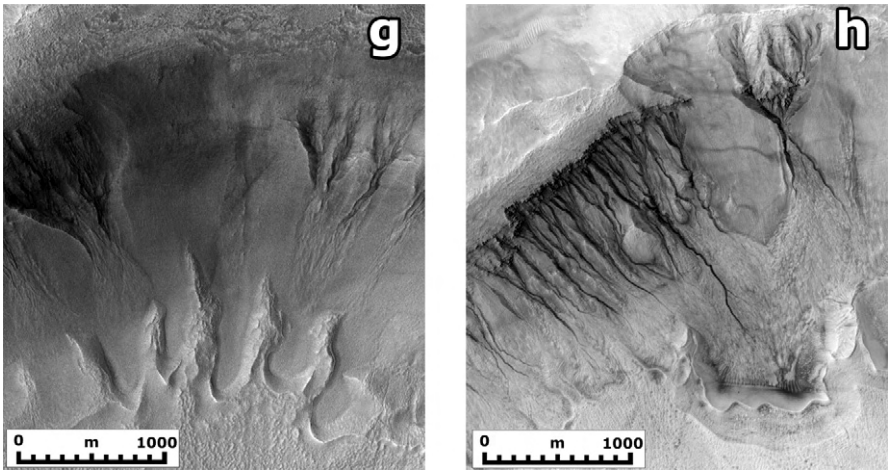

Fig. 21. (*continued*)

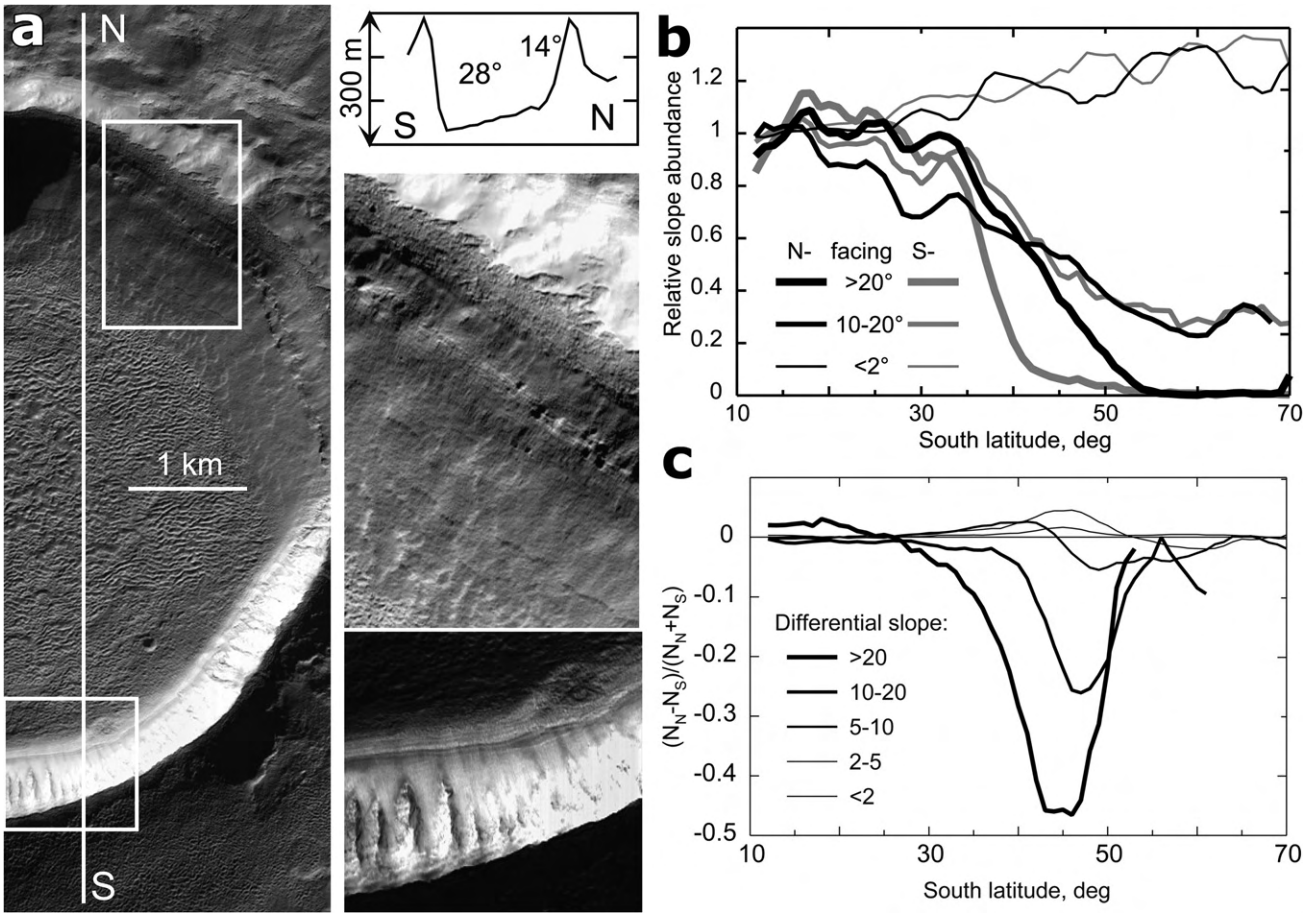

Fig. 22. The importance of slopes and their orientation in creating microenvironments and initiating geomorphological processes. (a) A typical crater interior at mid-latitudes. Crater is ∼6.5 km in diameter and located at 194.8° E and 43.5° S; north is approximately at the top of the image and illumination is from the upper left. Vertical line shows location of MOLA profile shown in box at upper right. Other boxes show locations of enlargements on right. The southern, equator-facing crater wall is steep and shows bedrock exposures and mass-wasted debris. The northern, pole-facing wall has been modified by formation of an active layer and transport of debris down onto the crater floor, smoothing the crater rim and modifying the crater interior (see the MOLA profile and the wall and floor slope asymmetry). (b) Abundance of N-facing and S-facing slopes relative to that of the typical equatorial highlands, plotted against latitude for Terra Cimmeria (180–220° W). The different curves correspond to different ranges of slopes in degrees, as shown, with black curves corresponding to N-facing slopes and gray curves to S-facing slopes. (c) Asymmetry of different slopes calculated with 150-km wide latitudinal zones in Terra Cimmeria and plotted against latitude. Different curves correspond to different ranges of differential slopes in degrees, as shown. From Kreslavsky et al. (2007). Compare to qualitative conditions in Fig. 15, and to ADV slope asymmetries in Fig. 4.

tic Dry Valleys (Marchant et al., 2002). Others (Figs. 18b and 18c) may correspond to the composite-wedge and sand-wedge polygons of the ADV inland mixed zone. Many patterns are superposed and have different scales (Fig. 18), suggesting recent climate change such as deposition of ice-rich layers during recent ice ages (e.g., Head et al., 2003) and the possible development of high-latitude active layers under conditions of higher spin-axis obliquity (e.g., Mangold, 2005; Kreslavsky et al., 2007).

Lobate, viscous-flow features and debris aprons (Figs. 19 and 20) similar to those seen in the ADV have been observed on Mars and both types of features display a limited distribution in latitude. Features with morphologies similar to debris-covered-glaciers cluster in latitude bands at about 45° (e.g., Milliken et al., 2003) and commonly occur in microenvironments on crater interior walls, where topography favors accumulation and preservation of ice and snow, where slopes are typically steeper, and where slope orientation may favor higher surface insolation and temperatures sufficient to cause flow (Fig. 15) (e.g., Hecht, 2002; Kreslavsky and Head, 2004; Kreslavsky et al., 2007). Larger lobate debris aprons commonly occur between 30° and 60° latitude and are concentrated around the base of massifs that are shedding debris (Fig. 20) (e.g., Squyres et al., 1992; Pierce and Crown, 2003; Head et al., 2005). These features are interpreted by many to be due to atmospheric water vapor diffusion causing deposition of ice in the pore spaces of debris fans, resulting in mobilization and flow (e.g., Mangold et al., 2002) during certain periods of the history of Mars. The lobate debris aprons could be closely related to the gelifluction lobes seen in the ADV inland mixed zone. Alternatively, recent evidence from Mars Express HRSC images suggests that at least some of these features are debris-covered glaciers (Fig. 20) (Head et al., 2005) rather than debris aprons with secondary ice undergoing creep or flow. Supporting evidence for the role of debris-covered glaciers in the formation of lobate debris aprons comes from the presence of adjacent debris-covered valley glaciers at the same latitudes (e.g., Head et al., 2006a, 2006b).

6.3.3. *Microscale landforms*

At the microscale, there are differences between the rocks and surface features found at different latitudes, such as at the high latitude Viking 2 landing site (47.7° N; Mutch et al., 1976a, 1977) and those at lower latitudes (Viking 1, Pathfinder, and Mars Exploration Rovers, all below 23° latitude; Mutch et al., 1976b; Binder et al., 1977; Golombek et al., 1999; Squyres et al., 2004a, 2004b, 2004c). Sediment-filled contraction-crack polygons similar to those seen in the ADV inland mixed zone are observed at the high-latitude Viking 2 site (Fig. 23) (Mutch et al., 1976a, 1977), and are also seen elsewhere in this latitude band in orbital MOC high-resolution images (e.g., Malin and Edgett, 2001; Mangold et al., 2004). Also observed at the Viking 2 site are heavily pitted rocks (Fig. 24) previously interpreted to be formed by vesiculation or differential weathering of clasts or phenocrysts (e.g., Mutch et al., 1976a). Allen and Conca (1991) suggest however that these features may form by processes much more similar to those that formed the pits in the Antarctic Dry Valley rocks in the SUZ (see also Parsons et al., 2005; Staiger et al., 2006). During winter at the Viking 2 site, deposition of frost and snow on rocks and on intervening ground was observed (Fig. 24; compare to Fig. 8), but was not seen at lower latitudes. These observations suggest that the deposition of snow on rocks with a thermal inertia sufficient to retain heat and cause localized melting of snowfall (Head and Kreslavsky, 2006), could have been a factor in the formation of the observed pitting, as appears to be the case in the stable upland zone and parts of the inland mixed zone of the Antarctic Dry Valleys (e.g., Allen and Conca, 1991).

6.4. *Equilibrium landforms and correlations between microclimate zones on the Earth and Mars*

In summary, there are numerous similarities between the hyper-arid cold desert Antarctic Dry Valley microclimate zones and the latitudinal and local microclimate zones observed on Mars (Fig. 1). Further, there are similarities in the type and range of geomorphic features observed at all scales (Figs. 18–21, 23 and 24). The ADV stable upland zone (SUZ) (Figs. 2 and 6), with its low moisture content, buried ice and perennial sub-zero temperatures, appears to be most analogous to the martian climate zone above about 50° latitude (Fig. 1). The ADV inland mixed zone (IMZ), with its mixed soil–water–ice content and slightly higher summertime temperatures, is most analogous to the high latitude zone on Mars for some periods in the recent geological past (Fig. 17), when a discontinuous active layer might have occurred. The ADV coastal thaw zone (CTZ) has no real equivalent on Mars today in that the current temperature–pressure environment on Mars (Fig. 13) does not support liquid water at the surface or in the near subsurface (Fig. 14a) under other than very exceptional circumstances (e.g., Kreslavsky et al., 2007). Regions equatorward of 30° latitude, although representing a hyperarid cold desert, are dehydrated in the near subsurface (Figs. 14b and 14c) (Mellon and Jakosky, 1995). The Amazonian climate history of Mars (the last ∼3 Ga) appears to be dominated by equatorward and poleward migration of these latitude-dependent environments in response to variations in spin axis/orbital parameters (e.g., Laskar et al., 2004; Head et al., 2003, 2005; Forget et al., 2006). Very ancient climates on Mars, such as those occurring during the Noachian period more than ∼3.7 Ga ago, may have been characterized by atmospheric temperatures and pressure conditions (Fig. 1; 300 mbar, 1000 mbar) that permitted pluvial activity (e.g., Craddock and Howard, 2002) during at least some part of the year, and thus may have been characterized by very different geomorphic processes and landforms, including some of those now operating in the CTZ of the Antarctic Dry Valleys (Fig. 1).

7. Geomorphic evidence for recent climate change on Mars

Both the Antarctic Dry Valleys and Mars are currently characterized by hyper-arid and extremely cold desert climates (Fig. 1). The recognition and documentation of three microclimate zones within the ADV (Fig. 1, within dashed oval, and

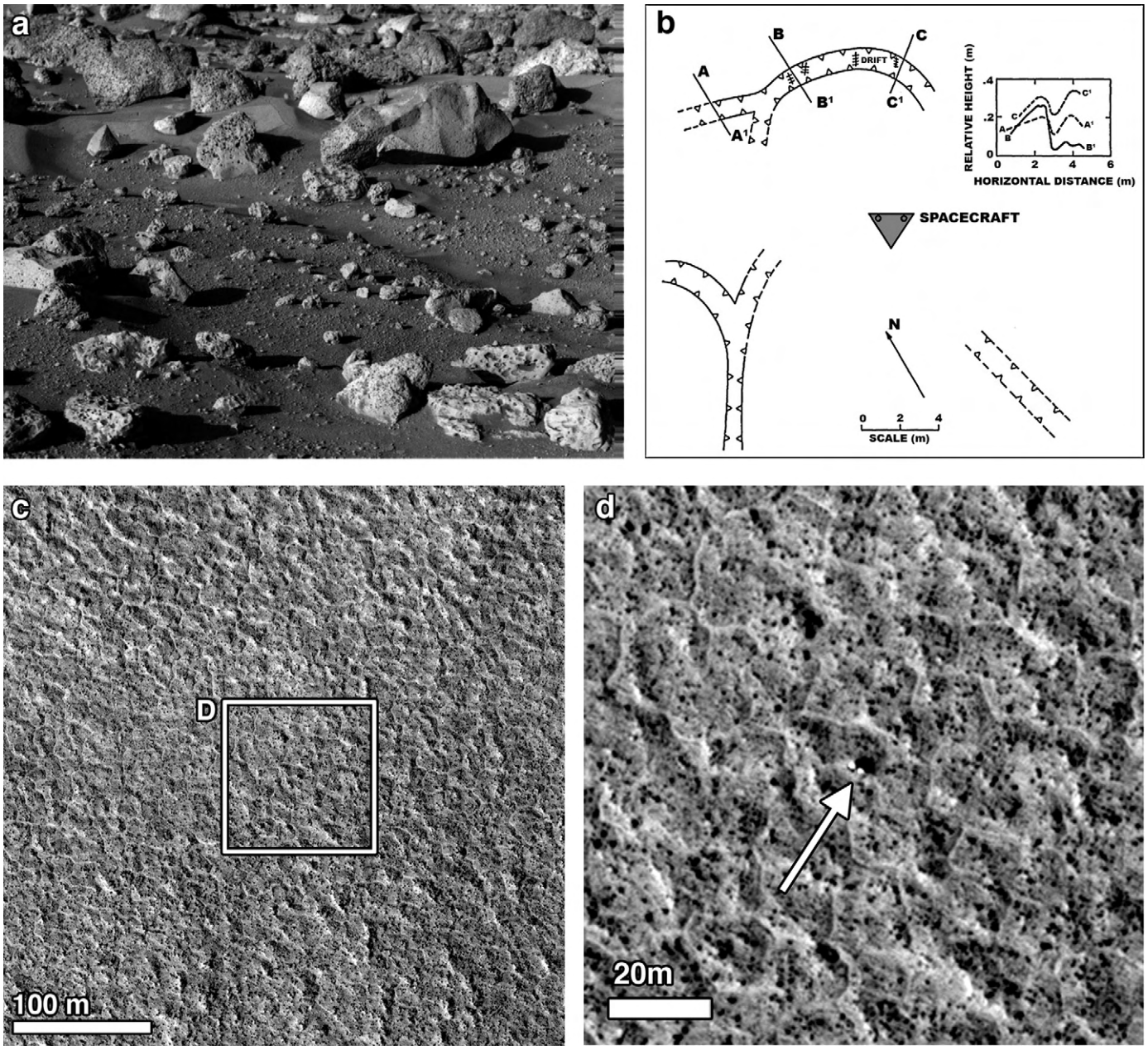

Fig. 23. Images of the Viking Lander 2 high-latitude landing site (47.97° N, 229.59° W) showing evidence for sand wedge and ice wedge polygons. (a) In the near field of the site, about 8 m north of the spacecraft, a trough ∼1 m across and ∼10 cm deep trends from the upper left to lower right and is filled with small drifts of fine-grained sediment. The trough is asymmetrical; the northern wall is relatively steep and high and a prominent upraised rim is seen along the northern edge. Blocks are relatively rare in the troughs, and rocks that are observed there are partly buried, in contrast to many in the adjacent terrain. Camera event 21A024. (b) The general distribution of troughs mapped in the vicinity of VL2, and topographic profiles across the northern trough (inset). Abrupt termination of troughs near the spacecraft are due to obscuration of the camera view by the spacecraft. The trough shown in (a) is the one to the north of the spacecraft. Profiles show the presence of a prominent raised rim on the northern edge, and more subtle differences in elevation suggest that the southern rim may also be raised. The presence of several trough junctions suggest a polygonal network. Similar features were not observed at the Viking Lander 1 site, at a more southerly latitude (22.48° N, 47.82° W) (from Mutch et al., 1976a, 1977). The combination of raised rims and sediment fill suggests that these features are analogous to sand wedge and ice wedge polygons in the ADV (Fig. 6). The depth to the current ice table at these latitudes (Fig. 14b), the amount of water ice in the substrate (Fig. 14c), and the annual temperature changes at the site, all indicate that thermal cycling could produce contraction-crack polygons, which became traps for fine-grained sediment. (c) Polygon networks in the region surrounding the VL 2 site are observed from orbit in HiRISE imagery [HiRISE image #PSP_001501_2280 for both (c) and (d)]. Box indicates location of (d), which shows the position of the VL 2 lander (arrow) and the generally polygonally textured landscape surrounding the site. Compare to surface images (a) and polygon scale (b) in the vicinity of the VL 2 lander.

Fig. 6), the variation of temperature, humidity, and soil water content among these microclimate zones (Fig. 1; Table 1), and the correlation of geomorphologic features at the micro-, meso-, and macro-scales with these zones, provides important insight into the origin of the diverse features and their stability with time and changing Antarctic climate conditions. Broadly similar climate zonation exists on Mars and is largely distributed as a function of latitude-dependent insolation and soil-moisture

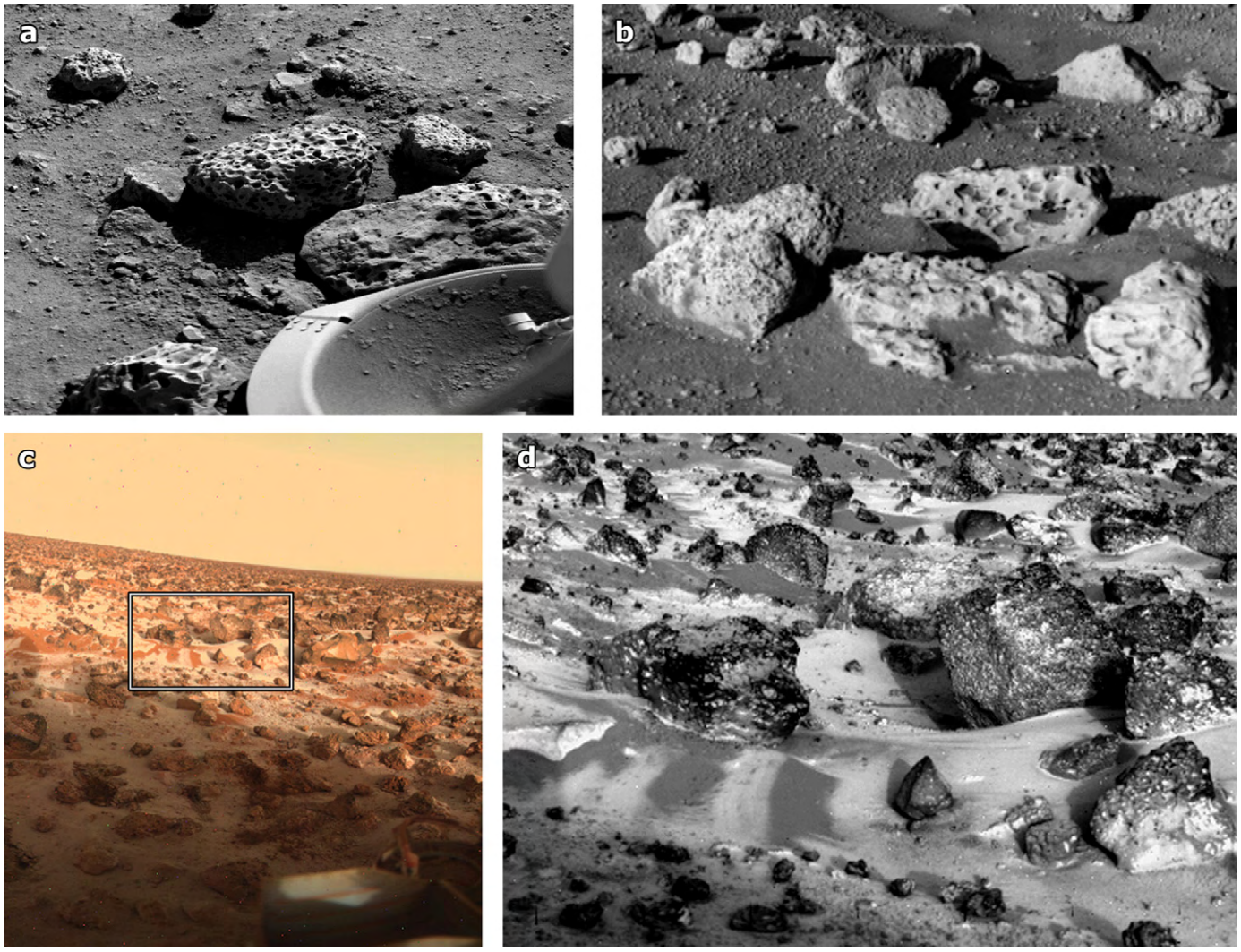

Fig. 24. Images of the Viking Lander 2 high-latitude landing site (47.97° N, 229.59° W) showing evidence for heavily pitted rock surfaces. (a) Pitted rocks in the vicinity of the lander footpad; the rock at the top of the footpad is ∼35 cm across (portion of 22A001). (b) Pitted rocks near the edge of a trough (top of image; see Fig. 23 for context) (portion of 21A024). Pits are ∼1–2 cm in diameter. (c) Frost and snow deposition at the VL 2 site in northern winter (image P21873). (d) Enlargement of area in the central part of (c) showing the location of snow and frost deposition in lows and small drifts between rocks and ripples, and in pits and troughs in the rocks. Seasonal snow and frost deposition (Jones et al., 1979; Wall, 1981) may lead to the formation of local meltwater on heated rock surfaces on Mars and focused chemical alteration to produce pits (Head and Kreslavsky, 2006), similar to the situation on Earth (see Fig. 8; see Parsons et al., 2005; Staiger et al., 2006).

content (Figs. 14 and 15). Detailed knowledge of the processes derived from the ADV microclimates can thus be applied to Mars and will be helpful in deconvolving the signal of climatic zonation and climate change there.

There is indeed evidence that Mars has undergone major changes in climate in the recent geological past (e.g., Head et al., 2003 and references therein); these changes have been linked to large variations in spin axis/orbital parameters (eccentricity and obliquity; Laskar et al., 2004), with indication of major lateral changes in ice deposition and stability, and 'ice age' deposits extending down to 30° latitude. Details of geomorphologic features and their stratigraphic relations support this view (e.g., Kreslavsky and Head, 2000, 2003; Mustard et al., 2001; Milliken et al., 2003), and individual geomorphologic features can be used to establish the sequence and sign of climate change.

For example, geomorphologic features on crater interior walls in mid-latitudes on Mars commonly reveal a sequence of events that illustrates the nature of changing climate (Fig. 25). In this specific case, the crater floor displays a rough-textured hummocky surface suggestive of sublimation polygons and aeolian modification. At the base of the crater wall, a series of concentric crenulate ridges mark the transition to the crater wall, with the edge of the floor marked by a wall-facing scarp (Fig. 25, #1). The ridges become increasingly sinuous toward the crater wall (Fig. 25, #2). The main features of the upper crater wall are alcoves in which blocks and bedrock are exposed. Below this, at the base of the wall, shallow linear lobate depressions extend toward the crater floor (Fig. 25, #3). Triangular talus cones form apices at the base of the alcoves, and broaden downslope, filling the shallow, linear, lobate depressions (Fig. 25, #4). These features are typical of many such

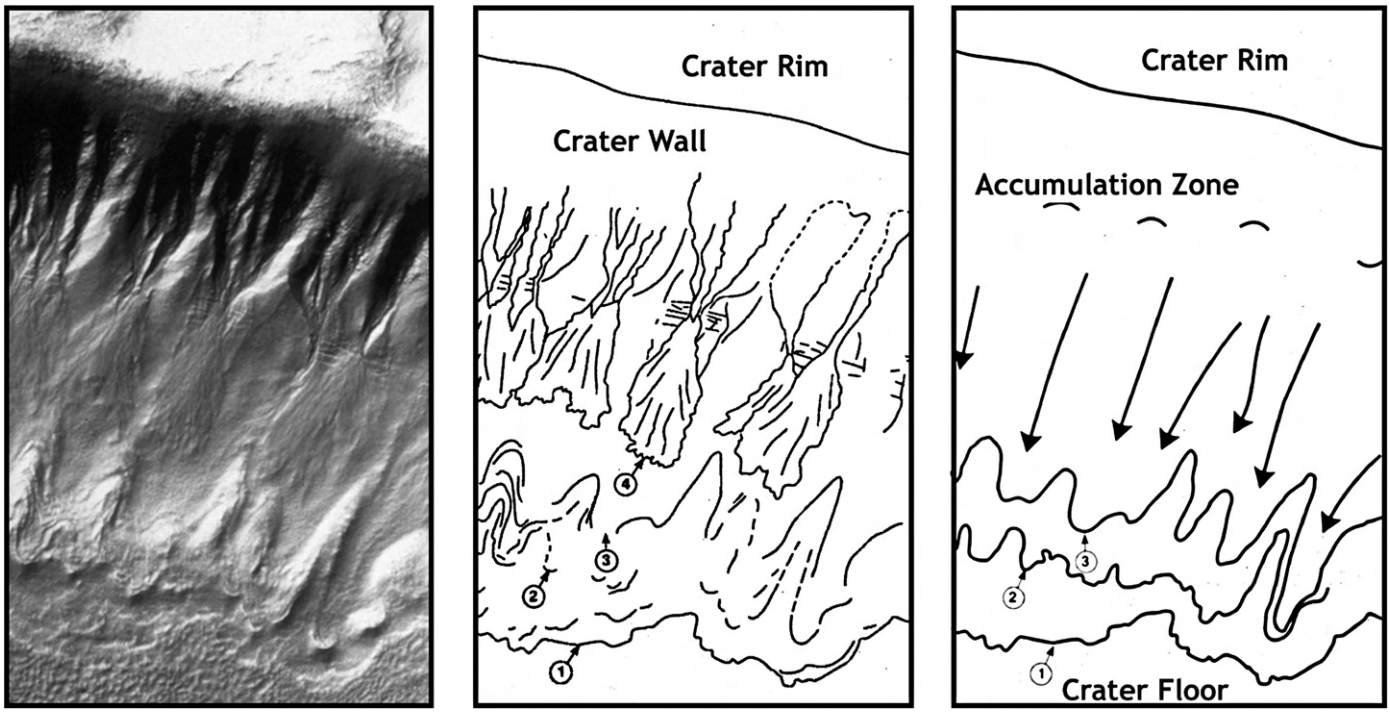

Fig. 25. Sequential development of climate-dependent landforms on Mars on the interior wall of an impact crater. Left: MOC image of a crater rim crest (top), wall (middle), and floor (bottom) showing the sequence of modification of the interior of a crater wall by glacial and mass wasting processes. Middle: Underlying the talus cones (4) is a sequence of units ranging from the upper alcoves, to debris-covered glacier remnants (1–3), to sublimation polygons and till on the crater floor. Right: These relationships suggest the former presence of a microclimate zone that included ice and snow accumulation, debris covered glaciers, and sublimation and polygon formation on the floor. Climate change caused retreat and ice loss, the formation of moraines, dehydration of the climate resulting in the advent of superposed dry talus cones (middle, 4). These types of relationships can be used to establish the nature of past microclimate zones and the sign (direction) of climate change.

features seen on crater walls at mid-latitudes (e.g., Malin and Edgett, 2000, 2001; Berman et al., 2005).

We interpret these geomorphologic features as evidence for changing climate on Mars. In this scenario, in the relatively recent geologic past, the climate was sufficiently different (e.g., Fig. 17) to cause the accumulation of snow and ice in the alcoves, leading to the formation of debris-covered glaciers (e.g., Fig. 19) that descended toward the crater floor (e.g., Milliken et al., 2003). In the past, sufficient ice and debris reached the crater floor to form the sublimation polygons seen there. As the climate changed to conditions less favorable for snow and ice deposition and retention, the debris-covered glaciers retreated, leaving a series of moraines (the zone of crenulate ridges) (Fig. 25, #2–3). With further climate change, the higher concentrations of ice in the regions proximal to the accumulation zones (below the alcoves) underwent sublimation, beheading the debris-covered glaciers and leaving the lobate depressions (Fig. 25, #3). In concert with final removal of ice from the alcoves, the microclimate environment entered a new phase that was dominated by relatively dry talus cone development (for example, the type of change from high obliquity to lower obliquity shown in Fig. 17). During this most recent time, alcove and crater wall debris weakened by the previous glacial action mass-wasted down the crater wall, filling the lows previously occupied by the debris-covered glaciers with talus cones (Fig. 25, #4). Indeed, some occurrences of young viscous flow features and lobate debris aprons show evidence for sinuous channels emerging from their distal portions (Figs. 19 and 20), suggesting that past conditions (e.g., Fig. 17) might also have included at least some seasonal melting and flow of water in local microenvironments (e.g., Costard et al., 2002; Head et al., 2007).

In summary, in a manner analogous to evidence for climate changes discussed for the Antarctic Dry Valleys, changing and superposed equilibrium landforms can be used to infer the sign of climate change on Mars. Mapping of similar microclimate zones and their superposition over the critical latitude-dependent transition zones on Mars holds promise for deconvolving the details of geologically recent climate change there (Fig. 17) (e.g., Head et al., 2003; Kreslavsky et al., 2007). Indeed, the upcoming Phoenix Mission to the northern high latitudes of Mars (Smith et al., 2007) will provide important new information on the climate conditions and the micro- and mesoscale geomorphology there.

8. Summary and conclusions

Analysis of the record of recent climate change on Mars is underway (e.g., Head and Marchant, 2003; Milkovich and Head, 2005; Laskar et al., 2002; Levrard et al., 2004; Tanaka, 2005; Kreslavsky et al., 2007; Forget et al., 2006) and will continue over the coming decades as automated spacecraft and eventually humans explore the planet, and begin to understand how to extrapolate the recent record to earlier peri-

ods of the climate history of Mars (e.g., Bibring et al., 2006; Carr, 2006). In parallel, the exploration and analysis of the Antarctic Dry Valley microclimate zones described here, and their comparison to the emerging details of similar zones on Mars, will provide important insight into the current climate on Mars, the nature and distribution of martian microclimate zones, and the geomorphological evidence for climate change in the past history of Mars (Fig. 1), including those climates most favorable for life.

Acknowledgments

We gratefully acknowledge the financial assistance of the National Science Foundation, Office of Polar Programs, through Grant NSF OPP-0338291 to D.R.M. and J.W.H., and of the National Aeronautics and Space Administration, Mars Fundamental Research Program through Grant NNX06AE32G to D.R.M., and the Mars Data Analysis Program, through Grant NNG04GJ99G to J.W.H. Thanks are also extended to Jay Dickson, Doug Kowalewski, Kate Swanger and Anne Côté for help in manuscript preparation, and to Joseph Levy, Mikhail Kreslavsky, David Shean, Christine McCarthy, Jay Dickson, Doug Kowalewski, Kate Swanger, Gareth Morgan, Seth Kadish, Samuel Schon and two anonymous reviewers for helpful reviews of the manuscript.

References

Allen, C.C., Conca, J.L., 1991. Weathering of basaltic rocks under cold, arid conditions—Antarctica and Mars. Proc. Lunar Sci. Conf. 21, 711–717.

Anderson, D.M., Gatto, L.W., Ugolini, F.C., 1972. An Antarctic analog of martian permafrost terrain. Antarct. J. U.S. 7, 114–116.

Arvidson, R.E., Guinness, E., Lee, S., 1979. Differential Aeolian redistribution rates on Mars. Nature 278, 533–535.

Augustinus, P.C., Selby, M.J., 1990. Rock slope development in McMurdo Oasis, Antarctica, and implications for interpretations of glacial history. Geogr. Ann. A 72, 55–62.

Baker, V.R., 2001. Water and the martian landscape. Nature 412, 228–236.

Banin, A., Clark, B.C., Wanke, H., 1992. Surface chemistry and mineralogy. In: Kieffer, H.H., Jakosky, B.M., Snyder, C.W., Matthews, M.S. (Eds.). Mars. Univ. of Arizona Press, Tucson, pp. 594–625.

Bao, H., Marchant, D.R., 2006. Quantifying sulfate components and their variations in soils of the McMurdo Dry Valleys, Antarctica. J. Geophys. Res. 111, doi:10.1029/2005JD006669.

Bao, H., Campbell, D.A., Bockheim, J.G., Thiemens, M.H., 2000. Origin of sulfate in Antarctic Dry Valley soils as deduced from anomalous ^{17}O compositions. Nature 407, 499–502.

Berg, T.E., Black, R.F., 1966. Preliminary measurements of growth of nonsorted polygons, Victoria Land, Antarctica. In: Tedrow, J.C.F. (Ed.), American Geophysical Union Antarctic Research Series, vol. 8. AGU, Washington, DC, pp. 61–108.

Berman, D.C., Hartmann, W.K., Crown, D.A., Baker, V.R., 2005. The role of arcuate ridges and gullies in the degradation of craters in the Newton Basin region of Mars. Icarus 178 (2), 465–486.

Beyer, L., Bockheim, J.G., Campbell, I.B., Claridge, G.G.C., 1999. Review: Genesis, properties, and sensitivity of Antarctic gelisols. Antarct. Sci. 11, 387–398.

Bibring, J.-B., Langevin, Y., Mustard, J.F., Poulet, F., Arvidson, R., Gendrin, A., Gondet, B., Mangold, N., Pinet, P., Forget, F., and the OMEGA Team, 2006. Global mineralogical and aqueous Mars history derived from OMEGA/Mars Express Data. Science 312, 400–404.

Binder, A.B., Arvidson, R.E., Guinness, E.A., Jones, K.L., Morris, E.C., Mutch, T.A., Pieri, D.C., Sagan, C., 1977. The geology of the Viking 1 landing site. J. Geophys. Res. 82, 4439–4451.

Black, R.F., 1973. Growth of patterned ground in Victoria Land, Antarctica. In: Permafrost Second International Conference. Nat. Acad. Sci., Yakutsk, Siberia, pp. 193–203.

Bocco, G., 1991. Gully erosion; process and models. Prog. Phys. Geogr. 15, 392–406.

Bockheim, J.G., 1997. Properties and classification of cold desert soils from Antarctica. Soil Soc. Am. J. 61 (1), 224–231.

Bockheim, J.G., 2002. Landform and soil development in the McMurdo Dry Valleys: A regional synthesis. Arct. Antarct. Alp. Res. 34, 308–317.

Bockheim, J.G., 2003. University of Wisconsin Antarctic Soils Database. National Snow and Ice Data Center/World Data Center for Glaciology, Boulder, CO. Digital Media.

Borgstrom, I., 1999. Basal ice temperatures during late Weichselian deglaciation; comparison of landform assemblages in west-central Sweden. Ann. Glaciol. 28, 9–15.

Boynton, W.V., and 24 colleagues, 2002. Distribution of hydrogen in the near-surface of Mars: Evidence for subsurface ice deposits. Science 296, 81–85.

Bradley, R.S., 1999. Paleoclimatology: Reconstructing Climates of the Quaternary. International Geophysics Series, vol. 64. Academic Press, London, 613 pp.

Brass, G.W., 1980. Stability of brines on Mars. Icarus 42, 20–28.

Bridges, N.T., Lackner, C.N., 2006. Northern hemisphere martian gullies and mantled terrain: Implications for near-surface water migration in Mars' recent past. J. Geophys. Res.—Planets 111, doi:10.1029/2006JE002702.

Bridges, J.C., Catling, D.C., Saxton, J.M., Swindle, T.D., Lyon, I.C., Grady, M.M., 2001. Alteration assemblages in martian meteorites: Implications for near-surface processes. Space Sci. Rev. 96, 365–392.

Brook, E.J., Brown, E.T., Kurz, M.D., Ackert, R.P., Raisbeck, G.M., Yiou, F., 1995. Constraints on age, erosion, and uplift of Neogene glacial deposits in the Transantarctic Mountains determined from in situ cosmogenic 10Beryllium and 26Aluminum. Geology 23, 1063–1066.

Brook, M.S., Kirkbride, M.P., Bock, B.W., 2006. Quantified time scale for glacial valley cross-profile evolution in Alpine mountains. Geology 34, 637–640.

Bullock, M.A., Moore, J.M., Mellon, M.T., 2004. Laboratory simulations of Mars aqueous geochemistry. Icarus 170, 404–423.

Burt, D.M., Knauth, L.P., 2003. Electrically conducting, Ca-rich brines, rather than water, expected in the martian subsurface. J. Geophys. Res. 108, doi:10.1029/2002JE001862.

Campbell, I.B., Claridge, G.G.C., 1969. A classification of frigic soils—The zonal soils of the Antarctic continent. Soil Sci. 107, 75–85.

Campbell, I.B., Claridge, G.G.C., 1987. Antarctica: Soils, Weathering Processes, and Environment. Developments in Soil Science, vol. 16. Elsevier, New York, 368 pp.

Campbell, I.B., Claridge, G.G.C., 2006. Permafrost properties, patterns and processes in the Transantarctic Mountains region. Permafrost Periglac. Process. 17, 215–232.

Campbell, I.B., Claridge, G.G.C., Balks, M.R., Campbell, D.I., 1997a. Moisture content in soils of the McMurdo Sound and Dry Valley region of Antarctica. In: Lyons, W.B., Howard-Williams, C., Hawes, I. (Eds.), Ecosystem Processes in Antarctic Ice Free Landscapes. A.A. Balkema, Rotterdam, Netherlands, pp. 61–76.

Campbell, D.I., MacCulloch, R.J.L., Campbell, I.B., 1997b. Thermal regimes of some soils in the McMurdo Sound and Dry Valley region. In: Lyons, W.B., Howard-Williams, C., Hawes, I. (Eds.), Ecosystem Processes in Antarctic Ice Free Landscapes. A.A. Balkema, Rotterdam, Netherlands, pp. 45–56.

Campbell, I.B., Claridge, G.G.C., Campbell, D.I., Balks, M.R., 1998. The soil environment of the McMurdo Dry Valleys, Antarctica. In: Priscu, J.C. (Ed.), Ecosystem Dynamics in a Polar Desert: The McMurdo Dry Valleys, Antarctica. In: Antarctic Research Series, vol. 72. AGU, Washington, DC, pp. 297–322.

Carr, M.H., 1981. The Surface of Mars. Yale Univ. Press, New Haven, CT.

Carr, M.H., 1996. Water on Mars. Oxford Univ. Press, New York.

Carr, M.H., 2006. The Surface of Mars. Cambridge Univ. Press, New York.

Chinn, T.J., 1980. Glacier balances in the Dry Valleys area, Victoria Land, Antarctica. In: Proceedings of the Riederlap Workshop. IAHS-AISH Publ. No. 126, pp. 237–247.

Chinn, T.J., 1981. Hydrology and climate in the Ross Sea area. J. Roy. Soc. New Zeal. 11 (4), 373–386.
Chinn, T.J., 1993. Physical hydrology of the Dry Valley lakes. In: Green, W.J., Friedman, E.I. (Eds.), Physical and Biogeochemical Processes in Antarctic Lakes. In: American Geophysical Union Antarctic Research Series, vol. 59. AGU, Washington, DC, pp. 1–51.
Christensen, P.R., 2003. Formation of recent martian gullies through melting of extensive water-rich snow deposits. Nature 422, 45–48.
Christensen, P.R., and 25 colleagues, 2001. Mars Global Surveyor Thermal Emission Spectrometer experiment: Investigation description and surface science results. J. Geophys. Res. 106 (E10), 23823–23872.
Claridge, G.G.C., Campbell, I.B., 1968. Soils of the Shackleton Glacier, Queen Maude Range, Antarctica. New Zeal. J. Sci. 11, 171–218.
Claridge, G.G.C., Campbell, I.B., 1977. The salts in Antarctic soils, their distribution and relationship to soil processes. Soil Sci. 28, 377–384.
Claridge, G.G.C., Campbell, I.B., 2005. Weathering processes in arid cryosols. In: Kimble, J. (Ed.), Cryosols Permafrost Affected Soils. Springer, Berlin/Heidelberg, pp. 447–458.
Clark, B.C., 1978. Implications of abundant hygroscopic materials in the martian regolith. Icarus 34, 645–665.
Clark, B.C., 1979. Chemical and physical microenvironments at the Viking landing sites. J. Mol. Evol. 14, 13–31.
Clark, B.C., Baird, A.K., 1979. Is the martian lithosphere sulfur rich? J. Geophys. Res. 84, 8395–8403.
Clark, B.C., Van Hart, D.C., 1981. The salts of Mars. Icarus 45, 370–378.
Clark, B.C., Baird, A.K., Weldon, R.J., Tsusaki, D.M., Schnabel, L., Candelaria, M.P., 1982. Chemical composition of martian fines. J. Geophys. Res. 87, 10059–10067.
Conca, J.L., Astor, A.M., 1987. Capillary moisture flow and the origin of cavernous weathering in dolerites of Bull Pass, Antarctica. Geology 15, 151–154.
Costard, F., Forget, F., Mangold, N., Peulvast, J.-P., 2002. Formation of recent martian debris flows by melting of near-surface ground ice at high obliquity. Science 295, 110–113.
Craddock, R.A., Howard, A.D., 2002. The case for rainfall on a warm, wet early Mars. J. Geophys. Res. 107 (E11), doi:10.1029/2001001505.
Cuffey, K.M., Conway, H., Gades, A.M., Hallet, B., Lorrain, R., Severinghaus, J.P., Steig, E.J., Vaughn, B., White, J.W.C., 2000. Entrainment at cold glacier beds. Geology 28, 351–354.
Dana, G.L., Wharton, R.A., Dubayah, R., 1998. Solar radiation in the McMurdo Dry Valleys, Antarctica. In: Priscu, J.C. (Ed.), Ecosystem Dynamics in a Polar Desert: The McMurdo Dry Valleys, Antarctica. In: Antarctic Research Series, vol. 72. AGU, Washington, DC, pp. 39–64.
Davis, N., 2001. Permafrost: A Guide to Frozen Ground in Transition. University of Alaska Press, Fairbanks, AK.
Denton, G.H., Marchant, D.R., 2000. The geologic basis for a reconstruction of a grounded ice sheet in McMurdo Sound, Antarctica, at the last glacial maximum. Geogr. Ann. A 82, 167–211.
Denton, G.H., Sugden, D.E., Marchant, D.R., Hall, B.L., Wilch, T.I., 1993. East Antarctic Ice Sheet sensitivity to Pliocene climatic change from a Dry Valleys perspective. Geogr. Ann. A 75, 155–204.
Dickinson, W.W., Rosen, M.R., 2003. Antarctic permafrost: An analogue for water and diagenetic minerals on Mars. Geology 31, 199–202, doi:10.1130/0091-7613.
Dickson, J.L., Head, J.W., Marchant, D.R., Morgan, G.A., Levy, J.S., 2007a. Recent gully activity on Mars: Clues from late-stage water flow in gully systems and channels in the Antarctic Dry Valleys. Lunar Planet. Sci. 38. Abstract 1678.
Dickson, J.L., Head, J.W., Kreslavsky, M., 2007b. Martian gullies in the southern mid-latitudes of Mars: Evidence for climate-controlled formation of young fluvial features. Icarus 188, 315–323.
Doran, P.T., McKay, C.P., Clow, G.D., Dana, G.L., Fountain, A.G., Nylen, T., Lyons, W.B., 2002. Valley floor climate observations from the McMurdo Dry Valleys, Antarctica, 1986–2000. J. Geophys. Res. 107 (D24), doi:10.1029/2001JD002045.
Elliot, D.E., Fleming, T.H., 2004. Occurrence and dispersal of magmas in the Jurrasic Ferrar large igneous province, Antarctica. Gondwana Res. 7 (1), 223–237.
Fabel, D., Stroeven, A.P., Harbor, J., Kleman, J., Elmore, D., Fink, D., 2002. Landscape preservation under Fennoscandian ice sheets determined from in situ produced ^{10}Be and ^{26}Al. Earth Planet. Sci. Lett. 201 (2), 397–406.
Farmer, C.B., 1976. Liquid water on Mars. Icarus 28, 279–289.
Farmer, C.B., Doms, P.E., 1979. Global seasonal variation of water vapor on Mars and the implications of permafrost. J. Geophys. Res. 84, 2881–2888.
Feldman, W.C., and 12 colleagues, 2002. Global distribution of neutrons from Mars: Results from Mars Odyssey. Science 297, 75–78.
Forget, F., Hourdin, F., Fournier, R., Hourdin, C., Talagrand, O., Collins, M., Lewis, S.R., Read, P.L., Huot, J.-P., 1999. Improved general circulation models of the martian atmosphere from the surface to above 80 km. J. Geophys. Res. 104 (E10), 24155–24176.
Forget, F., Haberle, R.M., Montmessin, F., Levrard, B., Head, J.W., 2006. Formation of glaciers on Mars by atmospheric precipitation at high obliquity. Science 311, 368–371.
Fountain, A.G., Lewis, K.J., Doran, P.T., 1999. Spatial climatic variation and its control on glacier equilibrium line altitude in Taylor Valley, Antarctica. Global Planet. Change 22, 1–10.
Frezotti, M., 1997. Ice front fluctuation, iceberg calving flux and mass balance of Victoria Land glaciers. Antarct. Sci. 9, 61–73.
Ghysels, G., Heyse, I., 2006. Composite-wedge pseudomorphs in Flanders, Belgium. Permafrost Periglac. Prosess. 17, 145–161.
Giardino, J.R., Shroder, J.F., Vitek, J.D., 1987. Rock Glaciers. Allen and Unwin, London, UK.
Gibson, E.K., Wentworth, S.T., McKay, D.S., 1983. Chemical weathering and diagenesis of a cold desert soil from Wright Valley, Antarctica: An analog for martian weathering processes. J. Geophys. Res. 88. (Suppl.), A812–A918.
Gooding, J.L., 1992. Soil mineralogy and chemistry on Mars: Possible clues from salts and clays in SNC meteorites. Icarus 99, 28–41.
Gooding, J.L., Wentworth, S.J., Zolensky, M.E., 1991. Aqueous alteration of the Nakhla meteorite. Meteoritics 26, 135–143.
Golombek, M.P., and 13 colleagues, 1997. Overview of the Mars Pathfinder Mission and Assessment of Landing Site predictions. Science 278, 1743.
Golombek, M.P., and 22 colleagues, 1999. Overview of the Mars Pathfinder Mission: Launch through landing, surface operations, data sets, and science results. J. Geophys. Res. 104 (E4), 8523–8554.
Gooseff, M.N., McKnight, D.M., Runkel, R.L., Vaughn, B.H., 2003a. Determining long time-scale hyporheic zone flow paths in Antarctic streams. Hydrol. Process. 17 (9), 1691–1710.
Gooseff, M.N., Barrett, J.E., Doran, P.T., Fountain, A.G., Lyons, W.B., Parsons, A.N., Porazinska, D.L., Virginia, R.A., Wall, D.H., 2003b. Snow-patch influence on soil biogeochemical proceses and ibertebrate distribution in the McMurdo Dry Valleys, Antarctica. Arct. Antarct. Alp. Res. 35, 92–100.
Haberle, R.M., McKay, C.P., Schaeffer, J., Cabrol, N.A., Grin, E.A., Zent, A.P., Quinn, R., 2001. On the possibility of liquid water on present-day Mars. J. Geophys. Res. 106 (E10), 23317–23326.
Hall, K.J., 1991. Mechanical weathering in the Antarctic: A maritime perspective. In: Dixon, J.C., Abrahams, A.D. (Eds.), Periglacial Geomorphology. John Wiley and Sons, Chichester, pp. 103–123.
Hall, B.L., Denton, G.H., Lux, D.R., Bockheim, J.G., 1993. Late Tertiary Antarctic paleoclimate and ice-sheet dynamics inferred from surficial deposits in Wright Valley. Geogr. Ann. A 75, 239–268.
Hallet, B., Waddington, D.E., 1991. Buoyancy forces induced by freeze-thaw in the active layer: implications for diapirism and soil circulation. In: Dixon, J.C., Abrahams, A.D. (Eds.), Periglacial Geomorphology. John Wiley and Sons, Chichester, pp. 251–279.
Hallet, B., Hunter, L., Bogen, J., 1996. Rates of erosion and sediment evacuation by glaciers: A review of field data and their implications. Global Planet. Change 12, 213–235.
Harris, K.J., Carey, A.E., Lyons, W.B., Welch, K.A., Fountain, A.G., 2007. Solute and isotope geochemistry of subsurface ice melt seeps in Taylor Valley, Antarctica. Geol. Soc. Am. Bull. 119, 548–555.
Hartman, B.N., 1998. Miocene paleoclimate and ice sheet dynamics as recorded in central Taylor Valley, Antarctica. Unpublished MS thesis, Boston University.
Haskin, L.A., and 29 colleagues, 2005. Water alteration of rocks and soils on Mars at the Spirit Rover site in Gusev crater. Nature 436, 66–69.

Hassinger, J.M., Mayewski, P.A., 1983. Morphology and dynamics of rock glaciers in southern Victoria Land, Antarctica. Arct. Alp. Res. 15, 351–368.
Head, J.W., Kreslavsky, M.A., 2006. Formation of weathering pits on rock surfaces in the Antarctic Dry Valleys and on Mars. Paper presented at the 44th Brown/Vernadsky Microsymposium, Moscow, Russia. Abstract m44–25.
Head, J.W., Marchant, D.R., 2003. Cold-based mountain glaciers on Mars: Western Arsia Mons. Geology 31 (7), 641–644.
Head, J.W., Marchant, D.R., 2006, Gullies and saline ponds in the cold hyperarid desert of the Antarctic Dry Valleys: Clues to interpreting climate conditions on Mars. Paper presented at the 44th Brown/Vernadsky Microsymposium, Moscow, Russia. Abstract m44–26.
Head, J.W., Mustard, J.F., Kreslavsky, M.A., Milliken, R.E., Marchant, D.R., 2003. Recent ice ages on Mars. Nature 426, 797–802.
Head, J.W., and 13 colleagues, 2005. Tropical to mid-latitude snow and ice accumulation, flow and glaciation on Mars. Nature 434, 346–351.
Head, J.W., Marchant, D.R., Agnew, M.C., Fassett, C.I., Kreslavsky, M.A., 2006a. Extensive valley glacier deposits in the northern mid-latitudes of Mars: Evidence for Late Amazonian obliquity-driven climate change. Earth Planet. Sci. Lett. 241, 663–671.
Head, J.W., Nahm, A.L., Marchant, D.R., Neukum, G., and the HRSC Co-Investigator Team, 2006b. Modification of the dichotomy boundary on Mars by Amazonian mid-latitude regional glaciation. Geophys. Res. Let. 33 (8), doi:10.1029/2005GL024360.
Head, J.W., Marchant, D.R., Dickson, J.L., Levy, J.S., Morgan, G.A., 2007. Mars gully analogs in the Antarctic Dry Valleys: Geological setting and processes. Lunar Planet. Sci. 38. Abstract 1617.
Healy, M., Webster-Brown, J.G., Brown, K.L., Lane, V., 2006. Chemistry and stratification of Antarctic meltwater ponds II: Inland ponds in the McMurdo Dry Valleys, Victoria Land. Antarct. Sci. 18, 525–533.
Hecht, M.H., 2002. Metastability of liquid water on Mars. Icarus 156, 373–386.
Heldmann, J.L., Mellon, M.T., 2004. Observations of martian gullies and constraints on potential formation mechanisms. Icarus 168, 285–304.
Huinink, H.P., Pel, L., Kopinga, K., 2004. Stimulating the growth of tafoni. Earth Surf. Proc. Land. 29 (10), 1225–1233.
Jakosky, B.M., Mellon, M.T., 2001. High-resolution thermal inertia mapping of Mars: Sites of exobiological interest. J. Geophys. Res. 106 (E10), 23887–23908.
Jones, K.L., Bragg, S.L., Wall, S.D., Carlston, C.E., Pidek, D.G., 1979. One Mars year: Viking lander imaging observations. Science 204, 799–806.
Kleman, J., Hattestrand, C., 1999. Frozen-bed Fennoscandian and Laurentide ice sheets during the last glacial maximum. Nature 402, 63–66.
Kleman, J., Marchant, D.R., Borgstrom, I., 2001. Late glacial ice dynamics on southern Baffin Island and in Hudson Strait. Arct. Antarct. Alp. Res. 33 (3), 249–257.
Knauth, L.P., Burt, D.M., 2002. Eutectic brine seeps on Mars: Origin and possible relation to young seepage features. Icarus 158, 267–271.
Koppes, M., Hallet, B., 2006. Erosion rates during rapid deglaciation in Icy Bay, Alaska. J. Geophys. Res. 111, doi:10.1029/2005JF000349.
Kostama, V.-P., Kreslavsky, M.A., Head, J.W., 2006. Recent high-latitude icy mantle in the northern plains of Mars: Characteristics and ages of emplacement. Geophys. Res. Lett. 33 (11), doi:10.1029/2006GL025946.
Kowalewski, D.E., Marchant, D.R., Levy, J.S., Head III, J.W., 2006. Quantifying low rates of summertime sublimation for buried glacier ice in Beacon Valley. Antarctica. Antarct. Sci. 18 (3), 421–428.
Kreslavsky, M.A., Head, J.W., 1999. Kilometer-scale slopes on Mars and their correlation with geologic units: Initial results from Mars Orbiter Laser Altimeter (MOLA) data. J. Geophys. Res. 104 (E9), 21911–21924.
Kreslavsky, M.A., Head, J.W., 2000. Kilometer-scale roughness of Mars: Results from MOLA data analysis. J. Geophys. Res. 105 (E11), 26695–26712.
Kreslavsky, M.A., Head, J.W., 2002a. Mars: Nature and evolution of young latitude-dependent water–ice-rich mantle. Geophys. Res. Lett. 29 (15), doi:10.1029/2002GL015392.
Kreslavsky, M.A., Head III, J.W., 2002b. Mars: Nature and evolution of young latitude-dependent water–ice-rich mantle. Geophys. Res. Lett. 29, doi:10.1029/2002GL015392.
Kreslavsky, M.A., Head, J.W., 2003. North–south topographic slope asymmetry on Mars: Evidence for insolation-related erosion at high obliquity. Geophys. Res. Lett. 30 (15), doi:10.1029/2003GL017795.
Kreslavsky, M.A., Head, J.W., 2004. Periods of active permafrost layer formation in the recent geological history of Mars. Lunar Planet. Sci. 35. Abstract 1201.
Kreslavsky, M.A., Head, J.W., 2005. Mars at very low obliquity: Atmospheric collapse and the fate of volatiles. Geophys. Res. Lett. 32, doi:10.1029/2005GL022645.
Kreslavsky, M.A., Head, J.W., Marchant, D.R., 2007. Periods of active permafrost layer formation during the geological history of Mars: Implications for circum-polar and mid-latitude surface processes. Planet. Space Sci., in press.
Kuzmin, R.O., Zabalueva, E.V., 1998. On salt solutions of the martian cryolithosphere. Solar Syst. Res. 32, 187–197.
Lachenbruch, A.H., 1962. Mechanics of thermal contraction cracks and ice-wedge polygons in permafrost. GSA Special Papers 70, 1–69.
Lancaster, N., 2002. Flux of eolian sediment in the McMurdo Dry Valleys, Antarctica: A preliminary assessment. Arct. Antarct. Alp. Res. 34 (3), 318–323.
Langbein, W.B., Schumm, S.A., 1958. Yield of sediment in relation to mean annual precipitation. AGU Trans. 39, 1023–1036.
Larsen, K.W., Arvidson, R.E., Jolliff, B.L., Clark, B.C., 2000. Correspondence and least-squares analysis of soil and rock compositions for the Viking Lander 1 and Pathfinder landing sites. J. Geophys. Res. 105, 29207–29221.
Laskar, J., Levrard, B., Mustard, J.F., 2002. Orbital forcing of the martian polar layered deposits. Nature 419, 375–377.
Laskar, J., Gastineau, M., Joutel, F., Robutel, P., Levrard, B., Correia, A., 2004. Long term evolution and chaotic diffusion of the insolation quantities of Mars. Icarus 170, 343–364.
Leovy, C., 2001. Weather and climate on Mars. Nature 412, 245–249.
Levrard, B., Forget, F., Montmessin, F., Laskar, J., 2004. Recent ice-rich deposits formed at high latitudes on Mars by sublimation of unstable equatorial ice during low obliquity. Nature 431, 1072–1075.
Levy, J.S., Marchant, D.R., Head III, J.W., 2006. Distribution and origin of patterned ground on Mullins Valley debris-covered glacier, Antarctica: The roles of ice flow and sublimation. Antarct. Sci. 18 (3), 385–397.
Levy, J., Head, J.W., Marchant, D.R., Morgan, G.A., Dickson, J.L., 2007. Gully surface and shallow subsurface structure in the South Fork of Wright Valley, Antarctic Dry Valleys: Implications for gully activity on Mars. Lunar Planet. Sci. 38. Abstract 1728.
Lewis, A.R., Marchant, D.R., Ashworth, A.C., Hemming, S.R., Machlus, M., 2007. Major middle Miocene global climate change: Evidence from East Antarctica and the Transantarctic Mountains. Geol. Soc. Am. Bull., in press.
Lyons, W.B., Welch, K.A., Carey, A.E., Doran, P.T., Wall, D.H., Virginia, R.A., Fountain, A.G., Csathó, B.M., Tremper, C.M., 2005. Groundwater seeps in Taylor Valley, Antarctica: An example of a subsurface melt event. Ann. Glaciol. 40, 200–206.
Lyons, W.B., Howard-Williams, C., Hawes, I. (Eds.), 1997. Ecosystem Processes in Antarctic Ice-Free Landscapes. A.A. Balkema, Rotterdam, Netherlands.
Mackay, J.R., 1977. The widths of ice wedges. Geol. Surv. Can. Prof. Paper 77 (1A), 43–44.
Mahaney, W.C., Dohm, J.M., Baker, V.R., Newsom, H.E., Malloch, D., Hancock, R.G.V., Campbell, I., Sheppard, D., Milner, M.W., 2001. Morphogenesis of Antarctic Paleosols: Martian analogue. Icarus 154 (1), 113–130.
Malin, M.C., 1974. Salt weathering on Mars. J. Geophys. Res. 79, 3888–3894.
Malin, M.C., 1984. Abrasion rate observations in Victoria Valley, Antarctica: 340-day experiment. Antarct. J. U.S. 19 (5), 14–16.
Malin, M.C., 1987. Abrasion in ice-free areas of southern Victoria Land, Antarctica. Antarct. J. U.S. 21 (5), 38–39.
Malin, M.C., Edgett, K.S., 2000. Evidence for recent groundwater seepage and surface runoff on Mars. Science 288, 2330–2335.
Malin, M.C., Edgett, K.S., 2001. Mars Global Surveyor Mars Orbiter Camera: Interplanetary cruise through primary mission. J. Geophys. Res. 106 (E10), 23429–23570.
Malin, M.C., Edgett, K.S., Posiolova, L.V., McColley, S.M., Noe Dobrea, E.Z., 2006. Present-day impact cratering rate and contemporary gully activity on Mars. Science 314, 1573–1577.
Mangold, N., 2005. High latitude patterned grounds on Mars: Classification, distribution and climatic control. Icarus 174, 336–359.

Mangold, N., Allemand, P., Duval, P., Geraud, Y., Thomas, P., 2002. Experimental and theoretical deformation of ice–rock mixtures: Implications on rheology and ice content of martian permafrost. Planet. Space Sci. 50 (4), 385–401.

Mangold, N., Maurice, S., Feldman, W.C., Costard, F., Forget, F., 2004. Spatial relationships between patterned ground and ground ice detected by the Neutron Spectrometer on Mars. J. Geophys. Res. 109 (E8), doi:10.1029/2004JE002235.

Marchant, D.R., Denton, G.H., 1996. Miocene and Pliocene paleoclimate of the Dry Valleys region, southern Victoria Land: A geomorphological approach. Mar. Micropaleontol. 27, 253–271.

Marchant, D.R., Head III, J.W., 2003. Origin of sublimation polygons in the Antarctic western Dry Valleys region: Implications for patterned ground development on Mars. Eos (Fall Suppl.) 84 (46). C12C-06.

Marchant, D.R., Head III, J.W., 2004. Microclimates zones of the Dry Valleys of Antarctica: Implications for landscape evolution and climate change on Mars. Lunar Planet. Sci. 35. Abstract 1405.

Marchant, D.R., Head III, J.W., 2005. Equilibrium landforms in the Dry Valleys of Antarctica: Implications for landscape evolution and climate change on Mars. Lunar Planet. Sci. 36. Abstract 1421.

Marchant, D.R., Denton, G.H., Swisher III, C.C., 1993a. Miocene–Pliocene–Pleistocene glacial history of Arena Valley, Quartermain Mountains, Antarctica. Geogr. Ann. A 75, 269–302.

Marchant, D.R., Denton, G.H., Sugden, D.E., 1993b. Miocene glacial stratigraphy and landscape evolution of the western Asgard Range, Antarctica. Geogr. Ann. A 75, 303–330.

Marchant, D.R., Denton, G.H., Swisher III, C.C., Potter Jr., N., 1996. Late Cenozoic Antarctic paleoclimate reconstructed from volcanic ashes in the Dry Valleys region, south Victoria Land. Geol. Soc. Am. Bull. 108 (2), 181–194.

Marchant, D.R., Lewis, A., Phillips, W.C., Moore, E.J., Souchez, R., Landis, G.P., 2002. Formation of patterned-ground and sublimation till over Miocene glacier ice in Beacon Valley, Antarctica. Geol. Soc. Am. Bull. 114, 718–730.

Margerison, H.R., Phillips, W.M., Stuart, F.M., Sugden, D.E., 2005. Cosmogenic He-3 concentrations in ancient flood deposits from the Coombs Hills, northern Dry Valleys, East Antarctica: Interpreting exposure ages and erosion rates. Earth Planet. Sci. Lett. 230, 163–175.

Marion, G.M., 1997. A theoretical evaluation of mineral stability in Don Juan Pond, Wright Valley, Victoria Land. Antarct. Sci. 9, 92–99.

Marshall, G.J., Turner, J., 1997. Katabatic wind propagation over the western Ross Sea observed using ERS-1 scatterometer data. Antarct. Sci. 9, 221–226.

Matsuoka, N., 2001. Solifluction rates, processes, and landforms: A global review. Earth Sci. Rev. 44, 107–134.

McKnight, D.M., Niyogi, D.K., Alger, A.S., Bomblies, A., Cenovitz, P.A., Tate, C.M., 1999. Dry Valley streams in Antarctica: Ecosystems waiting for water. Bioscience 49, 985–995, doi:10.2307/1313732.

Mellon, M.T., 1997. Small-scale polygonal features on Mars: Seasonal–sthermal contraction cracks in permafrost. J. Geophys. Res. 102, 25617–25628.

Mellon, M.T., 2003. Theory of ground ice on Mars and implications to the neutron leakage flux. Lunar Planet. Sci. 34. Abstract 1916.

Mellon, M.T., Jakosky, B.M., 1995. The distribution and behavior of martian ground ice during past and present epochs. J. Geophys. Res. 100, 11781–11799.

Milkovich, S.M., Head, J.W., 2005. North polar cap of Mars: Polar layered deposit characterization and identification of a fundamental climate signal. J. Geophys. Res. 110 (E1), doi:10.1029/2004JE002349.

Miller, G.H., Wolfe, A.P., Briner, J.P., Sauer, P.E., Nesje, A., 2005. Holocene glaciation and climate evolution of Baffin Island, Arctic Canada. Quaternary Sci. Rev. 24, 1703–1721.

Milliken, R.E., Mustard, J.F., Goldsby, D.L., 2003. Viscous flow features on the surface of Mars: Observations from high-resolution Mars Orbiter Camera (MOC) images. J. Geophys. Res. 108 (E6), doi:10.1029/2002JE002005.

Mitrofanov, I., and 11 colleagues, 2002. Maps of subsurface hydrogen from the high energy neutron detector, Mars Odyssey. Science 297, 78–81.

Morgan, G., Head, J.W., Marchant, D.R., Dickson, J.L., Levy, J.S., 2007. Gully formation on Mars: Testing the snowpack hypothesis from analysis of analogs in the Antarctic Dry Valleys. Lunar Planet. Sci. 38. Abstract 1656.

Murton, J.B., Worsley, P., Gozdzik, J., 2000. Sand veins and wedges in cold aeolian environments. Quaternary Sci. Rev. 19, 899–922.

Mustard, J.F., Cooper, C.D., Rifkin, M.K., 2001. Evidence for recent climate change on Mars from the identification of youthful near-surface ground ice. Nature 412, 411–414.

Mutch, T.A., Grenander, S.U., Jones, K.L., Patterson, W., Arvidson, R.E., Guinness, E.A., Avrin, P., Carlston, C.E., Binder, A.B., Sagan, C., 1976a. The surface of Mars—The view from the Viking 2 lander. Science 194, 1277–1283.

Mutch, T.A., Patterson, W.R., Binder, A.B., Huck, F.O., Taylor, G.R., Levinthal, E.C., Liebes, S., Morris, E.C., Pollack, J.B., Sagan, C., 1976b. The surface of Mars: The view from the Viking 1 lander. Science 193, 791–801.

Mutch, T.A., Arvidson, R.E., Guinness, E.A., Binder, A.B., Morris, E.C., 1977. The geology of the Viking Lander 2 site. J. Geophys. Res. 82, 4452–4467.

Nichols, R.L., 1968. Coastal geomorphology, McMurdo sound, Antarctica. J. Glaciol. 7, 449–478.

Nkem, J.N., Virginia, R.A., Barrett, J.E., Wall, D.H., Li, G., 2006. Salt tolerance and survival thresholds for two species of Antarctic soil nematodes. Polar Biol. 28 (8), 643–651.

Nylen, T., Fountain, A.G., Doran, P., 2004. Climatology of katabatic winds in the McMurdo Dry Valleys, southern Victoria land, Antarctica. J. Geophys. Res. 109, doi:10.1029/2003JD003937.

Paige, D.A., 2002. Near-surface liquid water on Mars. Lunar Planet. Sci. 33. Abstract 2049.

Parsons, R., Head, J.W., Marchant, D.R., 2005. Weathering pits in the Antarctic Dry Valleys: Insolation-induced heating and melting and applications to Mars. Lunar Planet. Sci. 36. Abstract 1138.

Patterson, W.S.B., 2001. The Physics of Glaciers. Butterworth–Heinman Publishing Co., London, UK.

Péwé, T.L., 1959. Sand-wedge polygons (tesselations) in the McMurdo Sound region, Antarctica—A progress report. Am. J. Sci. 257, 545–552.

Pierce, T.L., Crown, D.A., 2003. Morphologic and topographic analyses of debris aprons in the eastern Hellas region, Mars. Icarus 163, 46–65.

Pollack, J.B., Kasting, J.F., Richardson, S.M., Poliakoff, K., 1987. The case for a wet, warm climate on early Mars. Icarus 71, 203–224.

Prentice, M.L., Kleman, J.K., Stroeven, A.P., 1998. The composite glacial erosional landscape of the northern McMurdo Dry Valleys: Implications for Antarctic Tertiary glacial history. In: Priscu, J.C. (Ed.), The McMurdo Dry Valleys: A Cold-Desert Ecosystem. In: AGU Antarctic Research Series, vol. 72. AGU, Washington, DC, pp. 1–38.

Priscu, J.C. (Ed.), 1998. The McMurdo Dry Valleys: A Cold-Desert Ecosystem. AGU Antarctic Research Series, vol. 72. AGU, Washington, DC, p. 370.

Reiss, D., Jaumann, R., 2003. Recent debris flows on Mars: Seasonal observations of the Russell Crater dune field. Geophys. Res. Lett. 30 (6), doi:10.1029/2002GL016704.

Richardson, M.I., Mischna, M.A., 2005. Long-term evolution of transient liquid water on Mars. J. Geophys. Res. 110 (E3), doi:10.1029/2004JE002367.

Rieder, R., and 14 colleagues, 2004. Chemistry of rocks and soils at Meridiani Planum from the alpha particle X-ray Spectrometer. Science 306, 1746–1749.

Rignot, E., Hallet, B., Fountain, A., 2002. Rock glacier surface motion in Beacon Valley, Antarctica, from synthetic-aperture radar interferometry. Geophys. Res. Lett. 29 (12), doi:10.1029/2001GL013494.

Schaefer, J.M., Bauer, H., Denton, G.H., Ivy-Ochs, S., Marchant, D.R., Schlüchter, C., Wieler, R., 2000. The oldest ice on Earth in Beacon Valley, Antarctica: New evidence from surface exposure dating. Earth Planet. Sci. Lett. 179, 91–99.

Schumm, S.A., 1965. Quaternary paleohydrology. In: Wright, H.E., Frey, D.G. (Eds.), The Quaternary of the United States. Princeton Univ. Press, Princeton, NJ, p. 922.

Schumm, S.A., Lichty, R.W., 1965. Time, space and causality in geomorphology. Am. J. Sci. 263, 110–119.

Schwerdtfeger, W., 1984. Weather and Climate of the Antarctic. Developments in Atmospheric Science, vol. 15. Elsevier, Amsterdam, 262 pp.

Selby, M.J., 1971a. Slopes and their development in an ice-free, arid area of Antarctica. Geogr. Ann. A 53, 235–245.

Selby, M.J., 1971b. Some solifluction surfaces and terraces in the ice-free valleys of Victoria Land, Antarctica. New Zeal. J. Geol. Geophys. 14 (3), 469–476.

Selby, M.J., 1974. Slope evolution in an Antarctic oasis. New Zeal. Geogr. 30, 18–34.

Selby, M.J., 1977. Transverse erosional marks on ventifacts from Antarctica. New Zeal. J. Geol. Geophys. 20 (5), 949–969.

Seibert, N.M., Kargel, J.S., 2001. Small-scale martian polygonal terrain: Implications for liquid surface water. Geophys. Res. Lett. 28 (5), 899–902.

Settle, M., 1979. Formation and deposition of volcanic sulfate aerosols on Mars. J. Geophys. Res. 84, 8343–8354.

Siegel, B.Z., McMurty, G., Siegel, S.M., Chen, J., Larock, P., 1979. Life in the calcium chloride environment of Don Juan Pond, Antarctica. Nature 280, 828–829.

Sletten, R.S., Hallet, B., Fletcher, R.C., 2003. Resurfacing time of terrestrial surfaces by the formation and maturation of polygonally patterned ground. J. Geophys. Res. 108, doi:10.1029/2002JE001914.

Smith, D.E., and 23 colleagues, 2001. Mars Orbiter Laser Altimeter: Experiment summary after the first year of global mapping of Mars. J. Geophys. Res. 106, 23689–23722.

Smith, P.H., and the Phoenix Science Team, 2007. The Phoenix Mission. In: Seventh International Conference on Mars. Abstract 3180.

Spotila, J.A., Buscher, J.T., Meigs, A.J., Reiners, P.W., 2004. Long-term glacial erosion of active mountain belts: Example of the Chugach-St. Elias Range, Alaska. Geology 32, 501–504.

Squyres, S.W., Clifford, S.M., Kuzmin, R.O., Zimbelman, J.R., Costard, F.M., 1992. Ice in the martian regolith. In: Kieffer, H.H., Jakosky, B.M., Snyder, C.W., Matthews, M.S. (Eds.), Mars. Univ. of Arizona Press, Tucson, pp. 523–554.

Squyres, S.W., and 49 colleagues, 2004a. The Spirit Rover's Athena science investigation at Gusev crater, Mars. Science 305, 794–799.

Squyres, S.W., and 49 colleagues, 2004b. The Opportunity Rover's Athena science investigation at Meridiani Planum, Mars. Science 306, 1698–1703.

Squyres, S.W., and 17 colleagues, 2004c. In-situ evidence for an ancient aqueous environment at Meridiani Planum, Mars. Science 306, 1709–1714.

Squyres, S.W., and 17 colleagues, 2006. Two years at Meridiani Planum: Results from the Opportunity Rover. Science 313, 1403–1407.

Staiger, J.W., Marchant, D.R., Schaefer, J.M., Oberholzer, P., Johnson, J.V., Lewis, A.R., Swanger, K.M., 2006. Plio-Pleistocene history of Ferrar Glacier, Antarctica: Implications for climate and ice sheet stability. Earth Planet. Sci. Lett. 243, 489–503.

Sugden, D.E., Denton, G.H., Marchant, D.R., 1995a. Landscape evolution of the Dry Valleys, Transantarctic Mountains: Tectonic implications. J. Geophys. Res. 100 (B7), 9949–9967.

Sugden, D.E., Marchant, D.R., Potter Jr., N., Souchez, R., Denton, G.H., Swisher, C.C., Tison, J.-L., 1995b. Miocene glacier ice in Beacon Valley, Antarctica. Nature 376, 412–416.

Summerfield, M.A., Stuart, F.M., Cockburn, H.A.P., Sugden, D.E., Denton, G.H., Dunai, T., Marchant, D.R., 1998. Long-term rates of denudation in the Dry Valleys region of the Transantarctic Mountains, southern Victoria Land based on in-situ produced cosmogenic Ne-21. Geomorphology 27, 113–129.

Summerfield, M.A., Sugden, D.E., Denton, G.H., Marchant, D.R., Cockburn, H.A.P., Stuart, F.M., 1999. Cosmogenic isotope data support previous evidence of extremely low rates of denudation in the Dry Valleys region, southern Victoria Land, Antarctica. Geol. Soc. Lond. Spec. Publ. 162, 255–267.

Swanger, K.M., Marchant, D.R., 2007. Sensitivity of ice-cemented Antarctic soils to greenhouse-induced thawing: Are terrestrial archives at risk? Earth Planet. Sci. Lett. 259, 347–359.

Takamatsu, N., Kato, N., Matsumoto, G.I., 1998. The origin of salts in water bodies of the McMurdo Dry Valleys. Antarct. Sci. 10, 439–448.

Tanaka, K.L., 2005. Geology and insolation-driven climatic history of Amazonian north polar materials on Mars. Nature 437, 991–994.

Tillman, J.E., 1988. Mars global atmospheric oscillations: Annually synchronized, transient normal mode oscillations and the triggering of global dust storms. J. Geophys. Res. 93, 9433–9451.

Torii, T., Nakaya, S., Matsubaya, O., Matsumoto, G.I., Masuda, N., Kawano, T., Murayama, H., 1989. Chemical characteristics of pond waters in the Labyrinth of southern Victoria Land, Antarctica. Hydrobiologia 172, 255–264.

Tosca, N.J., McLennan, S.M., Clark, B.C., Grotzinger, J.P., Hurowitz, J.A., Knoll, A.H., Schröder, C., Squyres, S.W., 2005. Geochemical modeling of evaporation processes on Mars: Insight from the sedimentary record at Meridiani Planum. Earth Planet. Sci. Lett. 240, 122–148.

Toulmin, P., Baird, A.K., Clark, B.C., Keil, K., Rose, H.J., Christian, R.P., Evans, P.H., Kelliher, W.C., 1977. Geochemical and mineralogical interpretation of the Viking inorganic chemical results. J. Geophys. Res. 82, 4625–4634.

Vaniman, D.T., Chipera, S.J., 2006. Transformation of Mg- and Ca-sulfate hydrates in Mars regolith. Am. Mineral. 91, 1628–1642.

Wall, S.D., 1981. Analysis of condensates formed at the Viking 2 lander site—The first winter. Icarus 47, 173–183.

Wang, A., and 11 colleagues, 2007. Sulfate-rich soils exposed by Spirit Rover at multiple locations in Gusev crater on Mars. In: Seventh International Mars Conference. Abstract 3348.

Wentworth, S.K., Gibson, E.K., Velbel, M.A., McKay, D.S., 2005. Antarctic Dry Valleys and indigenous weathering in Mars meteorites: Implications for water and life on Mars. Icarus 174, 383–395.

Whalley, W.B., Palmer, C.F., 1998. A glacial interpretation for the origin and formation of the Marinet Rock Glacier, Alpes Maritimes, France. Geogr. Ann. 80, 221–236.

Wilson, L., 1969. Les relations entre les processus geomorphologique et le climat moderne comme méthode de paléoclimatologie. Rev. Géogr. Phys. Geol. Dynam. 11, 309–314.

Yershov, E.D., 1998. General Geocryology, Studies in Polar Research. Cambridge Univ. Press, Cambridge, UK, 580 pp.

Zent, A.P., Fanale, F.P., 1986. Possible Mars brines: Equilibrium and kinetic considerations. J. Geophys. Res. 91, 439–445.

Zent, A.P., Fanale, F.P., 1990. Possible martian brines: Radar observations and models. J. Geophys. Res. 95, 14531–14542.

Zent, A.P., Fanale, F.P., Salvail, J.R., Postawko, S.E., 1986. Distribution and state of H_2O in the high-latitude shallow subsurface of Mars. Icarus 67, 19–36.

Zurek, R., 1992. Comparative aspects of the climate of Mars: An introduction to the current atmosphere. In: Kieffer, H.H., Jakosky, B.M., Snyder, C.W., Matthews, M.S. (Eds.), Mars. Univ. of Arizona Press, Tucson, pp. 799–817.

Zurek, R.W., Barnes, J.R., Haberle, R.M., Pollack, J.B., Tillman, J.E., Leovy, C.B., 1992. Dynamics of the atmosphere of Mars. In: Kieffer, H.H., Jakosky, B.M., Snyder, C.W., Matthews, M.S. (Eds.), Mars. Univ. of Arizona Press, Tucson, pp. 835–933.